COATING SCIENCE AND TECHNOLOGY

PENNSYLVANIA STATE UNIVERSITY

PREPARED FOR
ROME AIR DEVELOPMENT CENTER

MARCH 1976

Unclassified

SECURITY CLASSIFICATION OF THIS PAGE (When Data Entered)

REPORT DOCUMENTATION PAGE		READ INSTRUCTIONS BEFORE COMPLETING FORM
1. REPORT NUMBER RADC-TR-76-95	2. GOVT ACCESSION NO.	3. RECIPIENT'S CATALOG NUMBER
4. TITLE (and Subtitle) COATING SCIENCE AND TECHNOLOGY		5. TYPE OF REPORT & PERIOD COVERED Final Report 2 January - 30 November 1975 6. PERFORMING ORG. REPORT NUMBER
7. AUTHOR(s) B.E. Knox K. Vedam		8. CONTRACT OR GRANT NUMBER(s) F19628-75-C-0110
9. PERFORMING ORGANIZATION NAME AND ADDRESS Materials Research Laboratory The Pennsylvania State University University Park, Pennsylvania 16802		10. PROGRAM ELEMENT, PROJECT, TASK AREA & WORK UNIT NUMBERS 61101E, 2415, T&WU n/a
11. CONTROLLING OFFICE NAME AND ADDRESS Defense Advanced Research Projects Agency 1400 Wilson Blvd. Arlington, VA 22209		12. REPORT DATE March 1976 13. NUMBER OF PAGES 88
14. MONITORING AGENCY NAME & ADDRESS(if different from Controlling Office) Deputy for Electronic Technology (RADC(ETSO)) Hanscom AFB, MA 01731 Contract Monitor: Joseph J. Comer/ETSO		15. SECURITY CLASS. (of this report) Unclassified 15a. DECLASSIFICATION/DOWNGRADING SCHEDULE

16. DISTRIBUTION STATEMENT (of this Report)

Approved for public release; distribution unlimited

17. DISTRIBUTION STATEMENT (of the abstract entered in Block 20, if different from Report)

18. SUPPLEMENTARY NOTES

This research was supported by the Defense Advanced Research Projects Agency. ARPA Order No. 2415

19. KEY WORDS (Continue on reverse side if necessary and identify by block number)

cadmium telluride, germanium oxidation, potassium chloride, tetrahedral carbon, diamond, zinc sulphide, sputter-deposited films, ion plating, plasma polymerization, electron microprobe, ellipsometry, ion scattering spectrometry, Auger electron spectrometry, electron microscopy, selected area diffraction, electron diffraction, x-ray diffraction.

20. ABSTRACT (Continue on reverse side if necessary and identify by block number)

The preparation of cadmium telluride films by sputter deposition was thoroughly investigated. The effect of substrate temperature on the phase content of the CdTe was studied. Higher rf power levels tend to favor the formation of cubic CdTe, and temperature is a definite factor in determining the preferred orientation of the crystallites. At low rf power levels, either amorphous or hexagonal CdTe is formed, depending on the argon pressure in the sputtering system and the substrate temperature. Substrate heating also reduced the impurity level of the films. Detailed x-ray examination of the sputtered films revealed the presence of preferential orien-

DD FORM 1 JAN 73 1473 EDITION OF 1 NOV 65 IS OBSOLETE
S/N 0102-014-6601

Unclassified

SECURITY CLASSIFICATION OF THIS PAGE (When Data Entered)

tation with the [100] direction perpendicular to the substrate for both cubic and hexagonal phases of CdTe.

Optical absorption studies were conducted with CdTe films deposited on KCl substrates. The optical absorption edge varies from 919 nm for cubic CdTe to 808 nm for the pure hexagonal phase. This is similar to ZnS polytypes, where the position of the optical absorption edge and the birefringence increase gradually as the degree of hexagonality increases from the cubic 3C phase to the hexagonal 2H phase. Ellipsometric measurements carried out on these films using λ5461Å as a function of angle of incidence do confirm the preferential orientation of the films and also the increase in the value of the refractive index with increasing hexagonality of the films. The birefringence of the 2H phase of CdTe is expected to be much larger than 24×10^{-3}. Ellipsometric measurements must be carried out in the 800-900 nm spectral region to arrive at an exact figure for the birefringence. Ellipsometry was also used to show the possible existence of voids in CdTe, similar to those known to exist in Si and Ge.

An automated ellipsometer was constructed utilizing a manual Rudolph ellipsometer, a locally-designed computer interface unit, and a PDP 11/20 data processor. On-line control, as well as data collection and reduction can be accomplished with this system. Measurement time for one data point has been reduced from about 1 hour to 1/50 sec., while maintaining the necessary high precision and accuracy.

Both ion scattering and Auger electron spectrometry were used to give compositional profile information about CdTe films on KCl. AES showed that the surface region of the films was tellurium-rich, while ISS showed the surface to be cadmium-rich. This discrepancy has not yet been explained. Bulk oxidation does not occur nor does oxygen diffusion into CdTe films pose any problem. Exposure to air for extended times does appear to degrade the films, however. An apparent artifact of the AES measurements is the diffusion of alkali away from the interface between the film and the substrate, leaving a chlorine-rich region at the interface. Some chlorine may even diffuse through the film to the surface.

The oxidation of germanium films sputter-deposited on KCl substrates was investigated. Films of various densities were prepared under controlled conditions and characterized by several different techniques. Bulk analysis was done with an electron microprobe, while compositional profiling was accomplished by ion scattering spectrometry. Low density Ge films do not undergo bulk oxidation in 20 hours. High density films should have a greater resistance to oxidation, but this was not observed within the range of our experimental error.

The ion scattering spectrometer was automated to assist in obtaining long-time compositional profiles, as well as to increase the accuracy of the counting techniques. The ISS unit was linked to a PDP 11/20 data processor through a multiplex unit and a computer interface unit designed and built in this laboratory.

An ion plating apparatus was constructed and used to prepare films of Ge and CdTe on glass and KCl substrates. While time did not permit complete characterization of these films, the adhesion and homogeneity appeared to be excellent.

Films prepared by plasma polymerization were characterized by electron microscopy using electron micrographs for texture comparison, selected area diffraction for phase identification, and high resolution diffraction to check the selected area diffraction results. Some of these films were amorphous and some were small crystallites in an amorphous second phase. The closest pattern fit was a cubic system with the lines indexing as "diamond". No (00ℓ) graphite lines were obtained. Three graphite (00ℓ) lines were obtained from one area of one film by glancing angle diffraction, pointing out the need for more extensive study. The presence of a "diamond-like" diffraction pattern does give support to a previously hypothesized tetrahedral carbon (diamond-like) building-block structure for these films.

COATING SCIENCE AND TECHNOLOGY

B. E. KNOX AND K. VEDAM
Materials Research Laboratory
The Pennsylvania State University
University Park, Penna. 16802

TECHNICAL SUMMARY

Technical Problem and Methodology

The objective of this research was to develop a thorough understanding of the science and technology of films applied as coatings on materials transparent to 10.6 and 3-5 μm radiation. The approach included the preparation of films by sputtering or ion-plating, chemical and physical vapor deposition, and plasma polymerization. The materials studied were inorganic, elemental and compound. An extension here was to be the exploration of the possibility of sputtering of ternary compounds effectively. New efforts to deposit tetrahedral carbon films were also included. Characterization techniques for the coatings included infrared spectrometry, laser-Raman spectrometry, ion scattering spectrometry, Auger electron spectrometry, scanning electron microscopy, x-ray diffraction, x-ray emission analysis, ellipsometry, and durability tests. Both single and multilayer films were to be evaluated on selected substrates. The results of these studies should provide guidelines for the selection of the best materials, processes and process controls for the production of good optical coatings for infrared components at wavelengths of 3-5 and 10.6 micrometers.

This research was to be the second phase of a larger effort started in April 1973. However, termination of the contract after only 40% of the effort had been expended necessarily meant that only a part of the objectives could be completed. The first phase of this program was reported in AFCRL-TR-75-0152 and the Proceedings of the Third and Fourth Conferences on High Power Infrared Laser Window Materials.

Technical Results

The preparation of cadmium telluride films by sputter deposition was thoroughly investigated. The effect of substrate temperature on the phase content of the CdTe was studied. Higher rf power levels tend to favor the

formation of cubic CdTe, and temperature is a definite factor in determining the preferred orientation of the crystallites. At low rf power levels, either amorphous or hexagonal CdTe is formed, depending on the argon pressure in the sputtering system and the substrate temperature. Substrate heating also reduced the impurity level of the films. Detailed x-ray examination of the sputtered films revealed the presence of preferential orientation with the [110] direction perpendicular to the substrate for both cubic and hexagonal phases of CdTe.

Optical absorption studies were conducted with CdTe films deposited on KCl substrates. The optical absorption edge varies from 919 nm for cubic CdTe to 808 nm for the pure hexagonal phase. This is similar to ZnS polytypes, where the position of the optical absorption edge and the birefringence increase gradually as the degree of hexagonality increases from the cubic 3C phase to the hexagonal 2H phase. Ellipsometric measurements carried out on these films using $\lambda 5461\text{Å}$ as a function of angle of incidence do confirm the preferential orientation of the films and also the increase in the value of the refractive index with increasing hexagonality of the films. The birefringence of the 2H phase of CdTe is expected to be much larger than 24×10^{-3}. Ellipsometric measurements must be carried out in the 800-900 nm spectral region to arrive at an exact figure for the birefringence. Ellipsometry was also used to show the possible existence of voids in CdTe, similar to those known to exist in Si and Ge.

An automated ellipsometer was constructed utilizing a manual Rudolph ellipsometer, a locally-designed computer interface unit, and a PDP 11/20 data processor. On-line control, as well as data collection and reduction can be accomplished with this system. Measurement time for one data point has been reduced from about 1 hour to 1/50 sec., while maintaining the necessary high precision and accuracy.

Both ion scattering and Auger electron spectrometry were used to give compositional profile information about CdTe films on KCl. AES showed that the surface region of the films was tellurium-rich, while ISS showed the surface to be cadmium-rich. This discrepency has not yet been explained. Bulk oxidation does not occur nor does oxygen diffusion into CdTe films pose any problem. Exposure to air for extended times does appear to degrade the films, however. An apparent artifact of the AES measurements is the diffusion of alkali away from the interface between the film and the substrate, leaving a chlorine-rich region at the interface. Some chlorine

may even diffuse through the film to the surface.

The oxidation of germanium films sputter-deposited on KCl substrates was investigated. Films of various densities were prepared under controlled conditions and characterized by several different techniques. Bulk analysis was done with an electron microprobe, while compositional profiling was accomplished by ion scattering spectrometry. Low density Ge films do not undergo bulk oxidation in 20 hours. High density films should have a greater resistance to oxidation, but this was not observed within the range of our experimental error.

The ion scattering spectrometer was automated to assist in obtaining long-time compositional profiles, as well as to increase the accuracy of the counting techniques. The ISS unit was linked to a PDP 11/20 data processor through a multiplex unit and a computer interface unit designed and built in this laboratory.

An ion plating apparatus was constructed and used to prepare films of Ge and CdTe on glass and KCl substrates. While time do not permit complete characterization of these films, the adhesion and homogeneity appeared to be excellent.

Films prepared by plasma polymerization were characterized by electron microscopy using electron micrographs for texture comparison, selected area diffraction for phase identification, and high resolution diffraction to check the selected area diffraction results. Some of these films were amorphous and some were small crystallites in an amorphous second phase. The closest pattern fit was a cubic system with the lines indexing as "diamond". No (00ℓ) graphite lines were obtained. Three graphite (00ℓ) lines were obtained from one area of one film by glancing angle diffraction, pointing out the need for more extensive study. The presence of a "diamond-like" diffraction pattern does give support to a previously hypothesized tetrahedral carbon (diamond-like) building-block structure for these films.

DoD Implications

The results of these studies will be used to provide guidelines for the selection of the best materials, processes and process controls for the production of good optical coatings for infrared components at wavelengths

of 10.6 and 3-5 micrometers. The plasma polymerization technique may lead to a new process for the deposition of "diamond-like" films for sealing and protecting optical components.

Further Research

No further work will be done under this contract, since it has expired. Some phases of the work may be continued under other auspices.

Specific Comments

No specific comments are offered at this time.

TABLE OF CONTENTS

LIST OF FIGURES

LIST OF TABLES

LIST OF APPENDICES

1. INTRODUCTION

The objective of this research program was to develop a thorough understanding of the science and technology of films applied as coatings on materials transparent to 10.6 and 3-5 μm radiation. The approach included the preparation of films by sputtering or ion-plating, chemical and physical vapor deposition, and plasma polymerization. The materials studied were inorganic, elemental and compound. An extension here was to be the exploration of the possibility of sputtering of ternary compounds effectively. New efforts to deposit tetrahedral carbon films were also included. Characterization techniques for the coatings included infrared spectrometry, laser-Raman spectrometry, ion scattering spectrometry, Auger electron spectrometry, scanning electron microscopy, x-ray diffraction, x-ray emission analysis, ellipsometry, and durability tests. Both single and multilayer films were to be evaluated on selected substrates. The results of these studies should provide guidelines for the selection of the best materials, processes and process controls for the production of good optical coatings for infrared components at wavelengths of 3-5 and 10.6 micrometers.

This research was to be the second phase of a larger effort started in April 1973. However, termination of the contract after only 40% of the effort had been expended necessarily meant that only a part of the objectives could be completed. The first phase of this program was reported in AFCRL-TR-75-0152 (1) and the Proceedings of the Third and Fourth Conferences on High Power Infrared Laser Window Materials (2,3).

2. SPUTTER-DEPOSITED CADMIUM TELLURIDE

2.1 Introduction

Several studies have been made on the effects of deposition conditions on the structure and phase content of CdTe evaporated films, but

none have been made on sputtered CdTe films. Sputtering generally produces films without fractionation of the more volatile components and with improved substrate-film adhesion. There are also several deposition parameters which can drastically influence the nature of the resulting film.

Cadmium telluride can be prepared either in a noncrystalline phase or in one of two crystalline phases, wurtzite or sphaelerite. The wurtzite phase has hexagonal symmetry, and the sphaelerite has cubic. These are analogous to the well-known polytypism of ZnS. As in ZnS, the phase content is a function of the sputtering gas pressure and the substrate temperature; the stable, room-temperature phase is cubic (4).

Of the studies made on evaporated CdTe, there was general agreement that higher substrate temperature promote stoichiometric, cubic films (5-9). Tolutis and Jasutic (8) found that cubic films were deposited on substrates held above 230°C, hexagonal films were found at substrate temperature between 140°C and 185°C, and mixed phases were formed at the other temperatures. There was also general agreement that Cd-rich films produced the hexagonal modification, while excess Te resulted in cubic films (5,6). Shalimova and Voronkov (9) determined the dependence between substrate temperature, deposition rate and phase content of CdTe evaporated films. They found that low substrate temperatures produced CdTe + Cd + Te at high deposition rates and CdTe + Te at low deposition rates. Single-phase CdTe was found only above 200°C at low deposition rates and above 350°C at high rates. These results are understandable in terms of the vapor pressure of the various constituents. CdTe has its boiling point at 1160°C, while Cd boils at 767°C and Te at 990°C.

2.2 Preparation

All films were sputtered from a 5" CdTe target in a turbomolecular-pumped Ultek 3140-6J rf sputtering system. The CdTe target was hot pressed and found to be cubic. The substrate-target distance was 52 mm. Initial system pressures were at least 3×10^{-6} torr before the titanium-purified Ar sputtering gas was admitted into the chamber. The substrates used were glass microscope slides ultrasonically cleaned with ethyl alcohol.

To determine the effect of substrate temperatures on the phase content of rf-sputtered CdTe, films were prepared at various rf powers and sputtering gas pressures. Substrate platens were held at room temperature by water cooling or heated to 230°C or 450°C.

The sputtering process heats the substrate through bombardment by energetic particles and secondary electrons produced at the target. The substrate temperature, T_s, is generally proportional to the rf power applied to the target. The sensor used to measure the temperature of the growing-film was a thin film of germanium deposited on a glass substrate (identical to the ones used to study CdTe structure). A 2μ thick layer of Ge was sputtered on these substrates, and molybdenum was deposited for electrical contacts. The surface of the sensor was coated with an insulating layer of SiO_2 to prevent shorting by any conductive deposits. After annealing for several hours at 400°C to eliminate any aging effects, the resistance of the sensor was measured between room temperature and 400°C. When placed on the substrate platens during deposition, the resistance of the sensors can be used to monitor T_s with an accuracy of about ±10°C. The germanium can also be used to measure the substrate self-bias that occurs during deposition. These sensors can be used only below 400°C, since the Ge film crystallizes at higher temperatures.

Figures 1 and 2 show T_s over the range of sputtering parameters used. The temperatures in Figure 1 were measured when the substrate platen was held near room temperature by water cooling. Those in Figure 2 were taken when the substrate platen was heated to 230°C by carbon elements. There is little difference in T_s for heated and unheated platens below 200 watts; the substrate surface is only weakly coupled to the platen temperature. Increasing the argon pressure can both increase heat conduction to the substrate from the platen and screen the substrate from some of the energetic particles that cause substrate heating. These two effects tend to cancel each other. The substrate self-bias shown in Figure 3 measures the difference between the number of electrons and positively charged argon ions incident on the substrate. The self-bias voltages for heated platens were similar to those indicated in Figure 3.

2.3 Film Structure

Each film was analyzed on a GE x-ray diffractometer using Cu Kα radiation between $2\Theta = 5°$ and 120°. Those films which showed only a broad (>2° width) peak in the neighborhood of $2\Theta = 24°$ were labeled amorphous. Most observed peaks could be identified as belonging to either the cubic or

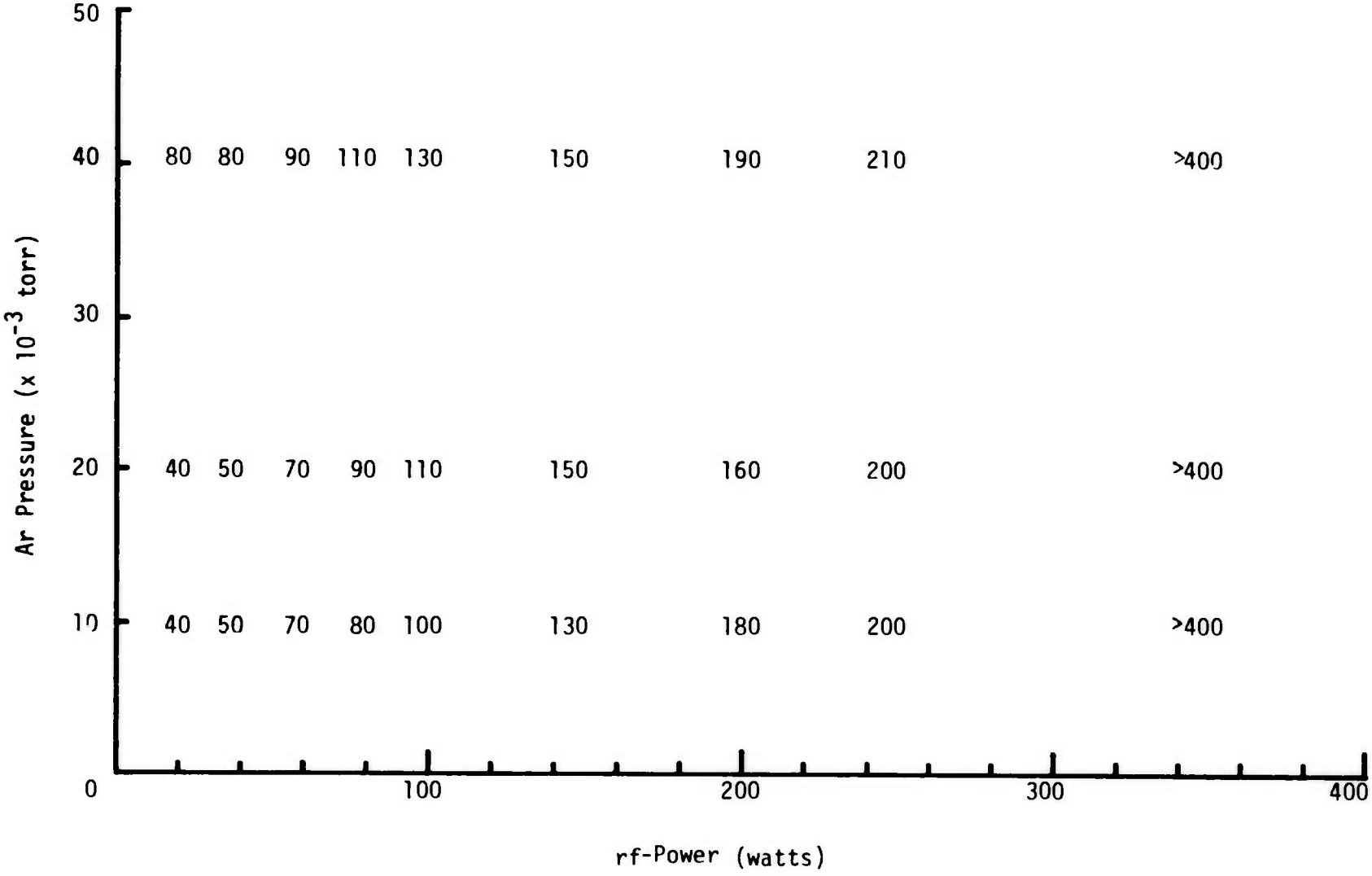

Figure 1. Temperature (°C) of Substrate with Platen Held at Room Temperature (Measured with Ge Thin Film Resistor).

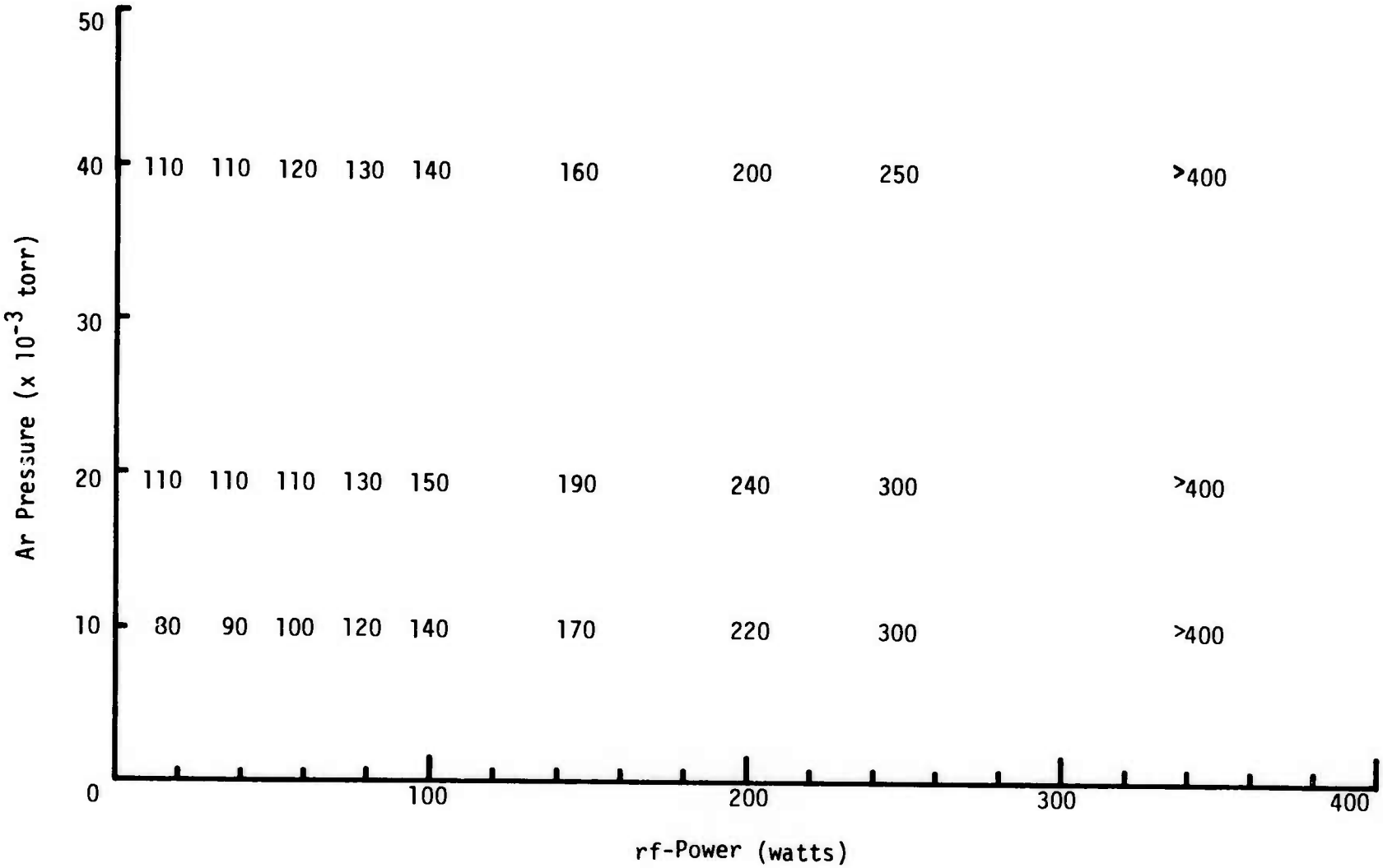

Figure 2. Temperature (°C) of Substrate with Platen Held at 230°C (Measured with Ge Thin Film Resistor).

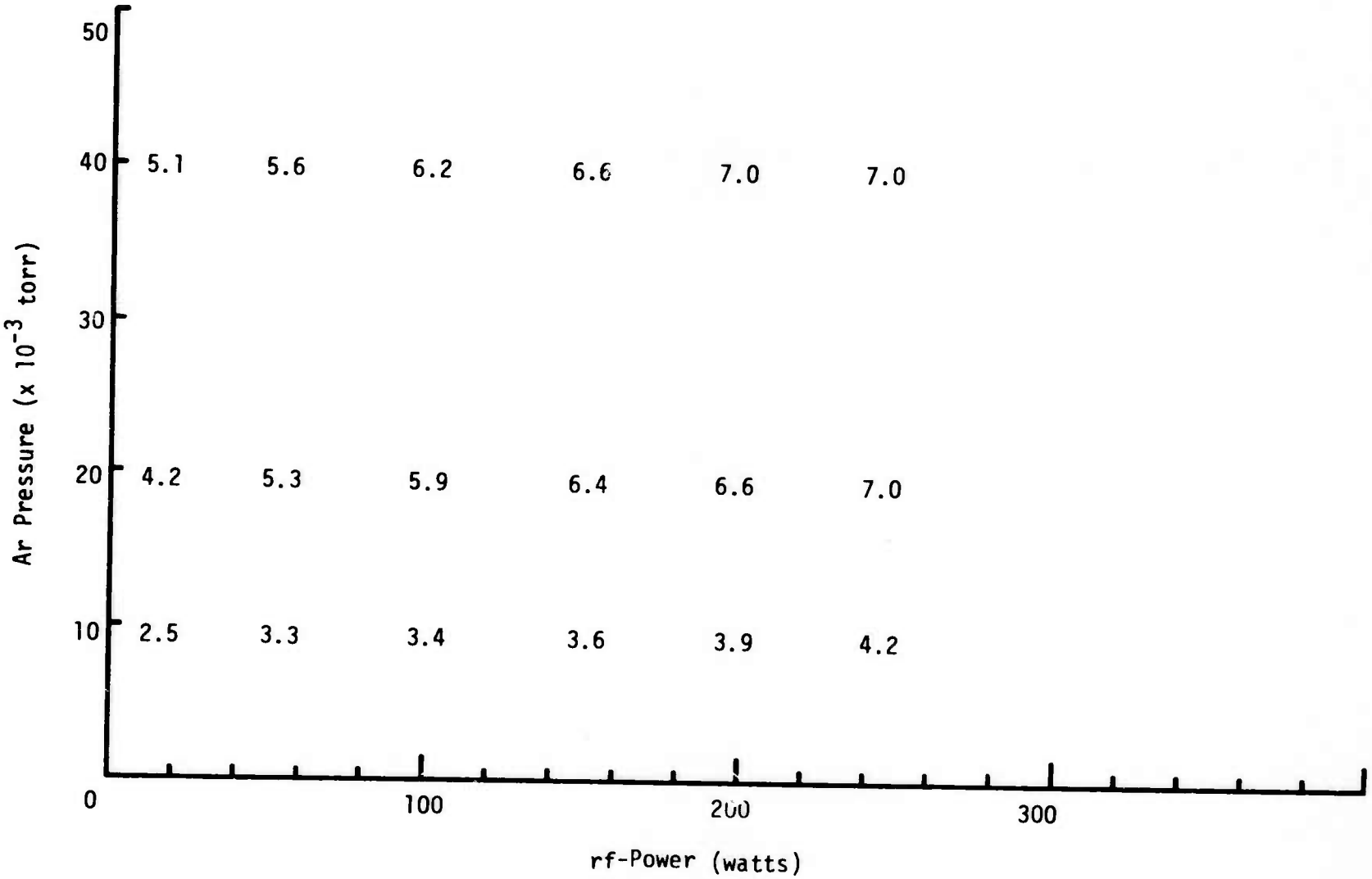

Figure 3. Substrate Self-Bias (Volts) Measured on Platen at Room Temperature.

hexagonal CdTe phases. Films prepared at the higher rf powers did show weak peaks at small angles (2θ = 8.2°, 12.5°, and 21.4°) which could not be identified as any known CdTe, Cd or Te crystalline phase. These have been reported in other studies and attributed to a superlattice (10), thermal scattering by acoustic phonons in the (110) planes, (11), and planar defects (12).

The sputtered films all showed high degree orientation in the form of a fibrous texture with the fiber axis perpendicular to the substrate surface. They were removed from the substrate, the orientation randomized, and then x-rayed again. Using the method of Short and Steward (13), the intensities of several diffraction lines were compared to determine the amount of cubic and hexagonal phases present. The films ranged from nearly completely hexagonal to cubic. For nearly every set of sputtering conditions, the amount of hexagonal phase decreased as the temperature of the substrate platen increased. For each film, the major phase and its orientation is shown in Figures 4, 5 and 6 for room temperature, 230°C, and 450°C platens, respectively. The orientations were determined from the major diffraction peak, which was generally 5 to 10 times the intensity of the next largest peak. The majority of the sputtering conditions which resulted in a cubic phase gave a (111) orientation, while the hexagonal phases showed several orientations.

2.4 Composition

The CdTe films were analyzed for Cd, Te, Ar and O content with an ARL microprobe and the results evaluated by Colby's Magic IV program (14). The average Te content of the films was 52 at% and was not dependent on substrate temperature. The average argon content was 1.7 at% for the room temperature depositions and 1.5 at% for those deposited at high temperatures. The argon content did exhibit the well-known decrease at higher Ar pressures. A heated substrate appeared to reduce the oxygen content by about 30%, but quantitative results for light elements are difficult to obtain in thin films because of low signal-to-noise ratios.

2.5 Conclusion

Since the purpose of this program was to investigate the possibilities of using rf-sputtered CdTe as a laser window coating for 10.6 μm radiation, the wide variety of structures produced by rf-sputtering should be examined in terms of optical loss. Those films which were single-phase

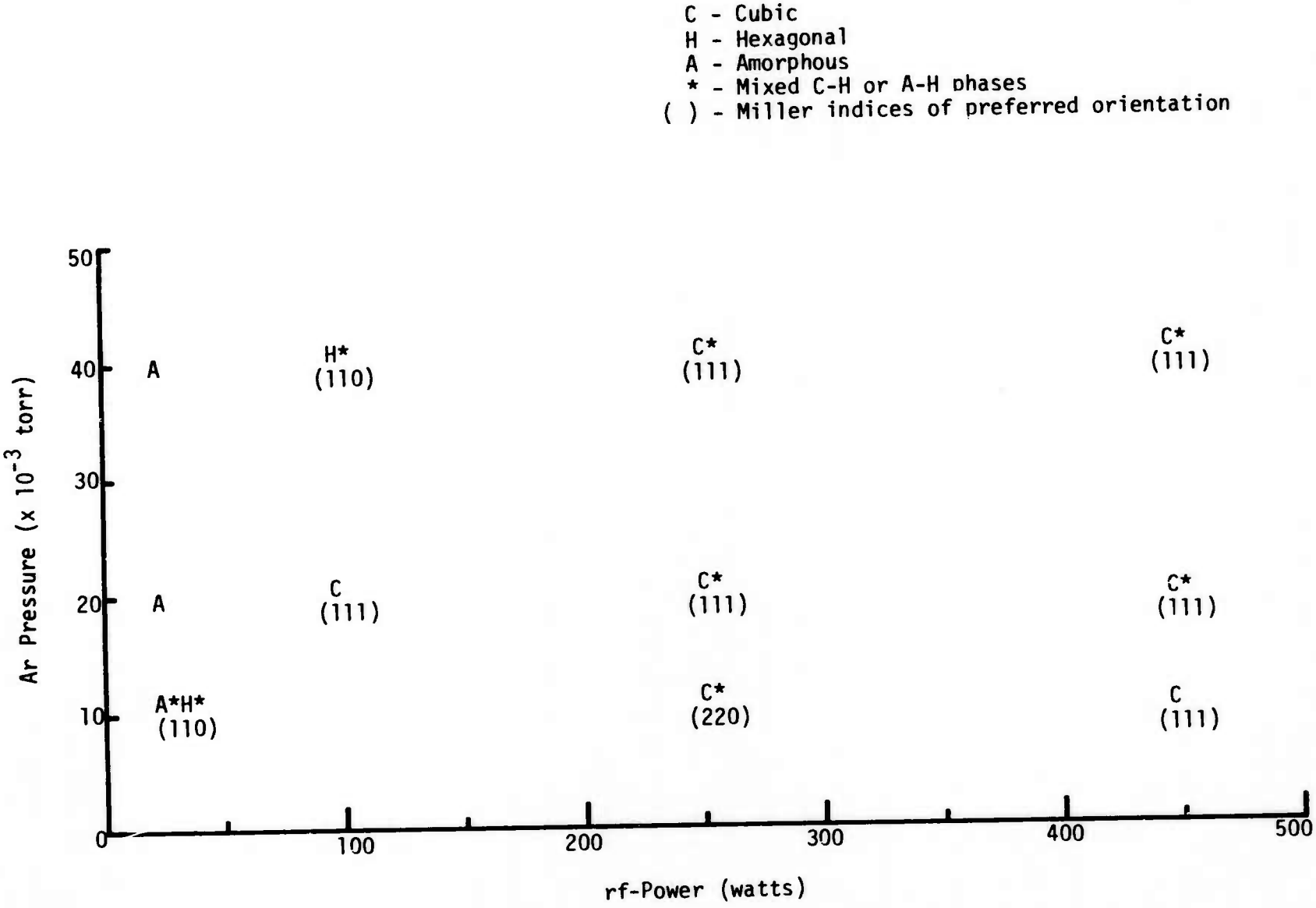

Figure 4. Structure of CdTe Deposited on Platen at Room Temperature.

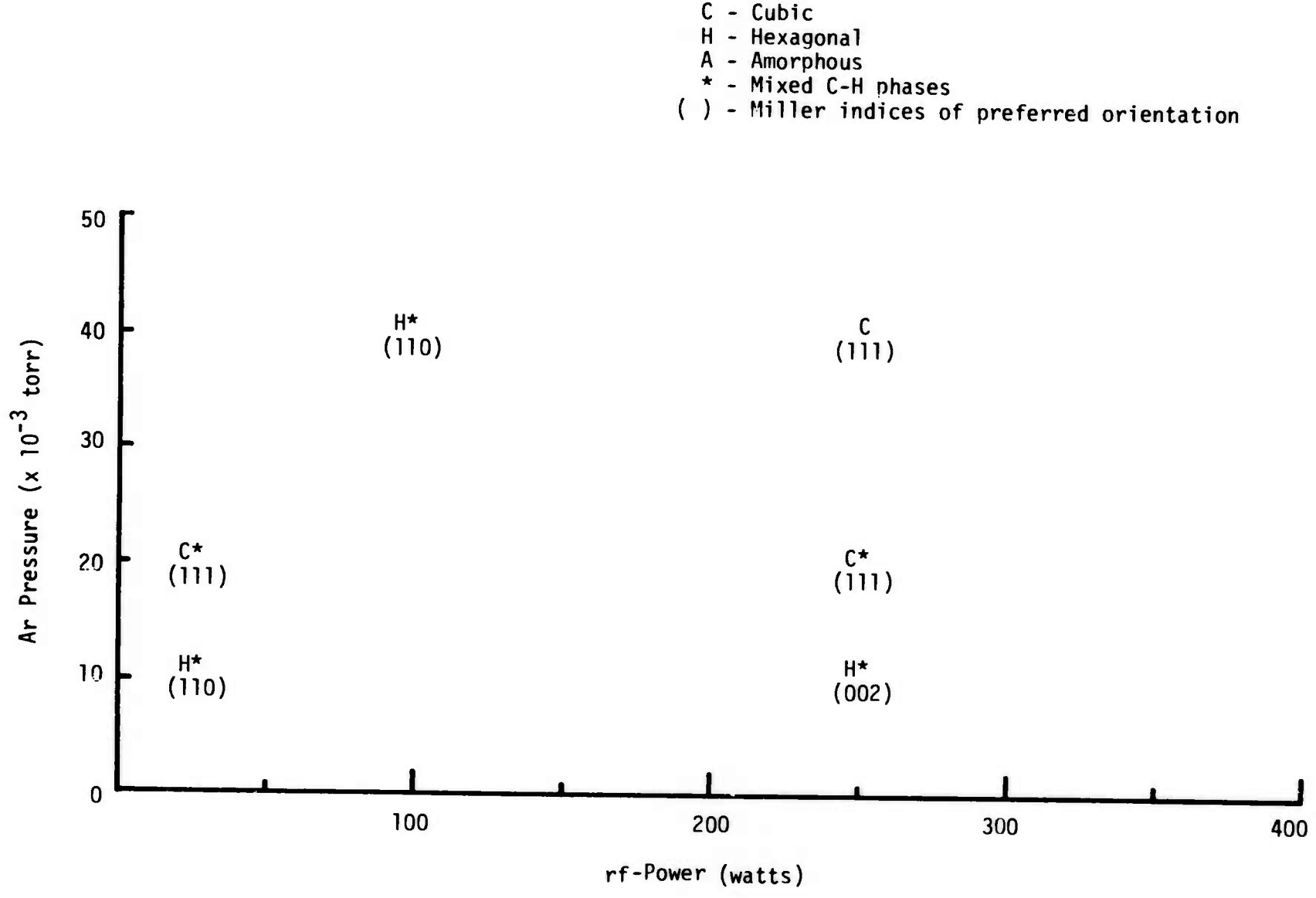

Figure 5. Structure of CdTe Deposited on Platen at 230°C.

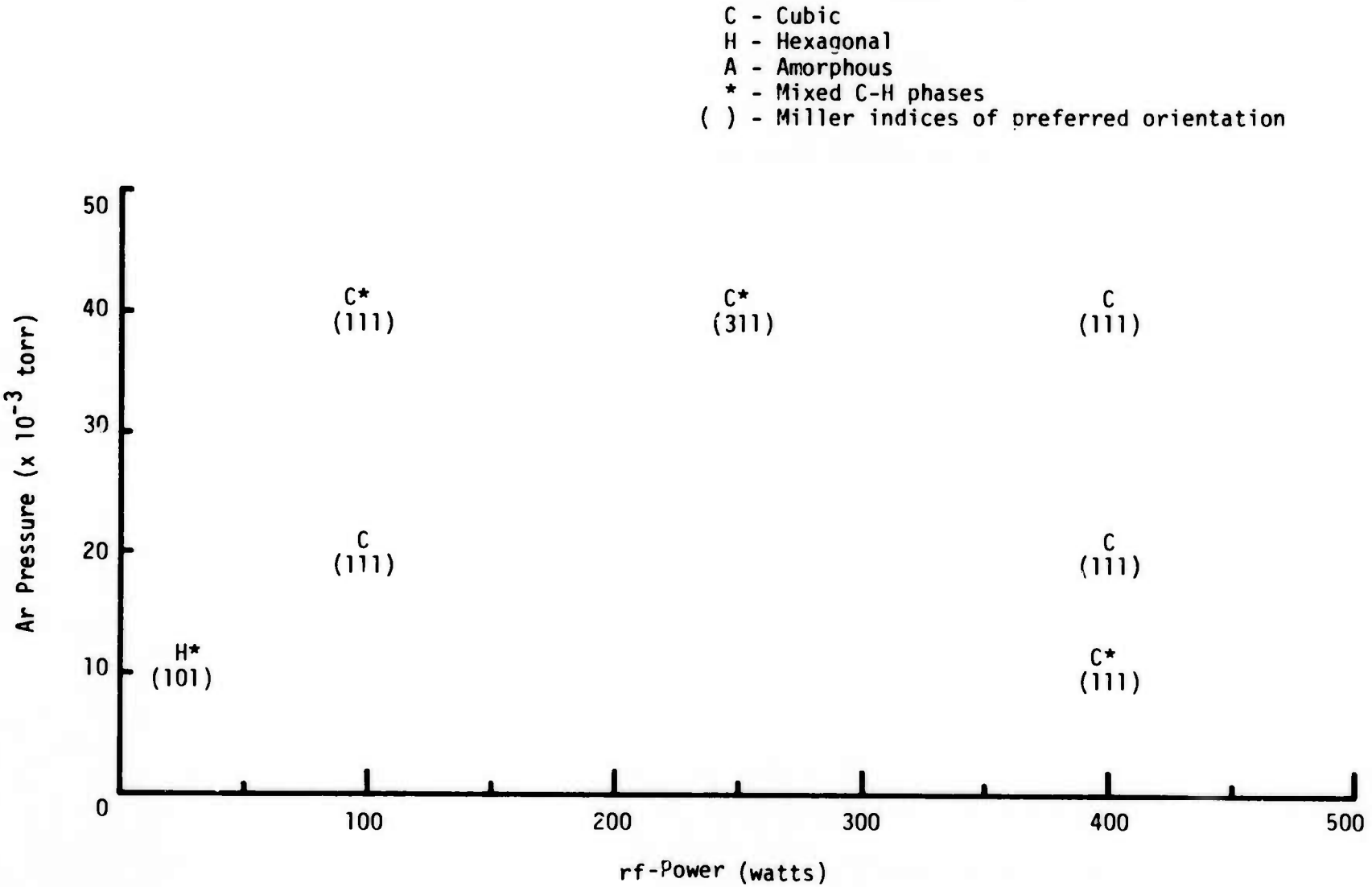

Figure 6. Structure of CdTe Deposited on Platen at 450°C.

and isotropic should be the best choice. This would be either an amorphous or a fully cubic layer. Substrate heating was shown to reduce the impurity content of the films. While it was not attempted, changing the Cd/Te ratio in the target or employing a D-target should result in films of any desired composition.

3. OPTICAL ABSORPTION STUDIES ON SPUTTERED CdTe FILMS

Data on the optical absorption edges of the CdTe sputtered films were obtained with a Cary 14 double beam recording spectrophotometer. All the measurements reported in this and the next section were made on sputtered films prepared with the platen kept at room temperature. The results are given in Figure 7.

We see that the absorption edge for the cubic phase is at 808.0 nm, while that for the hexagonal phase with RF 200 volts and argon pressure of 5 microns is 919.0 nm. The absorption edges for the other CdTe films sputtered under different conditions fall in between these two extreme values. This is reminiscent of the case of ZnS, another II-VI compound.

Brafman and Steinberger (15) have demonstrated in the case of ZnS polytypes that the optical band gap (position of the absorption edge) as well as the degree of birefringence varies in a linear manner with the percentage of hexagonality between the two limits corresponding to the 2H wurtzite and the 3C sphalerite polytype. Table I summarizes their results on various ZnS polytypes. It is seen from this table that the absorption edge for 3C type was observed to be 341 nm, while those for the hexagonal 2H type were 331.5 nm and 334.5 nm for $E \| C$ and $E \perp C$, respectively. The absorption edges for the various other polytypes fell in between these two limits. Similarly, the birefringence observed for the different polytypes varied between the limits 0 and 24×10^{-3}.

Likewise, in the case of CdTe, the observed shift in the position of the absorption edge and the results of the x-ray diffraction studies indicate the possible presence of polytypic phases in these films.

Through arrangement of the atoms, both cubic and hexagonal structures of ZnS (and possibly CdTe as well) can be considered as made up of pairs of layers, one plane in each pair being Zn and the other plane in the pair being S. The layer-pairs in both structures are stacked one above the

TABLE I

EFFECT OF POLYTYPISM ON THE OPTICAL PROPERTIES OF ZnS

Polytype	Percent Hexagonality α	Absorption Edge (nm) $\lambda_{o\|\|}$	Absorption Edge (nm) $\lambda_{o\|}$	$n_\varepsilon - n_\omega$ ($\times 10^3$)
3H	0	341.0		0
120H or 40H	10	340.0	340.4	2.4
10H	20	339.0	339.7	4.8
6H	33.3	337.5	338.8	8.2
4H	50	336.1	337.8	12.0
2H	100	331.5	334.5	23.8

other, and successive layer-pairs are displaced horizontally. A displacement is necessary to preserve the tetrahedral bond scheme; without a displacement sequence S-Zn-S would link in a straight line, contrary to the tetrahedral scheme which requires an angle of 109°28' between these bonds. Polytypism can arise when different ZnS (or CdTe) structures result from different stacking sequences of the layer-pairs. If the layer-pairs are numbered sequentially in cubic ZnS, they are displaced so that layer-pairs labeled 0, 3, 6 ... lie exactly above each other without sidewise displacement. Thus the stacking sequence in cubic ZnS is written as 012012012 or as ABCABCABC. The stacking scheme in hexagonal ZnS is such that layer-pairs 0, 2, 4 ... lie exactly above each other, and the stacking sequence is written as 010101 or as ABABAB. All nearest neighbor bonds are tetrahedral in both schemes. If we look only at the nearest neighbors to a given atom, we cannot tell whether we are in a cubic or hexagonal crystal, but if we look beyond the nearest-neighbors to the second-nearest-neighbor atoms we can distinguish the cubic and hexagonal structures. The nearest-neighbor bond lengths in ZnS are nearly equal in the two structures.

In addition to the above mentioned two main types, there are also those in which the stacking sequence is periodic in four or more layer-pairs; for example, the hexagonal 4H polytype whose stacking sequence is ABACABAC...., hexagonal 6H with the stacking sequence ABABACABABAC..., etc.

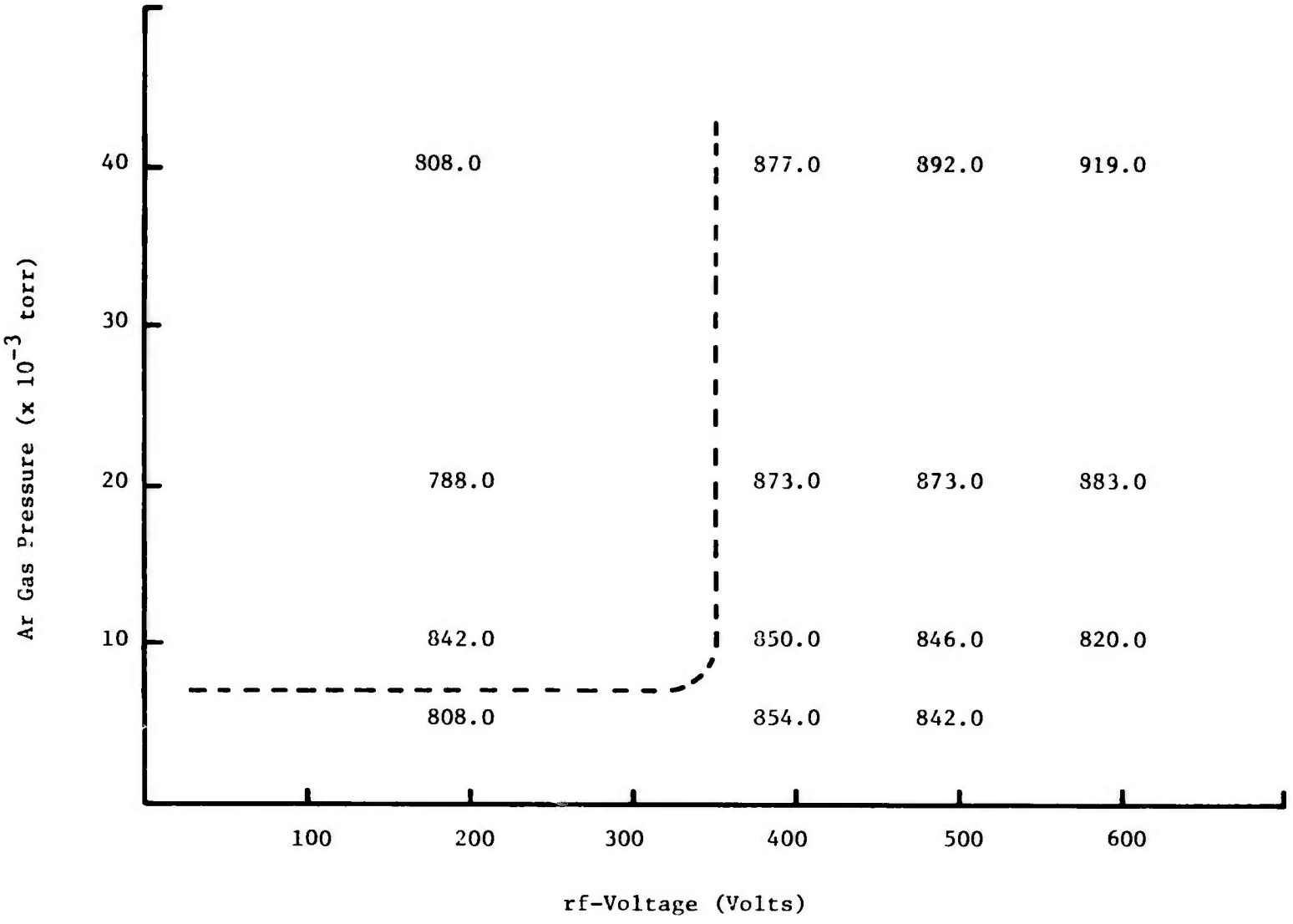

Figure 7. Optical Absorption Edges for Sputter-Deposited CdTe Films.

The percentage of hexagonality, α, in any noncubic polytype may be defined as the percentage of close-packed planes which are in a hexagonal, nearest-neighbor environment. For example, in the case of the 4H polytype, the B's and C's are in hexagonal environments, and thus $\alpha = 50$. Evidently, $\alpha = 100$ for wurtzite, and $\alpha = 0$ for zincblende (15).

4. ELLIPSOMETRIC MEASUREMENTS

Ellipsometric measurements were made on the CdTe films at an angle of incidence, $\phi_o = 70°$, and a wavelength, $\lambda = 5461\text{Å}$. The results of these measurements are shown in Figures 8 and 9.

At this point it will be useful to estimate the maximum experimental error in our ellipsometric measurements and consider its effect on the values of $\bar{n}_2$ and $\bar{k}_2$ evaluated from these measurements. Neglecting for the moment any possible systematic errors, it is estimated that the maximum errors in the ellipsometric parameters, Δ and ψ, are $\pm 0.05°$ and $\pm 0.02°$, respectively. For the case of CdTe such errors in Δ and ψ imply an uncertainty in the value of $\bar{n}_2$ of ± 0.004 and in $\bar{k}_2$ of $\pm .00003$.

Figure 8 shows a systematic variation in $\bar{n}_2$ with Ar gas pressure and r.f. voltage. The value of $\bar{n}_2$ increases as the percentage of hexagonality of the sputtered films increases across the Ar pressure-r.f. voltage field from the upper right to the lower left corner. This, again, is consistent with the work of Brafman and Steinberger (15) on ZnS polytypes.

The α-ZnS system shows a positive birefringence, Δn, where $n = n_\varepsilon - n_\omega$. The CdTe system shows a similar behavior. In order to confirm that the above-observed variation in $\bar{n}_2$ is due to the effect of positive birefringence of CdTe polytypes, another set of ellipsometric measurements was made on these same specimens at an angle of incidence $\phi_o = 58°$. The results of these measurements, together with those for $\phi_o = 70°$, are given in Figures 9 and 10. Notice that the observed differences in $\bar{n}_2$ and $\bar{k}_2$ for the two angles of incidence are well above the experimental error limits. Therefore, they can be considered as genuine and not an artifact of the experimental measurements.

CdTe in its cubic phase is optically isotropic; thus, the index of refraction is independent of the angle of incidence. However, in its

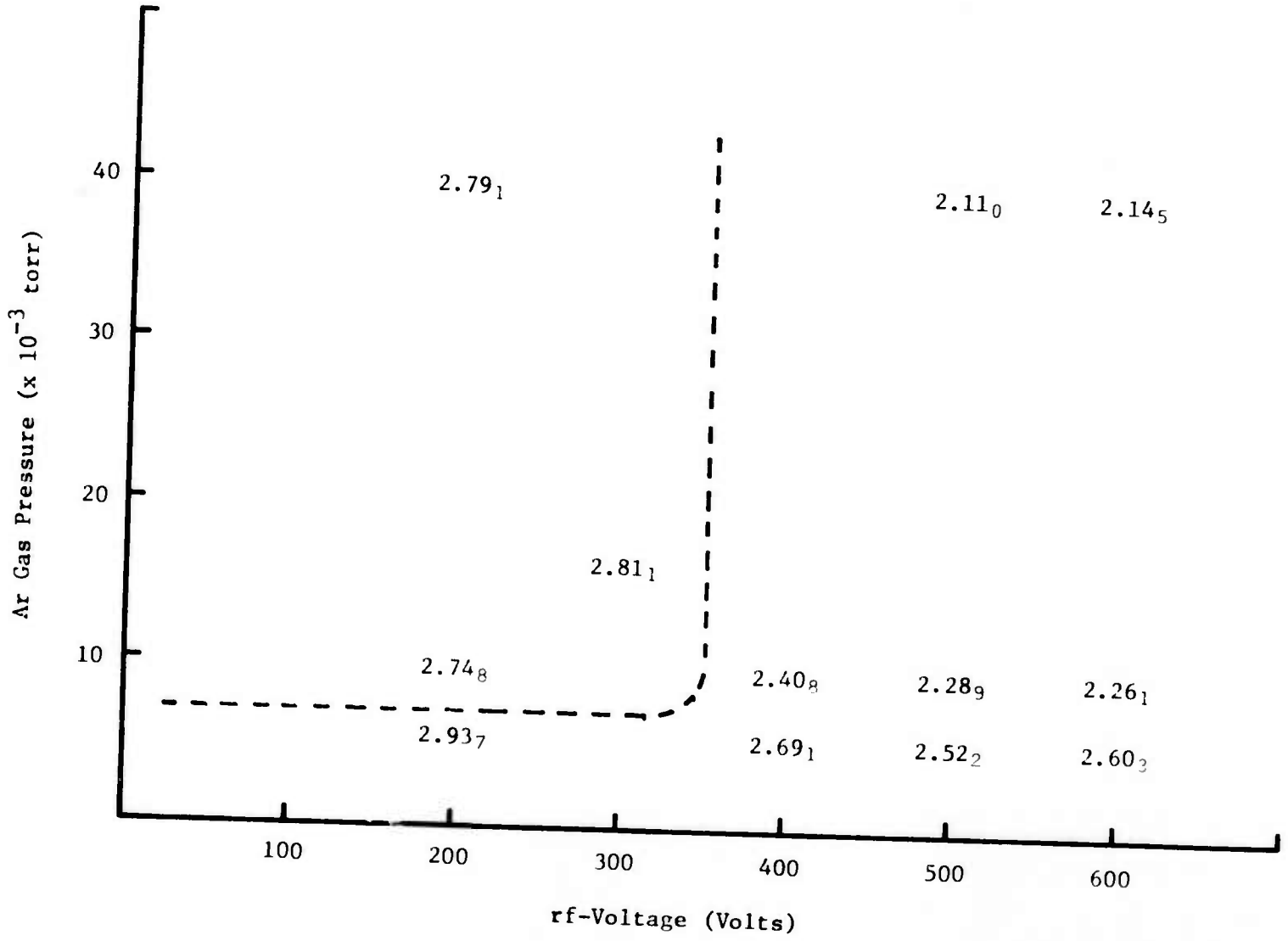

Figure 8. $\bar{n}_2$ for Sputter-Deposited CdTe Films for ϕ_o = 70° and λ = 5461Å.

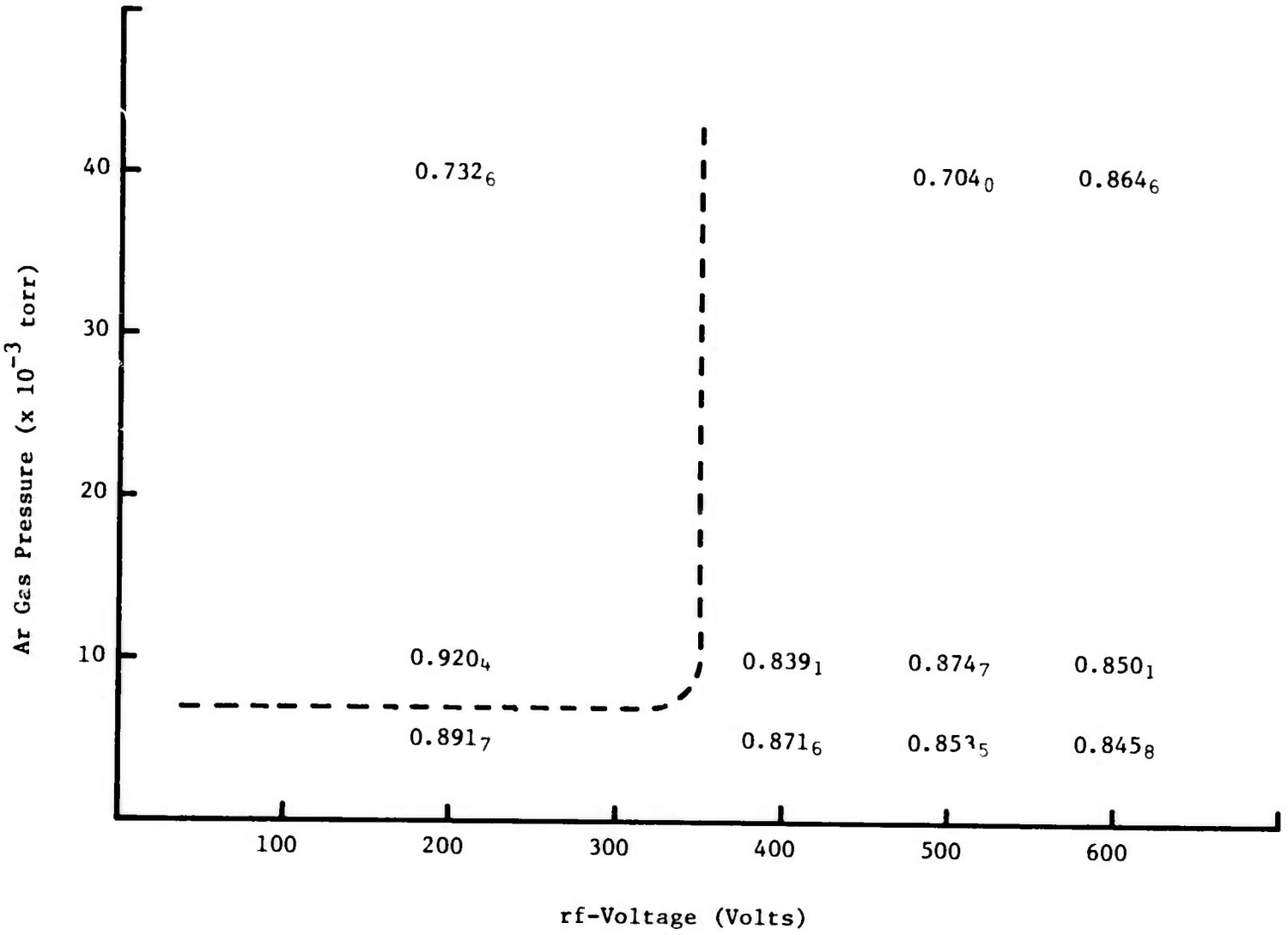

Figure 9. $\bar{k}_2$ for Sputter-Deposited CdTe Films for $\phi_o = 70°$ and $\lambda = 5461\text{Å}$.

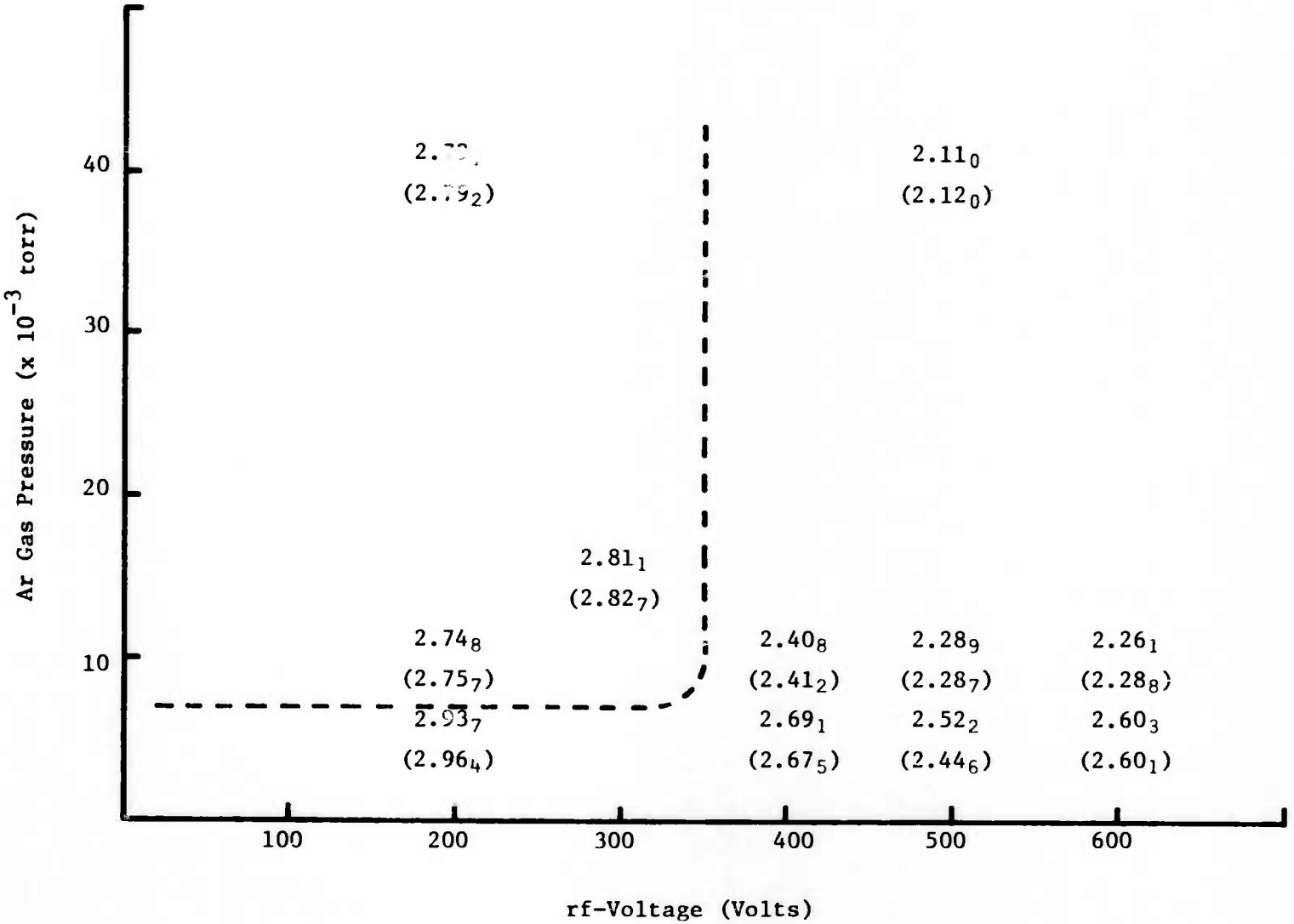

Figure 10. $\bar{n}_2$ for Sputter-Deposited CdTe Films for ϕ_o = 70° and 58° (Values in Parentheses) and λ = 5461Å.

hexagonal phase the material is birefringent, and hence the effective index of refraction, $\bar{n}_2$, is dependent on ϕ_o. Therefore, for the hexagonal phase we should see a difference in $\bar{n}_2$ for $\phi_o = 70°$ and $\phi_o = 58°$, and, indeed, such a difference does exist. Identical reasoning can be advanced for the behavior of the optical absorption coefficient or, equivalently, in the value of $\bar{k}_2$. Here again, we do notice such a trend as can be seen from Figure 10.

It should be mentioned here that the x-ray studies revealed the presence of hexagonal phases of CdTe in many of the films prepared by sputtering. The films studied are not epitaxial single crystal films, but polycrystalline films with some degree of preferred orientation. Hence, as a first approximation, the ellipsometric measurements were interpreted assuming that the film was isotropic and uniform. This means that we can report the optical properties of each film with the effective complex refractive index, $n_2 - ik_2$. The values so computed are given in Figures 8-11. The effect of preferential orientation on these measurements will now be considered.

Recall that the preferred orientation of the CdTe crystallites in the sputtered films is such that the (110) plane of the crystallites is parallel to the substrate, i.e., the c-crystallographic axis lies parallel to the substrate. This axis is also the optic axis of the indicatrix of the hexagonal CdTe.

Now consider the case of light incident on a uniaxial crystal with its optic axis in the plane of the reflecting surface. Depending on the orientation of the crystal, the optic axis may lie in the plane of incidence, perpendicular to it, or at any position between these two extremes. When the optic axis lies in the plane of incidence, n_s, the index of refraction for E_s, the electric vector of the incident light perpendicular to the plane of incidence, is indentical to n . However, n_p, the index for E_p, the electric vector in the plane of incidence, lies between n_ω and n_ε. On the other hand for the optic axis perpendicular to the plane of incidence, $n_p = n_\omega$ and $n_s = n_\varepsilon$. For random orientations of the optic axis between these two positions, the values of n_s and n_p both lie between n_ω and n_ε. Hence, $\bar{n}_2$, the effective value of the index of refraction, must lie between n_ω and n_ε. Since $n_\omega < n_\varepsilon$ for crystals having a positive birefringence, we would expect, therefore, the value of $\bar{n}_2$ to be larger than n_ω.

Next let us consider the effect of changing ϕ_o, the angle of incidence of a light beam striking the surface of a uniaxial crystal. Assume that the optic axis is in the plane of the crystal's surface. We again start by considering the E_s and E_p components of the incident electric vector. Changing ϕ_o will not affect E_s, but it will influence the characteristics of E_p in the crystal. Therefore we will only consider the E_p component in this discussion

Once more we consider the two extreme cases: the optic axis parallel to the plane of incidence and the optic axis perpendicular to the plane of incidence. In the first case, n_p may be resolved into components along the axes of the indicatrix. For $\phi_o = 0°$, $n_p = n_\varepsilon$, and for $\phi_o = 90°$, $n_p = n_\omega$. Since $n_\varepsilon > n_\omega$, we conclude that as ϕ_o is increased from 0° to 90°, n_p decreases. Also, since n_s is uneffected by changing ϕ_o, the total effect of increasing ϕ_o is to decrease $\bar{n}_2$. In the second case $n_p = n_\omega$ regardless of ϕ_o; thus changing ϕ_o for this case will not reveal any birefringence and, hence $\bar{n}_2$ is independent of ϕ_o. Therefore, for any case between these two extremes, increasing ϕ_o will decrease $\bar{n}_2$.

The sputtered films we are considering are composed of such crystallites. Their optic axes are randomly oriented in the plane of the film. Thus, we can expect the effective value of the index of refraction to lie between n_ε and n_ω. We also expect that ($\bar{n}_2$ measured at $\phi_o = 70°$) will be less than $\bar{n}_2$ measured at $\phi_o = 58°$, as indeed is generally found to be the case.

Before closing it would be worthwhile to compare the value of $\bar{n}_2$ of the cubic CdTe films prepared by sputtering techniques with the value of n reported in the literature on hot pressed CdTe. Obviously, the latter value corresponds to the cubic phase of the material and hence, this value must correspond to the value for the cubic phase of the sputtered CdTe (namely, the material prepared with r.f. voltage at 600 volts and Ar pressure at 4[illegible] x 10^{-3} torr). It is seen that the refractive index of the sputtered film, $\bar{n}_2 = (2.145)$ is much lower than the refractive of the bulk material (2.66) (16). This large a difference in the value of n cannot be attributed solely to the lower value of density of the sputtered film (5.62 gm/cm^3) as compared to the bulk density (6.20 gm/cm^3) (17), since the application of the Lorentz-Lorenz equation

$$\frac{n^2 - 1}{n^2 + 2} = \frac{4\pi}{3} N\alpha$$

reveals that the reduced density accounts for only about 5% of the reduction in refractive index. At this point it may be useful to look at the values of $\bar{n}_2$ for sputtered Ge films and see how these values compare with the index of refraction of films which were recrystallized by high temperature annealing and also with that for bulk Ge. These values are listed in Table II. Note that the values of the refractive index for the sputtered films are always less than those of both the recrystallized and bulk samples. This difference is most likely due to the presence of voids in the sputter-deposited samples which increase the surface-to-volume ratio. In these surface regions, the bulk crystalline electronic bonds are distorted and shifted by local strains. The strains may be a few atoms away from the surface, but in the surface layers shifts as large as 0.1Å in interatomic spacing have been deduced from LEED observations (21). This is a huge strain (of order of 5%) and is not ordinarily obtainable in the usual kind of hydrostatic pressure or uniaxial stress experiments. In addition to strains, the surface regions of the voids can have large electric fields due to band bending induced by charged dangling bonds and other surface states (22). This undoubtedly affects the optical constants of the material with the probable results of lowering the index of refraction at λ = 546.1 nm.

Agarwal (23) has found that the glassy semiconductors which include the chalcogenide alloys show very little or no electron spin resonance signal. This, however, does not preclude the presence of dangling bonds in the CdTe samples. Very recently Street and Mott (24) have extended the model proposed by Anderson (25) to show that dangling bonds do exist in the chalcogenides although there may be no free electron spins to give rise to an ESR signal. According to this model, there are more bonding states than pairs of electrons, and all such states are either doubly occupied or empty. That is, at the dangling bond sites there are either two electrons whose spins cancel or no electrons.

We can, therefore, surmise the presence of dangling bonds in the sputtered CdTe films. These dangling bonds, then, most likely account for the unusually low value of $\bar{n}_2$ for the cubic sputter-deposited film.

Similarly, both the ordinary and extraordinary refractive indices of the 2H hexagonal phase of CdTe are expected to be larger than 2.937 given

TABLE II

OPTICAL CONSTANTS OF GERMANIUM AT λ = 5436.1 nm.

n_2	k_2	Substrate Temperature During Deposition	Reference
3.7	2.1	20°	G. Jungk (18)
3.8	2.25	100°	G. Jungk (18)
4.1	2.3	200°	G. Jungk (18)
4.9	2.0	300°	G. Jungk (18)
3.7	2.4	400°	G. Jungk (18)
4.5	2.5	25°	Connel, et al. (44) (19)
4.7	2.3	350°	Connel, et al. (44) (19)
5.0	2.4	(single crystal)	G. Jungk (18)
5.46	1.75	(single crystal)	Knausenberger, Vedam (20)

in Figure 8. Further, by analogy of the values of $\Delta n = (n_\varepsilon - n_\omega)$ and the absorption edges for α-ZnS given in Table I, the birefringence of the 2H phase of CdTe is also expected to be much larger than 24×10^{-3}.

Thus, we have shown that the term, "sputtered film," is ambiguous. Unless the sputtering parameters are given, the structure of such a film is unknown, as are many of its properties. Only by giving the r.f. voltage and Ar gas pressure of a sputter-deposited CdTe film can we identify it as cubic, hexagonal, or amorphous. We have also shown that ellipsometry can indicate the presence of polytypic phases in these films and also indicate the possible presence of voids in CdTe similar to those known to exist in Ge and Si. Further work, including ESR measurements, is needed to confirm the presence of these voids and thus give a better understanding of the CdTe system.

5. AUTOMATED ELLIPSOMETER

As discussed earlier in Section 4 of this report, ellipsometry was one of the methods employed to nondestructively characterize KCl substrates as

well as the CdTe films that were deposited on KCl. With the support of this project it has been possible to obtain a Rudolph manual ellipsometer and to automate it by linking it with an existing, on-line PDP 11/20 data processor. As is well known it usually takes about one hour to carry out one measurement on any sample using a manual ellipsometer. On the other hand with the automated system, it is now possible to perform this experiment in about 1/50 second, after the ellipsometer has been calibrated.

The principle involved as well as the various specifications of this automated ellipsometer are essentially the same as has been described in detail by Aspnes (26-28). Since these details are available in the open literature, they are not being repeated here. The only information which is not available in the literature is the software necessary to operate the ellipsometer with the on-line data processor as well as to collect and process the data, which is included in this report as Appendix A. Since the program is written in BASIC language, the program is essentially self-explanatory.

6. OXIDATION OF GERMANIUM FILMS

6.1 Background

According to Green (29), the first oxide monolayer on crystalline germanium films forms in six seconds. Subsequent oxidation is much slower, following a logarithmic rate law. Thus, crystalline germanium has a thin oxide layer on any surface exposed to air.

Helms, et al. (30) reported bulk oxidation effects upon exposure of amorphous germanium to air which were not observed for crystalline germanium. The amorphous germanium was prepared to be void-free by electron-gun deposition onto a flat glass substrate. Helms suggested that the bulk oxidation was due to the "openness" of the amorphous lattice with respect to the crystalline lattice, providing an easy diffusion path for gases into the bulk. This observation of strong bulk oxidation effects on void-free, high density amorphous germanium was done with ultraviolet reflectance spectroscopy. The samples were oxidized by filling the sample chamber with air for a specified amount of time.

Henrich and Fan (31,32) did oxidation studies of sputtered and electron-beam evaporated amorphous germanium films using Auger electron spectrometry (AES). The samples, deposited on glass, were exposed to dry air and room air for periods of one half hour to two weeks. In the analysis, successive sample layers were sputtered off, and the surface then analyzed using AES. For the amorphous, electron-gun deposited films, oxygen was detected up to 250Å , but heavily oxidized regions were limited to a region 10-12Å into the film from the surface. Henrich also stated that sputtered amorphous films oxidize no more than single crystal germanium does. His results showed sputtered amorphous germanium films have oxygen present only 5-10Å into the film. It is also important to note that in these studies, the observed oxygen level for sputtered films after four days in dry air was no greater than the observed oxygen level after one half hour exposure time to room air. This was the time needed to transfer the samples from the sputtering unit to pumpdown in the AES unit.

Samples exposed to room air for four days showed an increase in oxygen signal, but all the oxygen was still confined to the 5-10Å depth. This agrees with ellipsometric data from work by Connell, et al. (33), who estimated the oxide layer formed on the sputtered amorphous Ge films to be about 10Å.

Henrich concluded that the presence of oxygen in amorphous electron-gun deposited films was due to the presence of pores, but disagreed with the extent of oxidation claimed by Helms. Henrich also believed that the argon detected throughout the sputtered film was trapped during growth, and that the argon gas prohibited oxidation of the films by preventing oxygen gas from diffusing into the film.

Previous studies of Ge films on KCl substrates performed in this laboratory using infrared spectrophotometry and ion scattering spectrometry showed bulk oxidation of the amorphous germanium films (1). However, these films were made at sputtering conditions such that the density was about 4.8 gm/cm^3, i.e., very porous with many voids.

6.2 Preparation of the Films

For this study amorphous films with thicknesses in the range of 500 - 700Å and densities varying between 5.2 - 5.8 gms/cm^3 were prepared. The r.f. power was varied to achieve these different densities, maintaining

the argon sputtering gas pressure at a constant value. The substrate temperature during sputtering was not measured, but previous studies of Ge on glass done by Messier (34) showed that for r.f. powers of 100 - 200 watts, the substrate temperature varied between 320 - 400°C. The substrate temperatures for this study are believed not to have exceeded those values but rather to have been much lower. The water "welding" technique used to bond the substrates to the platen makes much better thermal contact, as shown by the marked decrease in sputter damage to the "welded" substrates.

Several films were made at each power level in order to determine the extent of oxidation, not only according to film density, but also according to the length of exposure time to air. Table III shows the sputtering parameters for some of the films. All films were made from a five inch germanium target using Ti-purified argon. The films were allowed to cool while still in vacuum in the sputtering unit. All films except those immediately placed in the ISS vacuum system were stored in vacuum dessicators until used.

TABLE III

SPUTTERING PARAMETERS FOR Ge FILMS DEPOSITED ON KCl SUBSTRATES*

Film Number	r.f. Power (watts)	r.f. Voltage (watts)	Sputter Time (sec)	Film Thickness (Å)	Deposition Rate (Å/sec)	Film Density (34) (gm/cm^3)
LRG-86+	100	650	300	665	2.2	5.2
LRG-159	100	700	73	530	7.3	5.2
LRG-146	150	900	58	605	10.4	5.5
LRG-148	200	1100	52	588	11.3	5.8

*Base Pressure - 10^{-6} torr, Ar pressure - 30 mtorr, target separation - 2.5 cm.

+Different sputtering unit: Base pressure - 3×10^{-7} torr, Ar pressure - 30 mtorr, target separation - 5 cm.

Film thicknesses were determined with a Varian A-Scope Interferometer using sodium light at $\lambda = 5893\text{Å}$. Densities were derived from work by Messier (34). All films were deposited on the (100) plane of KCl as determined by a Picker-Siemens X-Ray Diffractometer with Cu Kα radiation ($\lambda = 1.54178\text{Å}$).

Exposure times of 15 minutes in room air (the time needed to transfer the samples from vacuum into the ISS unit), 2 hours in dry air plus 15 minutes transfer time and 20 hours dry air plus 15 minutes transfer time were made for all wattage films. Either argon or nitrogen was blown on the samples during the 15 minute exposure required for transfer of the samples. A sample prepared at 100 watts was exposed to dry air for 3 months and room air for two hours in order to determine if bulk oxidation did eventually occur and if the ISS unit would have enough sensitivity to detect oxygen through the film.

In addition films approximately 1 μm thick were prepared using identical sputtering conditions except for sputtering time. These films were analyzed by electron microprobe and were kept in vacuum until they were transferred to the analyzer. Nitrogen gas was blown on the films to inhibit oxidation during the 15 minute transfer.

6.3 Electron Microprobe Analysis

Bulk analyses of the 1 μm thick Ge films was done in an ARL Electron Microprobe X-Ray Analyzer. The beam voltage was 10 Kev, and the sample current was maintained at 1.5×10^{-8} amps during all analyses. Three standards were used:

1) A GeO_2 single crystal,
2) Ge, 99.99% pure, and
3) 2.95 at% Ar, 97 at% Ge.

The results are shown in Table IV.

The 100 watt sputtered film, which had the lowest density ($\simeq 5.2$ gms/cm^3) of all the films made, had the lowest argon and germanium content. It also had the highest oxygen content of the three different density films, approximately 17 at%, compared to about 3 at% for the other films.

The electron microprobe analyses showed that without extended exposure to air, low density Ge sputtered films oxidize more readily than the more dense germanium films. The analyses also seem to indicate that films with

TABLE IV

ELECTRON MICROPROBE ANALYSES OF Ge FILMS

Film by r.f. Power (watts)	Argon Content (At%)	Germanium Content (At%)	Oxygen Content (At%)
100	.35 ± .1	81.9 ± 2.8	17.7 ± 2.8
150	1.32 ± .1	95.5 ± 1.1	3.1 ± 1.2
200	1.50 ± .3	95.2 ± 2.0	3.3 ± 2.0

densities between 5.5 - 5.8 gms/cm^3 have the same initial tendency toward oxidation.

6.4 Analysis of Ge Films by Ion Scattering Spectrometry

Scattered ion spectra were obtained using a hybrid ion scattering spectrometer (3M) - Auger electron spectrometer (Physical Electronics Industries) shown schematically in Figure 11.

For these analyses the base pressure of the system was in the mid 10^{-8} torr range after bake-out. Sorption and titanium sublimation pumping were used for roughing; the main pumping was accomplished with an ion pump; and cryopumping was used to maintain a low background pressure during analysis. Because profiles of the oxygen in the films was desired, He^4 was used as the probe gas, with a backfill pressure of 7.0×10^{-5} torr. The energy of the primary ions was 1500 ev. Charge neutralization was used to prevent a buildup of positive charge on the surface during analysis and to reduce field-enhanced diffusion of chlorine ions from the potassium chloride substrate into the film.

The beam current varied slightly depending on the sample being analyzed. The usual value for beam current using He^4 was 180 na, which resulted in a current density of 63.5 μa/cm^2.*

*The current density was calculated from:

$$J_0 = \frac{0.88\ I}{FWHM}$$

where I is the beam current in amperes.

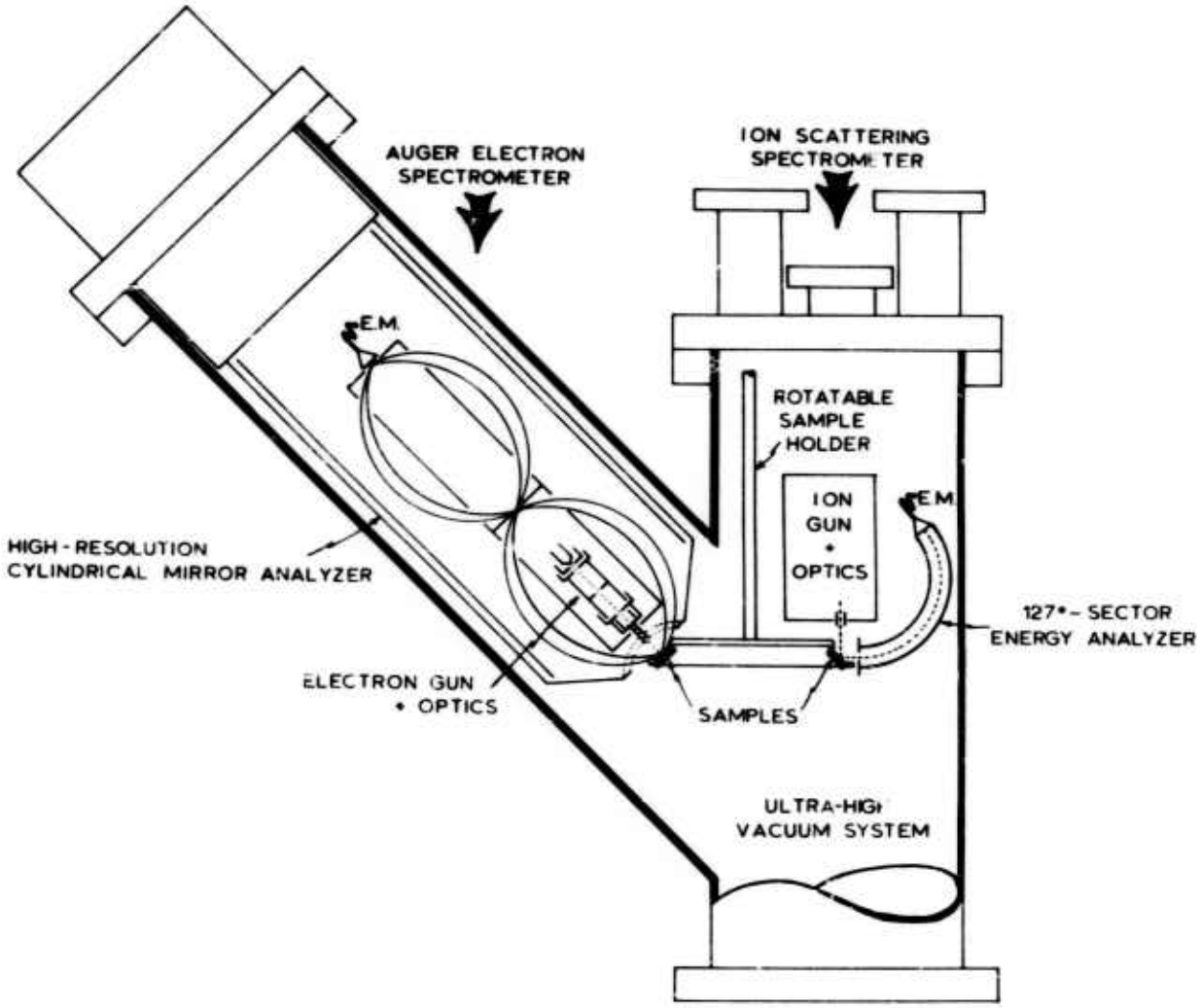

Figure 11. ION SCATTERING-AUGER ELECTRON SPECTROMETER

In order to minimize edge effects, the depth profile was made using beam rastering and signal gating. The FWHM of the ion beam used was nominally 0.5 mm. The raster controls were set such that the beam was deflected 1.5 FWHM, resulting in a raster length of 0.146 cm and a rastered area of 0.02 cm^2. The signal was electronically gated such that the signal from the central 35% of the rastered area was measured.

To an order of magnitude, the ISS sensitivity for the elements is about 10^{-3} monolayer. Because of the interest in the oxygen content of the films, the ISS sensitivity for oxygen was determined using He^4. The sensitivity for the oxygen signal was calculated to be of the order of 10^{-2} monolayer.

For the germanium film samples, the sputtered-ion, oxygen, potassium-chlorine, and germanium peaks were monitored. (Potassium and chlorine are difficult to resolve using He^4.) The sputtered ion peaks yield information on film thickness and interface depth. However, it is difficult to resolve the separate sputtered ion peaks in the low energy ratio region, and the sputtered ion peaks merge with the result that only one sputtered ion peak height can be monitored. Initially, sputtered germanium ions dominate; as the potassium chloride interface is approached, the sputtered peak becomes a mixture of potassium and germanium ions, with the potassium contribution quickly exceeding that from the germanium because of its lower ionization potential. The various peak heights versus time are then plotted to obtain a compositional profile of the film. Also, the O/Ge ratio is plotted, where applicable, to determine the oxygen distribution within the films. The use of ratios avoids errors due to small changes in the gain of the measuring system over the long time periods of some of the measurements.

Film 1 (LRG-86) was exposed to dry air for three months and room air for two hours. Bulk oxidation of the film occurred within this time as shown in Figure 12. A drastic increase in the sputtered ion peak accompanied by a decrease in the germanium peak indicated when the interface was reached. The interface was reached after 11.0 hours of sputtering by the primary ion beam of the ion scattering spectrometer, corresponding to a sputtering rate of 1 Å/min. As expected, the germanium signal did not reach a maximum until the first few monolayers of the film were sputtered away. These first monolayers contained adsorbed oxygen and other contaminants and were oxidized

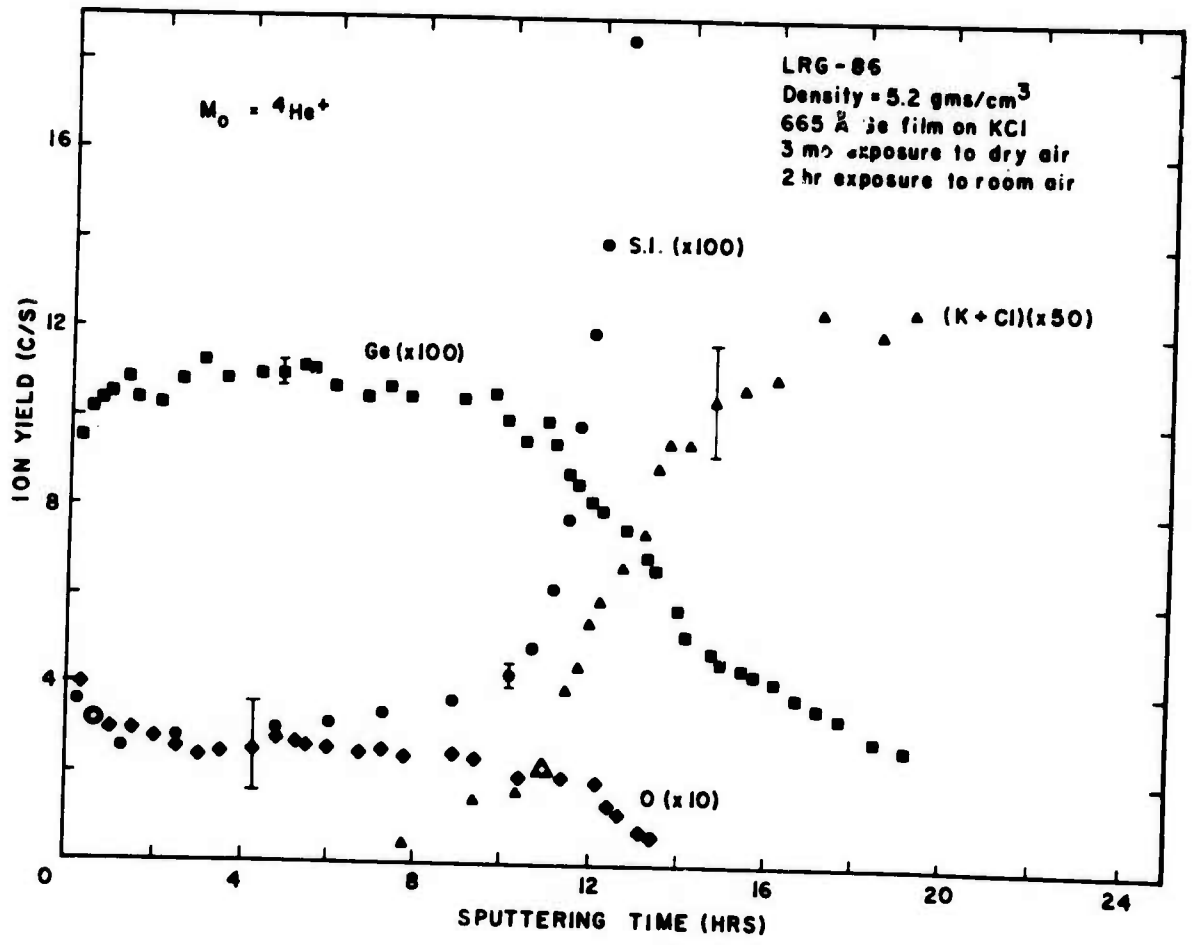

Figure 12. Depth Profile of Sputtered Ge Film 1.

to a higher degree. This was verified by a decrease in the sputtered ion signal after the first few minutes. The Ge signal then remained constant through the rest of the film. Correspondingly, the oxygen signal decreased and then leveled off as the first monolayers were sputtered away. The combined potassium and chlorine signal increased dramatically at the interface. This peak was labeled (K + Cl), since their masses are close together, and it is difficult to differentiate between them using He^4 as the probe gas. The (K + Cl) peak appeared after about eight hours of sputtering time. The presence of the (K + Cl) peak before the interface was reached can be accounted for in a number of ways:

1) K and/or Cl ion diffusion into the film from the substrate;
2) the absence of a sharp line of demarcation between the film and the substrate caused by damage to the KCl substrate during the sputtering process, and

3) the presence of argon near the interface.

Argon was the sputtering gas used in making the films. The argon peak could be interpreted as the (K + Cl) peak because their characteristic energy ratio peaks fall close to each other. However, it is highly unlikely that the premature (K + Cl) signal could be due to argon. If argon were present, it should be uniformly distributed throughout the whole film, which was not observed.

The more probable explanation for this is the combination effect of Cl ion diffusion from the substrate into the film and the absence of a sharp line of demarcation between the film and the substrate, implying the existence of an interfacial layer composed of Ge, K and Cl.

An examination of Figure 12, as well as other curves to follow, reveals at least one shoulder to the (K + Cl) peak occurring in the region of the interface. The small (K + Cl) signal that is observed as the interface is approached could be due to the Cl ion diffusion into the film from the interfacial layer.

The slow decay of the germanium and oxygen signals is caused by edge effects which were not completely eliminated by the rastering and gating system. The germanium and oxygen signal came from successive layers of the film exposed on the sloping sides of the crater, as well as from the Gaussian distribution of ions in the primary ion beam.

The O/Ge ratio for this film was also plotted. Figure 13 shows that, except for the film surface, the O/Ge ratio remains essentially constant throughout the film.

The analysis of this film clearly shows that germanium sputtered films of density 5.2 gms/cm^3 eventually oxidize throughout the film.

Film 2 (LRG-148) was exposed to room air only during transfer from the vacuum dessicator to the ion scattering sample chamber. As with Film 1, the Ge signal reached a maximum after the first monolayers were sputtered off. By the time the second scan was made (10 minutes), the oxygen signal had decreased. After 30 minutes, the oxygen signal disappeared and did not reappear at any time during the profile. The sputtered ion peak decreased after the first few minutes and then leveled off until the interface was reached. The combined (K + Cl) peak appeared at the beginning of the profile, disappeared through the bulk of the film, and reappeared at the inter-

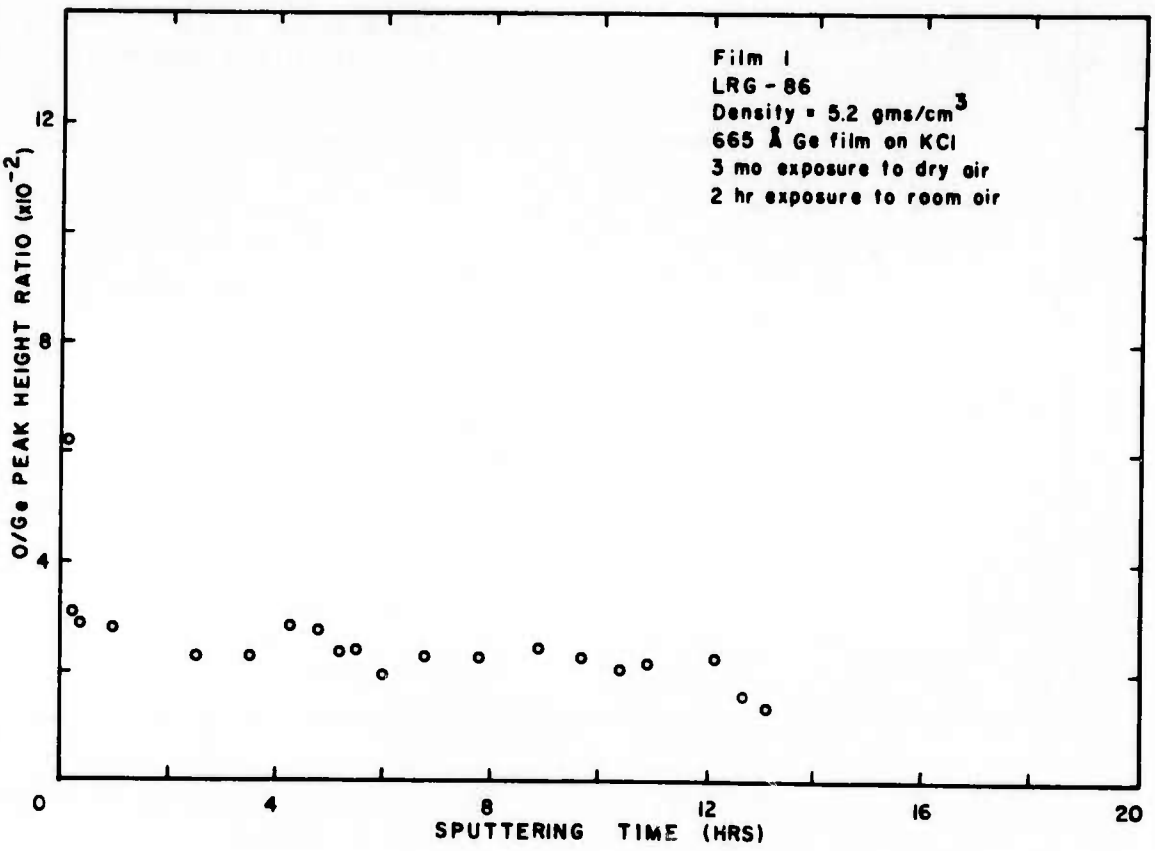

Figure 13. O/Ge Peak Height Ratio Profile of Film 1.

face. The presence of (K + Cl) on the surface of the film cannot be explained. The first (K + Cl) point at zero hours may be argon that was blown on the sample to inhibit oxidation. The reason for the detection of the (K + Cl) peak up to one half hour sputtering time cannot be explained. The decrease in the Ge signal at 1.9 hours, as well as the increase after 3 hours, can possible be explained as resulting from a change in the gain of the measuring system.

It is obvious that no bulk oxidation of Film 2 occurred during the 15 minute exposure to room air.

Figure 14 is the compositional depth profile of Film 2 which was exposed to room air for only 15 minutes during transfer. Figures 15-17 show the results for Film 3 (LRG-148), Film 4 (LRG-146) and Film 5 (LRG-159), respectively. Although these 3 films were exposed to dry air for 2 hours in addition to the 15 minute transfer, their compositional profiles are

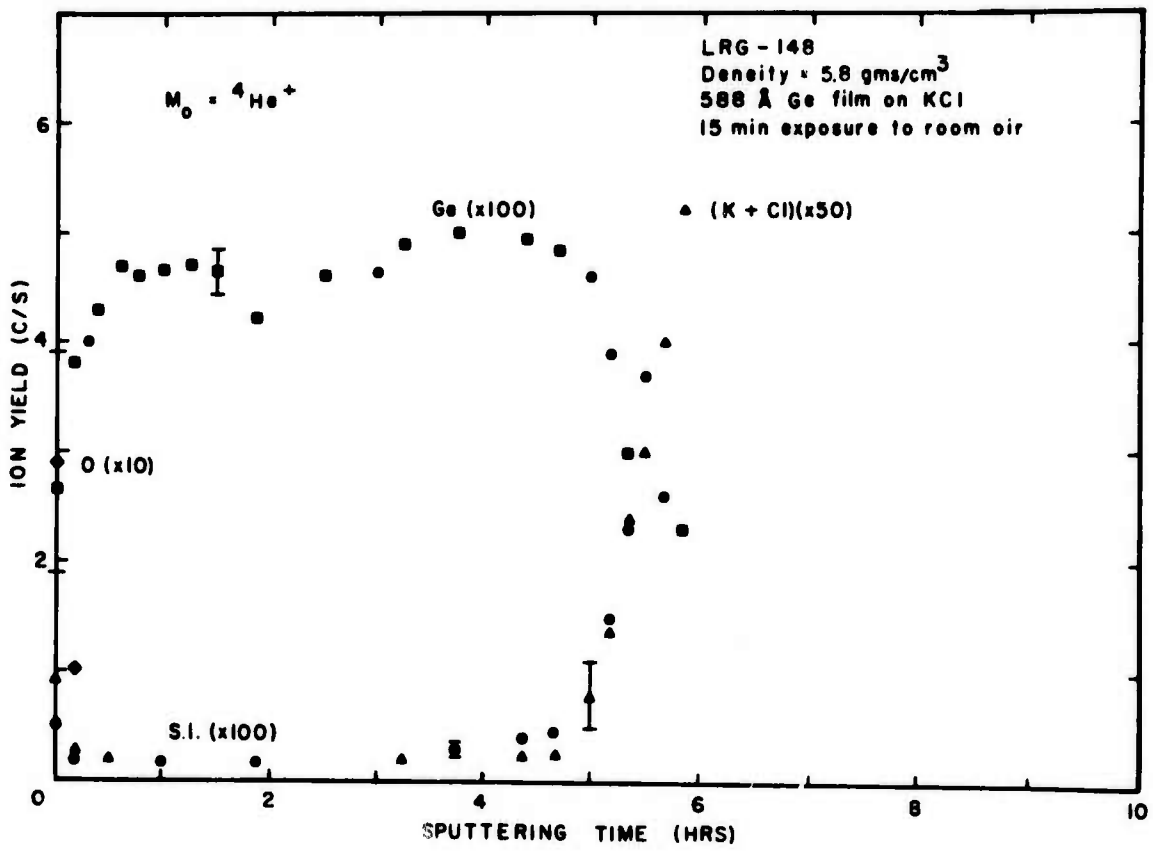

Figure 14. Depth Profile of Sputtered Ge Film 2.

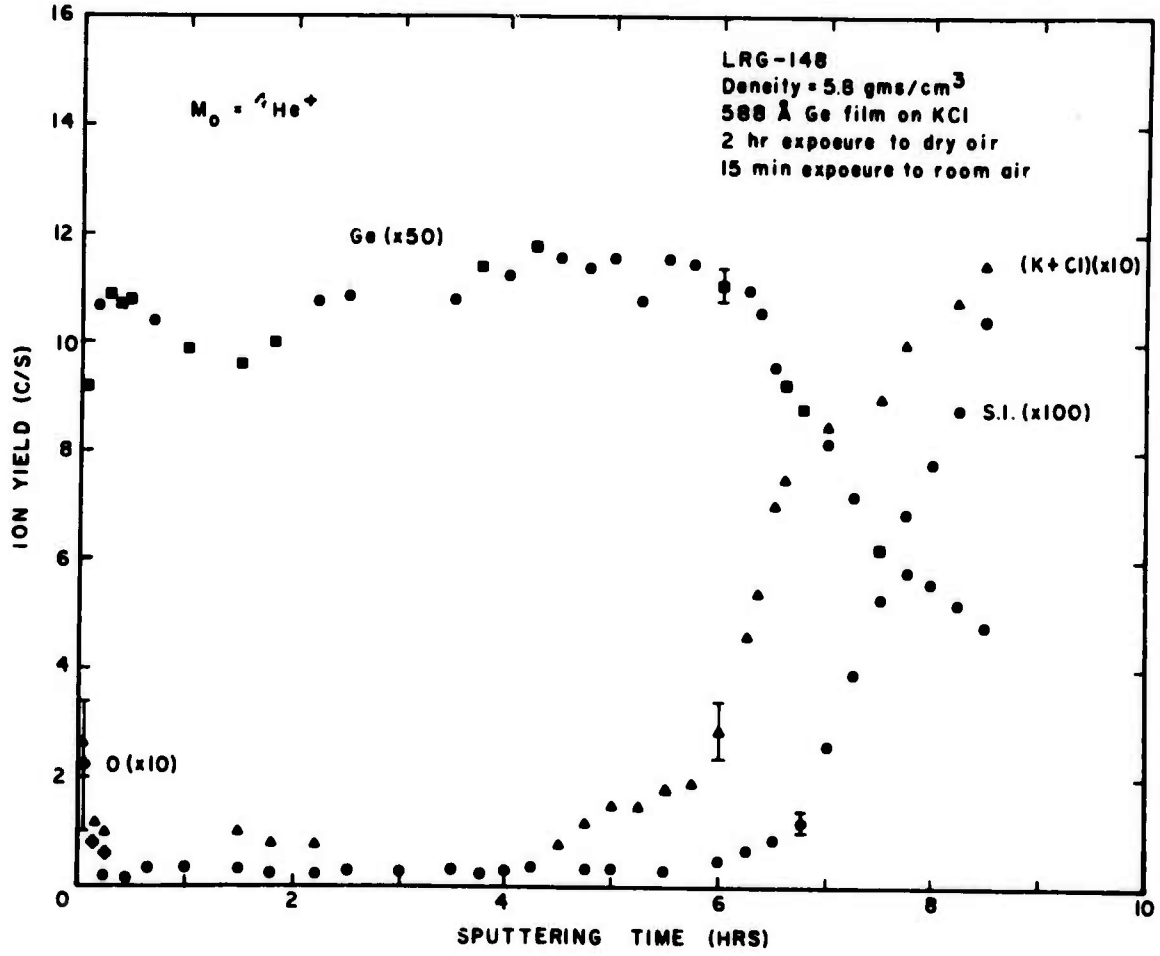

Figure 15. Depth Profile of Sputtered Ge Film 3.

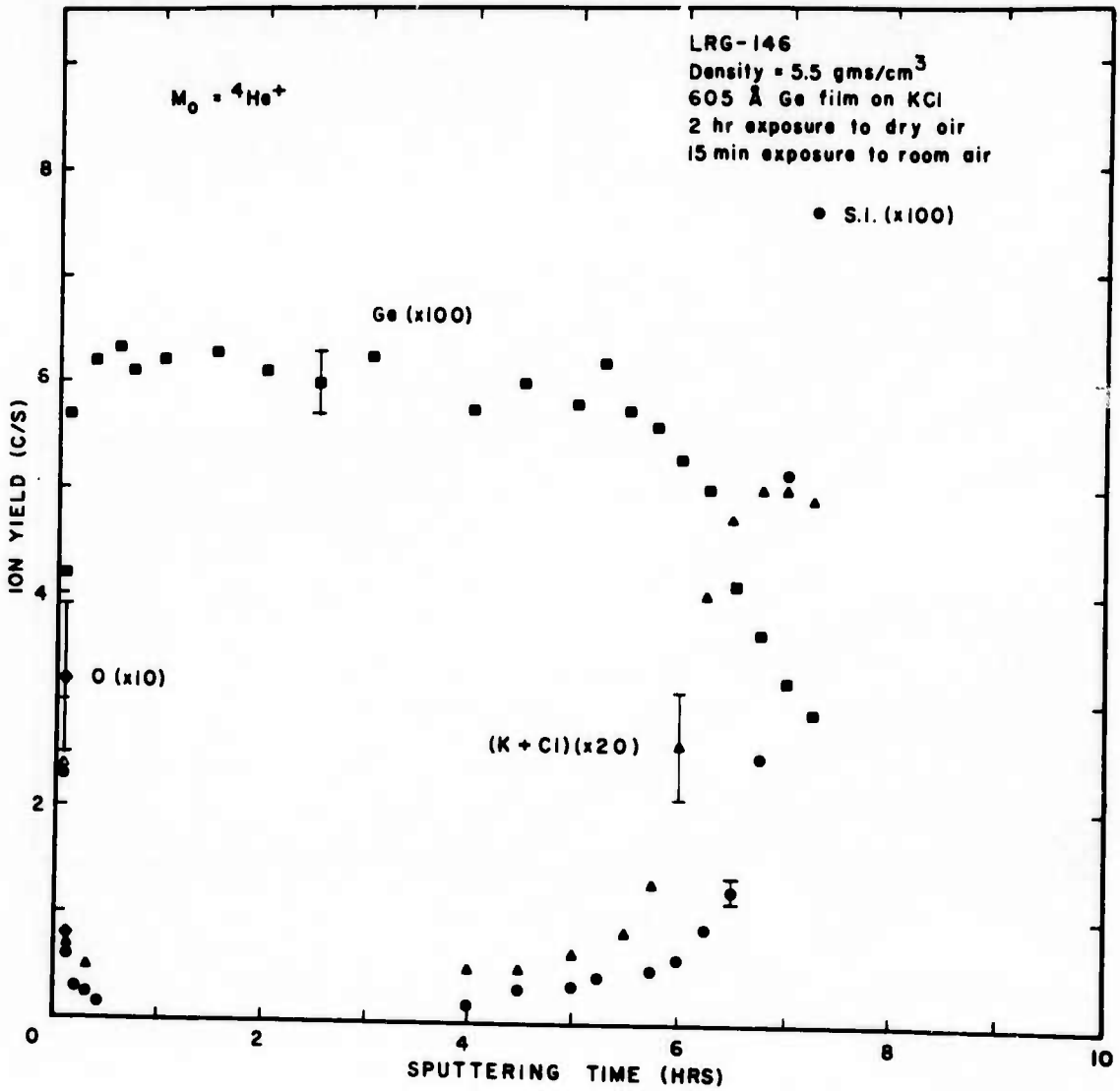

Figure 16. Depth Profile of Sputtered Ge Film 4.

comparable to that for Film 2. In no case was the oxygen signal detected beyond about 22Å into the film. The Ge, O, and sputtered ion peaks follow the same pattern as for Film 2. The (K + Cl) peak appeared at the beginning of each profile, and with the exception of Film 3 (Figure 15), disappeared until the interface was reached, as indicated by a rapid increase in signal. There is no obvious explanation why the (K + Cl) peak reappeared in Film 3 after 1-1/2 hours of sputtering time and then disappeared again. The fluctuating peak height of Ge in this same film (Figure 15), can probably be explained by changes in the gain of the system.

The last film analyzed, Film 6, was a low density film that had been exposed to dry air for 20 hours and room air for about 15 minutes (Figure 18). This film showed no more oxidation than the other films did. The profile for

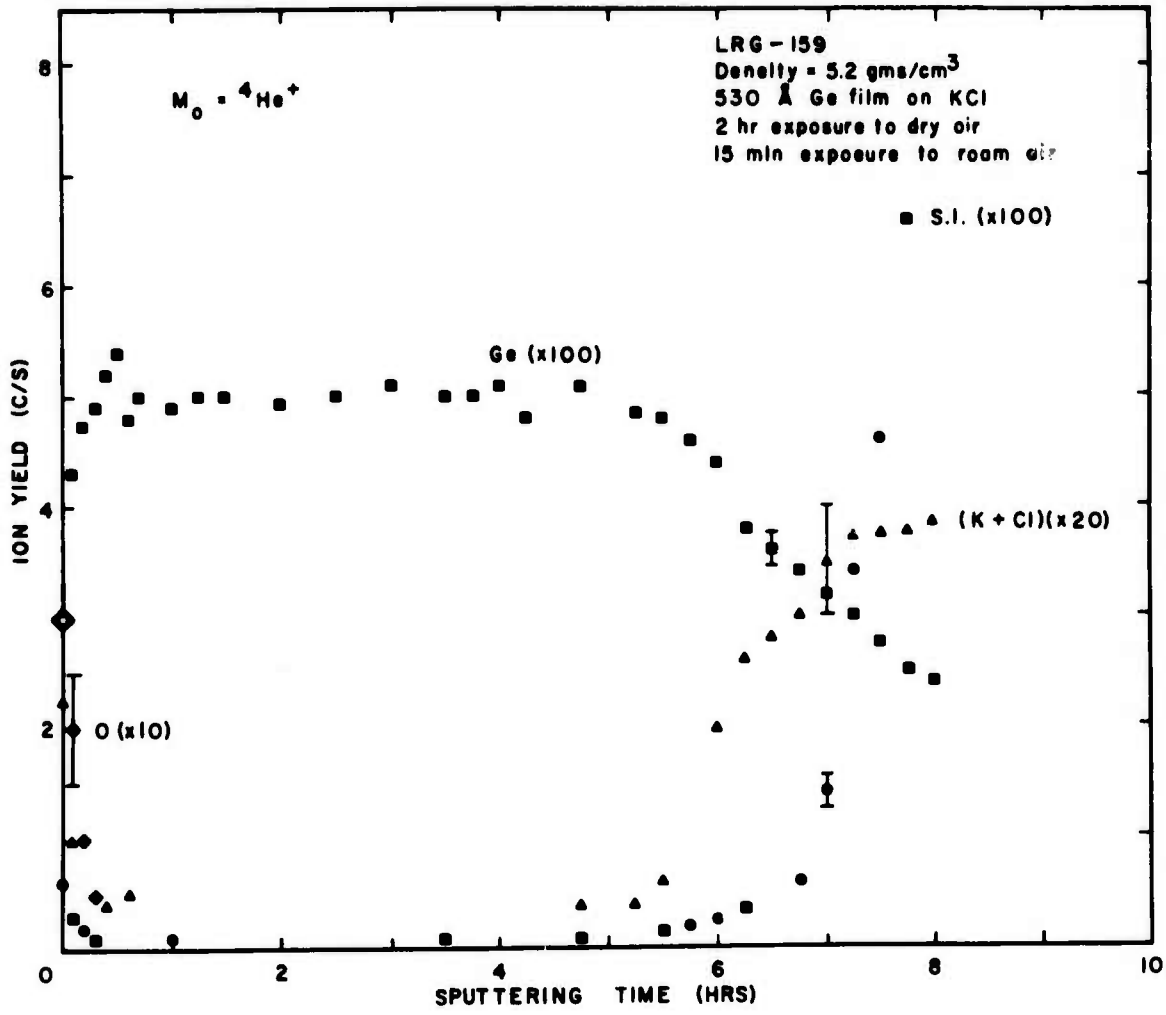

Figure 17. Depth Profile of Sputtered Ge Film 5.

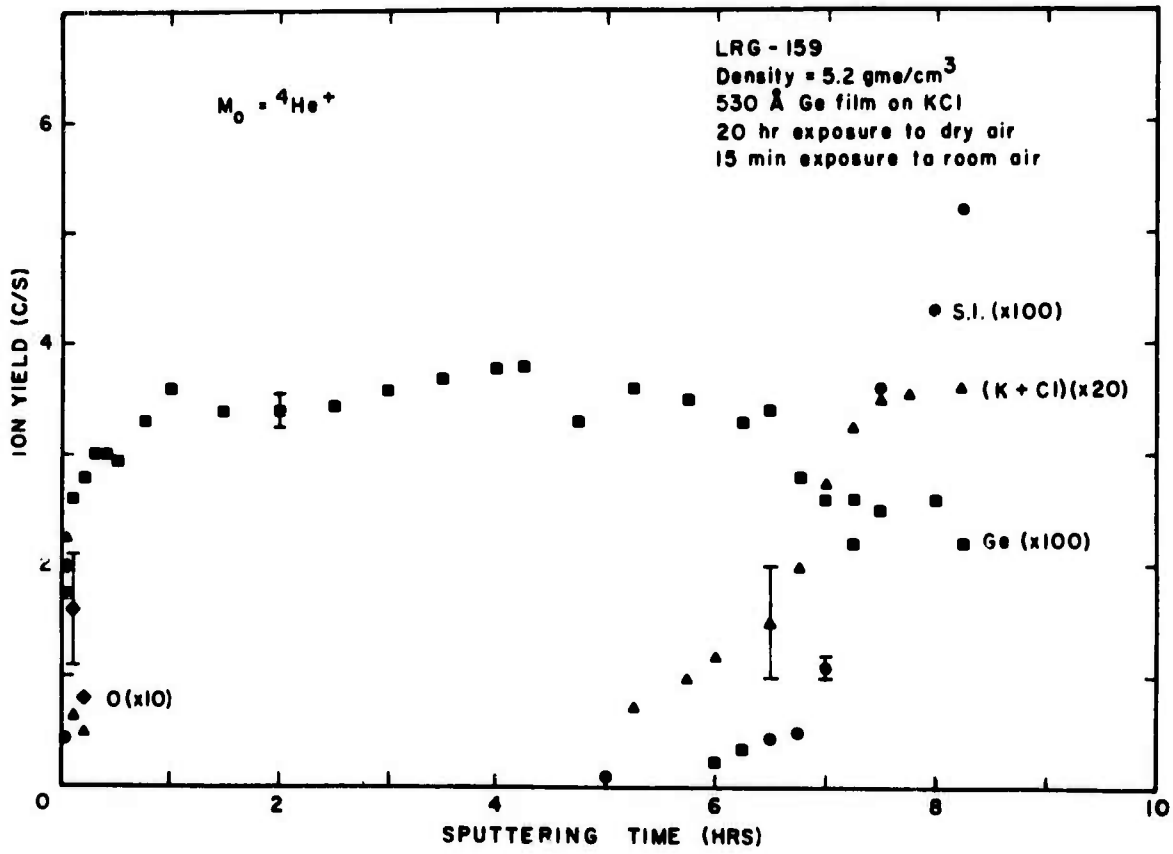

Figure 18. Depth Profile of Sputtered Ge Film 6.

this film was comparable to those of Films 2-5. No obvious deviation could be found.

Because the oxygen signal disappears rather abruptly for all films except the one exposed to air for three months and does not reappear, the oxidation of the amorphous Ge film is believed to occur by a diffusion process. Diffusion is a layer by layer process, and the sudden disappearance of the oxygen signal is what would be expected if the oxidation occurred by diffusion.

Table V summarizes the ISS results. It can be seen from the ISS depth profiles that the low density germanium films made under the previously specified condition do not undergo bulk oxidation in 20 hours. Higher density Ge films should have greater resistance to oxidation. Within experimental error, neither the low nor the high density films showed a greater tendency toward oxidation within two hours of exposure to room air.

6.5 Comparison of ISS Results with the Electron Microprobe Analysis

The electron microprobe results indicated that the less dense Ge films had a greater tendency to oxidize than the more dense Ge films. The ISS results do not agree. In the time span allowed, the less dense Ge films oxidized no more readily than the more dense Ge films did.

The results of the electron microprobe work on the least dense Ge film exposed to air a minimal amount of time indicated that 17 at% of this film was oxygen. The ISS revealed that this same type film exposed for 20 hours had oxidized only on the surface.

Measurement of oxygen with the electron microprobe, especially in small amounts, is somewhat troublesome; there are many places for errors. Calibration in the low range is difficult, and signal-to-noise ratios are low. Although no clear explanation could be found for this discrepency, the tendency is to fault the microprobe analysis in favor of the ISS results in this case.

It is difficult to believe that a germanium film can pick up 17% oxygen in 15 minutes. The denser films have more plausible oxygen contents of about 3% which can be explained in terms of surface oxidation.

TABLE V

SUMMARY OF ISS RESULTS FOR SPUTTERED GE FILMS.

	Film 1	Film 2	Film 3	Film 4	Film 5	Film 6
Density (gms/cm^3)	5.2	5.8	5.8	5.5	5.2	5.2
Exposure Time						
Dry Air (hrs)	3 months	0	2	2	2	20
Room Air (min)	120	15	15	15	15	15
Film Thickness (Å)	665	588	588	605	530	530
Sputtering Time to Damaged Substrate (hrs)	11.0	5.0	6.8	6.2	7	7
Sputtering Rate (Å/min)	1.01	1.96	1.44	1.62	1.27	1.27
Maximum Depth of Oxygen Signal (Å)	665	17.0	20.4	10.0	21.6	15.2

6.6 Analysis of Ge Films by Auger Electron Spectrometry

An attempt was made to use Auger electron spectrometry to verify the results of the ion scattering experiments. However, there is no suitable charge neutralization system available for the AES unit. To eliminate or lessen charging effects, one normally uses grazing incidence excitation ($\cong 60°$). However, the Auger electron spectrometer used here is equipped for normal incidence excitation only. Thus, charging of the sample surface occurred, and meaningful analyses could not be obtained.

7. CADMIUM TELLURIDE COMPOSITIONAL PROFILING WITH ION SCATTERING AND AUGER ELECTRON SPECTROMETRY

7.1 Film Preparation

A series of cadmium telluride films were sputter-deposited on KCl substrates for compositional profiling with ion scattering and Auger electron spectrometry. The substrates were prepared according to standardized techniques developed before (1). The CdTe films were prepared in a sputtering system having a turbomolecular pump as the main component of the vacuum system. A freon-refrigerated baffle was used to prevent pump oils from entering the sputtering chamber. This system was maintained as a "clean" unit for the preparation of optical coatings.

The base pressure before deposition was in the low 10^{-6} torr region. A gate valve throttled the flow of argon through the system so that a pressure of 10 mtorr was maintained during the deposition. All argon power at 200 volts were used as sputtering conditions so that amorphous films were obtained. Deposition proceeded for 9 minutes at a rate of about 1Å/sec., giving films which were measured to be 510Å thick using a Varian interferometer. A 5-inch target of 5-nines pure CdTe was used with the substrates mounted at a distance of 5 cm from the target. All films were stored in dry air until analyzed.

7.2 Analytical Conditions

The hybrid ion scattering-Auger electron spectrometer was utilized in obtaining the profiles which will be discussed. The primary ion beam in the scattering experiments was He^4 for films 3 and 5 and Ne^{20} for film 4. The primary beam energy was 1.5 kev, the beam diameter was 0.5 mm FWHM, the beam current was maintained at 180 na giving a current density of about 65 $\mu a/cm^2$,

the rastered area was about 0.02 cm^2, the signal was gated from the central 35% of the rastered area, and the sputtering rate was about 1.5Å/min. No oxygen was detected by ISS in any of the films; the measured oxygen sensitivity was about 10^{-2} monolayers.

For AES analysis, the electron beam was set to give an energy of 1.5 kev at 2 ma, giving target currents of 8-10 μa. The modulation was set at 3 volts and a time constant of 0.1 msec was used.

The first step in each analysis was to obtain an Auger spectrum from the surface of each film (the "a" spectrum in each series). The sample was positioned for ISS analysis, and the ion beam was switched on to begin the scattering experiment. After the beam had sputtered through the film to the substrate, the sample was again positioned for Auger electron analysis and another spectrum obtained (spectrum "c" in each series). The electron beam was moved to intercept the side of the sputtered crater and a third spectrum obtained (spectrum "b" in each series). All of this was necessary because we did not have a precision sample rotator to move the sample back and forth between the ISS and AES positions. (This unit is currently under construction and will feature a computer-controlled stepping motor for precision alignment, thus allowing simultaneous profiles to be obtained).

7.3 ISS Profiles and AES Spectra

The results of these profiling studies are shown in Figures 19-24. Film 3 was exposed to room air only long enough to transfer it from the sputtering chamber to a desiccator for storage and from there to the ISS vacuum chamber. Figure 19 is the composition profile for this film, and it shows a rather uniform cadmium/tellurium profile throughout the film. The rapid rise in the sputtered ion peak is a very good indicator that the substrate has been reached, since the lower ionization potential of the potassium ions in the substrate (compared to cadmium and tellurium which had made up the bulk of the sputtered ions to that point) gives a higher percentage of ions in the sputtered species and hence an increased ion signal. Ion scattering signals from potassium and chlorine appear at the same time, confirming that the substrate indeed has been reached. The increase in the cadmium + tellurium peak after about 1/2 hour sputtering cannot be explained.

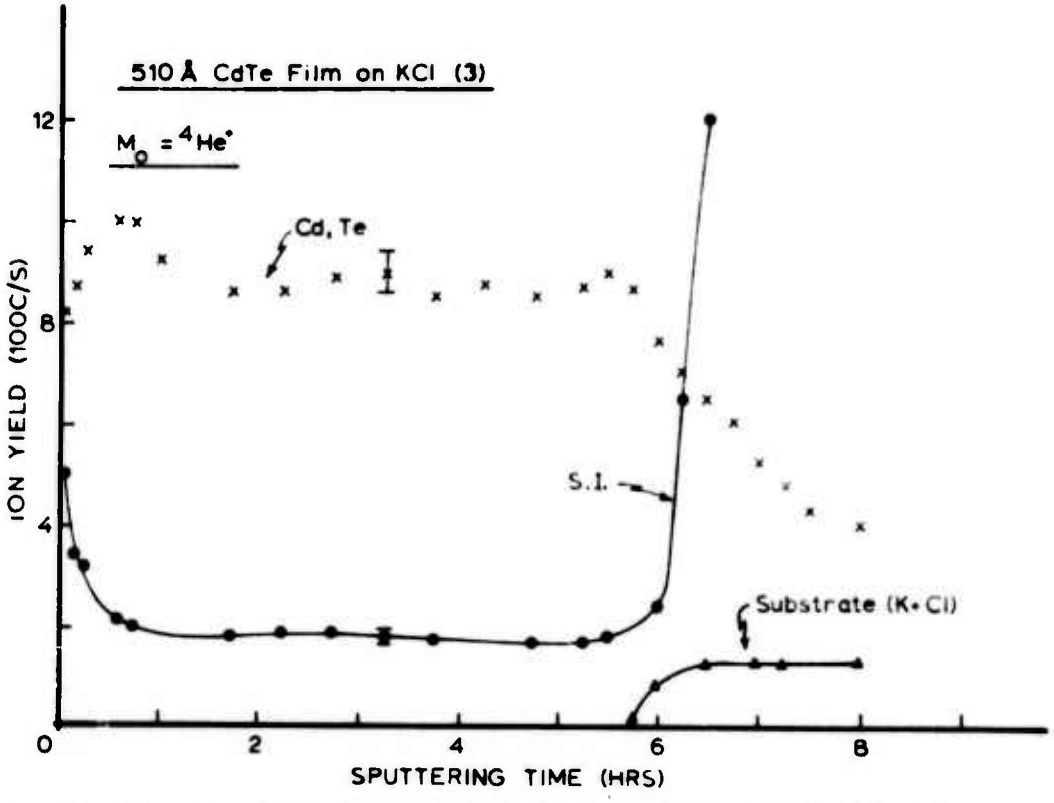

Figure 19. Ion Scattering Profile of Sputtered CdTe Film 3.

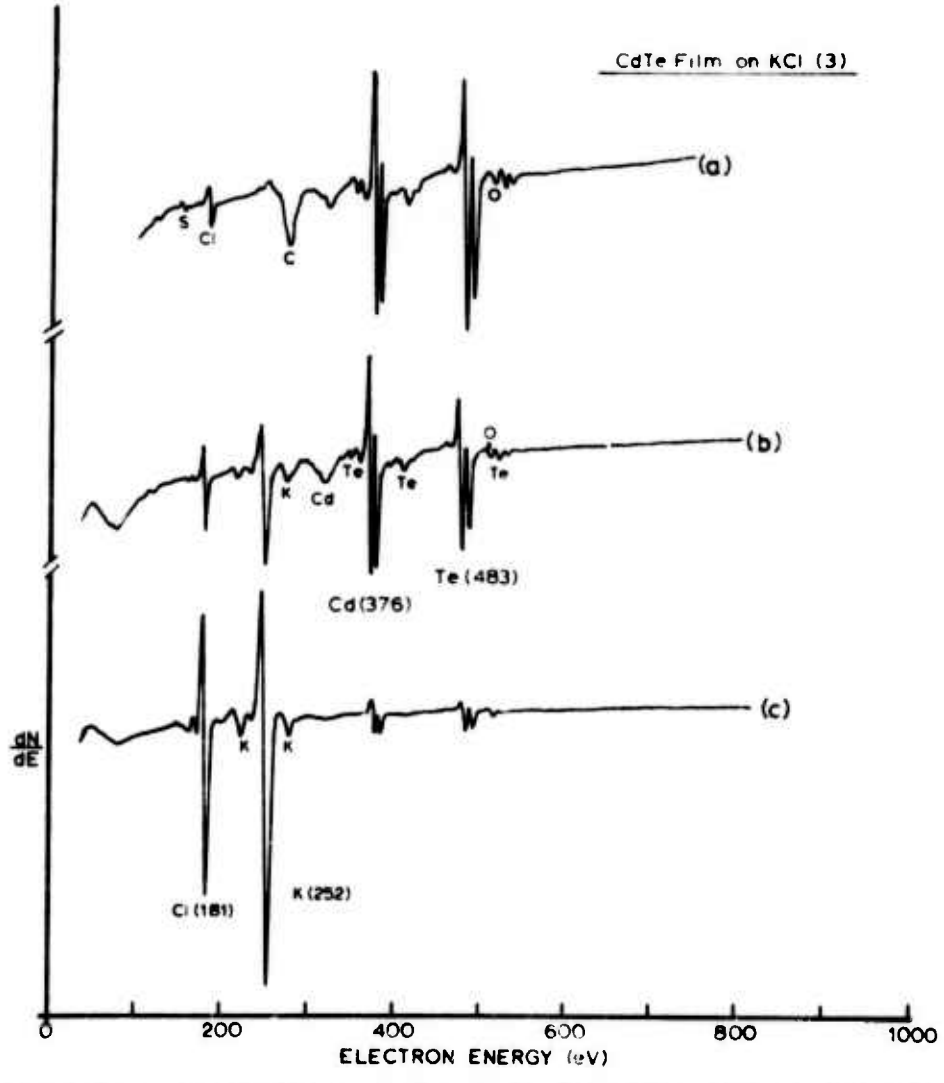

Figure 20: Auger Electron Spectra of Sputtered CdTe Film 3: (a) Surface of Film, (b) Halfway Down Crater Wall, (c) Bottom of Crater.

Figure 20 shows three Auger electron spectra taken from Film 3 at the specific points indicated. S, Cl, C, and O appear as impurities on the surface. The sulfur, carbon and oxygen probably arise from pump fluids in the vacuum system of the sputtering unit, as well as residuals from the ISS vacuum system. C and O probably arise from the cracking of CO and CO_2 by the electron beam interacting with the surface. Note that the surface appears to be tellurium-rich. In spectrum "b" the cadmium and tellurium are approximately stoichiometric. There appears to be a great deal of potassium at this level, perhaps diffusing from the substrate. Analysis of the bottom of the crater shows a chlorine-rich surface. This is opposite to what might be expected according to others who have studied the effect of electron beams on alkali halides (35,36). Essentially, the electron beam causes the surface region to become depleted in the halide, leaving an alkali-rich surface. Perhaps in the case where a film in deposited on the alkali halide the film acts as a barrier to the halide movement, causing a build-up of halide ions at this interface; or perhaps the film enhances the diffusion of the alkali, leaving a halide-rich interface. This clearly needs more study, such as an ISS investigation of the compositional profile through such a film after an extended exposure to an electron beam. The primary ion beams used in ISS do not seem to affect the alkali halides in the same manner as electron beams.

Figure 21 shows the ISS profile of CdTe Film 5 which had been exposed to room air for about 17 hours. Although no oxygen was detected, the film did seem to be degraded in some manner. The Cd,Te peak did not fall off sharply at the interface as in the previous film. In addition the signals from the ion scattering experiment were quite erratic.

The Auger electron spectra shown in Figure 22 indicate P, S, Cl, C and O impurities on the surface of Film 5. As before, the surface is tellurium-rich. Part way through the film, the composition is still tellurium-rich, with a significant amount of potassium present, as well. As in the previous film, the interface region at the surface of the substrate assayed very chlorine-rich.

Helium-4 was used as a probe gas in the ion scattering experiments conducted with the previous two films, because we were interested in detecting the presence of oxygen anywhere in the film. Using $^4He^+$ it is not possible to separate the signals derived from cadmium from those derived from tellurium. Thus, $^{20}Ne^+$ was used for the ion scattering experiments on Film 4. The ISS spectra (Figure 23) indicate a cadmium-rich surface, just like the previous

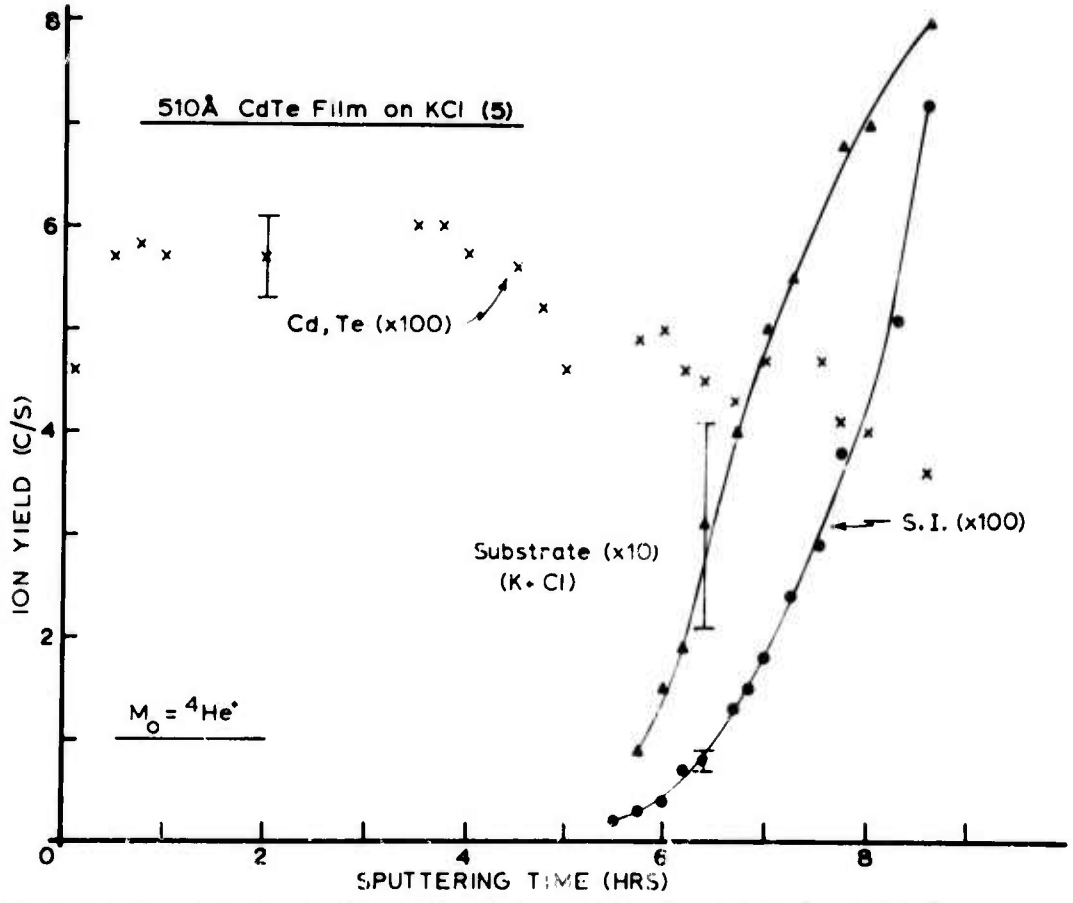

Figure 21. Ion Scattering Profile of Sputtered CdTe Film 5.

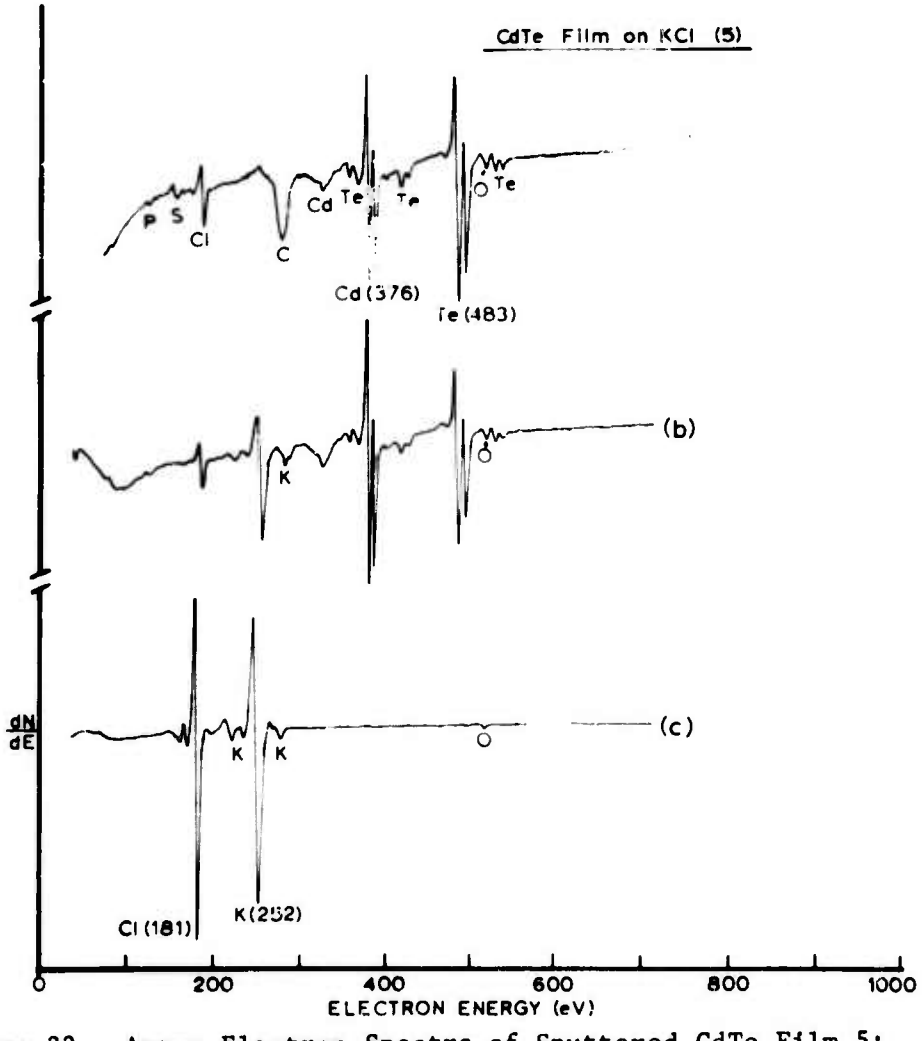

Figure 22. Auger Electron Spectra of Sputtered CdTe Film 5: (a) Surface of Film, (b) Halfway Down Crater Wall, (c) Bottom of Crater.

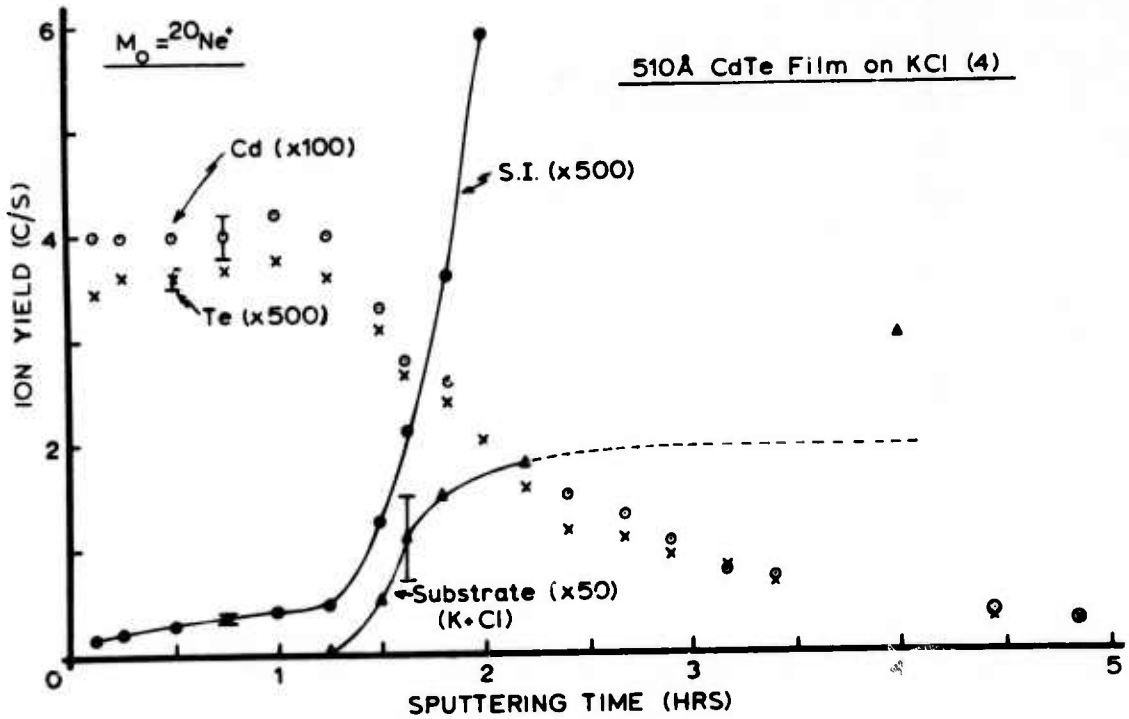

Figure 23. Ion Scattering Profile of Sputtered CdTe Film 4.

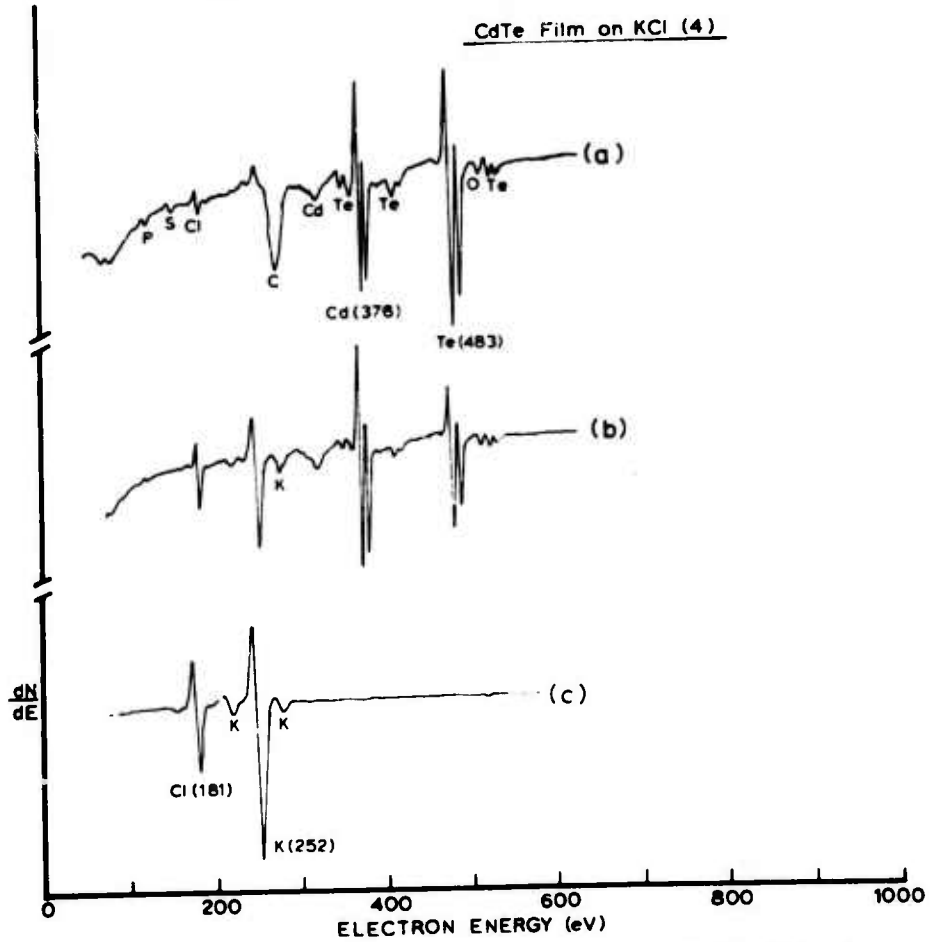

Figure 24. Auger Electron Spectra of Sputtered CdTe Film 4: (a) Surface of Film, (b) Halfway Down Crater Wall, (c) Bottom of Crater.

two films. The same impurities occur on the surface as before. However, part way through the film, the Auger electron spectrum (b) shows the film to be cadmium-rich. Potassium is also present at this location in the film, as well as some chlorine. Spectrum "c" shows the bottom of the crater to be potassium-rich, unlike the previous two films. These differences have not been explained at this time.

Another disturbing finding is shown in the two Auger electron spectra in Figure 25. Two CdTe films were prepared under identical sputtering conditions, using the same target, in two different sputter deposition systems.

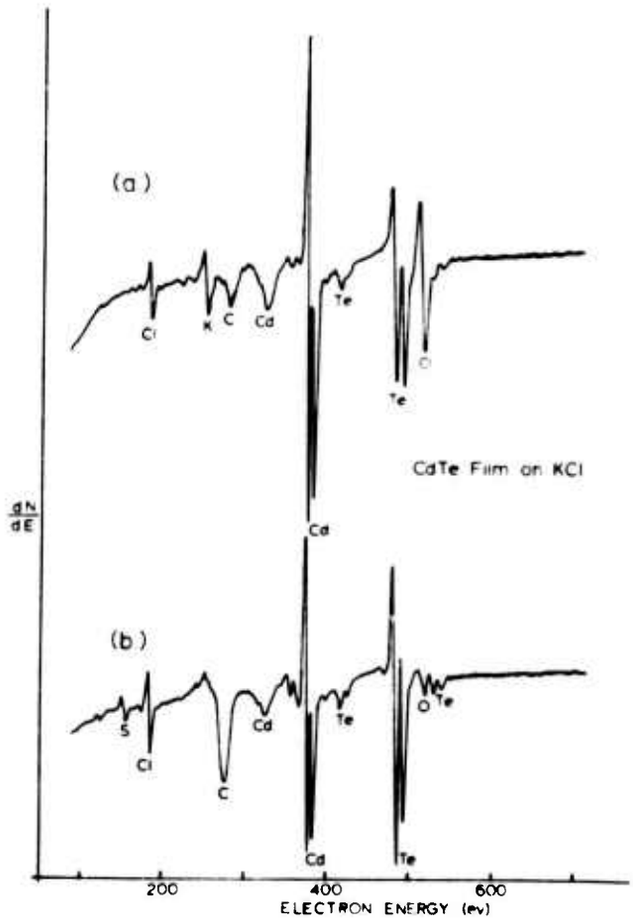

Figure 25. Auger Electron Spectra of Sputtered CdTe Films Prepared in: (a) An Oil-Pumped MRC System and (b) a Turbomolecular-Pumped Airco Temescal System.

The film from which spectrum "a" was obtained was made in a oil-pumped MRC system. The surface contained chlorine, carbon and a great deal of oxygen as impurities, and it assayed very cadmium-rich. Spectrum "b" was obtained from a film made in a turbomolecular-pumped Airco Temescal system. This film was tellurium-rich and contained some sulfur and phosphorus, a little oxygen and a lot of carbon. Thus it appears that the type of sputtering apparatus, or at least the type of vacuum system used on such an apparatus, is an important parameter to give, along with the r.f. power and voltage, and the sputtering gas pressure.

8. AUTOMATION OF THE ION SCATTERING SPECTROMETER

Automatic control of the ion scattering spectrometer by a PDP 11/20 computer is accomplished through a 3M Eight Channel Digital Multiplex System and a computer interface unit (C.I.U.) designed in this laboratory. The computer controls the channel, counting and scan sequences. A maximum of eight (8) different channels or segments of the ISS spectrum can be scanned sequentially.

The width of each channel can be selected in order to integrate the counts over a given peak, or the width can be narrowed down to measure the height of a given peak. The counting scheme can be programmed to store either the counts per channel over a fixed time interval or the time required to obtain a fixed total count (2^0 to 2^{15}). In addition successive readings of an individual segment can be specified (1, 3 or 5) before proceeding to the next channel. A copy of the basic program for an automatic, computer-controlled ISS profile is given in Appendix B. The definition of variables used in the program is listed in Appendix C.

In a typical profile a manual scan is first made with the multiplex unit and an XY recorder. This enables one to select the segments or channels to be investigated and to determine the proper counting level for each channel. A typical ISS spectrum of 1.5 kev $^{20}Ne^+$ ions scattered from a 990Å CdTe film sputter-deposited on a KCl substrate, obtained 12 minutes after the ion beam was turned on, is shown in Figure 26. This is a plot of the ion yield (counts/sec) vs. the energy ratio E_s/E_o, where E_o is the energy of the incident probe $^{20}Ne^+$ ions, and E_s is the energy of the elastically scattered neon ions. Chemical identification of the scattering target atom

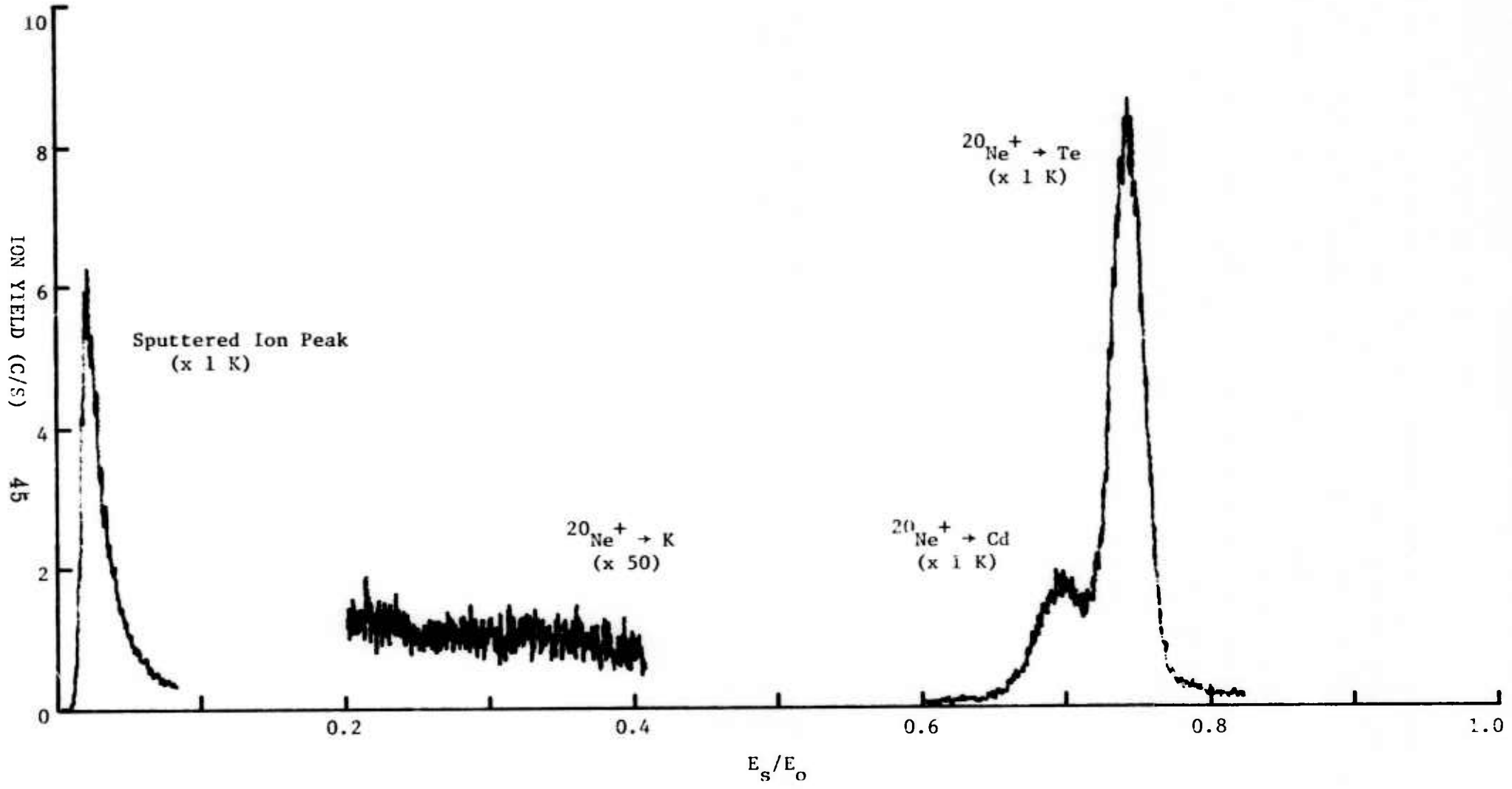

Figure 26. Spectrum of 1.5 kev $^{20}Ne^{+}$ Ions Scattered from a 990Å CdTe Film on KCl Substrate.

is obtained by measuring the energy ratio E_s/E_o. In Figure 26 the two major peaks correspond to neon ions elastically scattered from Cd and Te atoms on the sample surface. The energy ratio (E_s/E_o) region between 0.32 to 0.36 corresponds to $^{20}Ne^+$ ions elastically scattered from K atoms. No peak is observed in this region.

An additional peak which occurs in the low energy region of the ISS spectrum is the sputtered ions (S.I.) peak. The interaction of the ion beam with the sample sputters successive layers of atoms from this surface. Some of the sputtered atoms are ejected as ions at typical energies of 2-10 ev. The yield of sputtered ions depends upon the element and the state in which it exists on the surface. Low ionization potential elements, such as Ca, K and Na, are easily sputtered as ions, while elements that are chemically combined, such as oxides, produce enhanced ion yields. By monitoring the sputtered ion peak in a compositional depth profile, additional information about the interfacial region between the CdTe film and the KCl substrate can be obtained.

A spectrum is scanned by sweeping the voltage applied to the electrostatic energy analyzer and displaying the counting rate versus the ratio of the energy of the scattered ions to the energy of the incident ions. The spectrum shown in Figure 26 was obtained at a slow sweep speed (100 ev/min). Some information can be lost before the next scan is initiated. With a computerized profile, faster data acquisition is achieved and counting statistics greatly improved by repetitive counting. Thus, more detailed studies of compositional homogeneity with depth and diffusion profiles in the films can be made.

The complete profile of a 990A CdTe film is shown in Figure 27. The sample was deposited on a KCl substrate by sputtering from a 5-inch CdTe target in a diffusion-pumped vacuum system. The deposition conditions were:

P_{Ar}:	40 millitorr (Ti purified)
rf voltage:	500 volts
rf power:	180 watts
Substrate-target distance:	5.2 cm
Deposition time:	200 sec
Base pressure:	2×10^{-6} torr

The film thickness was 990Å, measured with a Varian Interferometer.

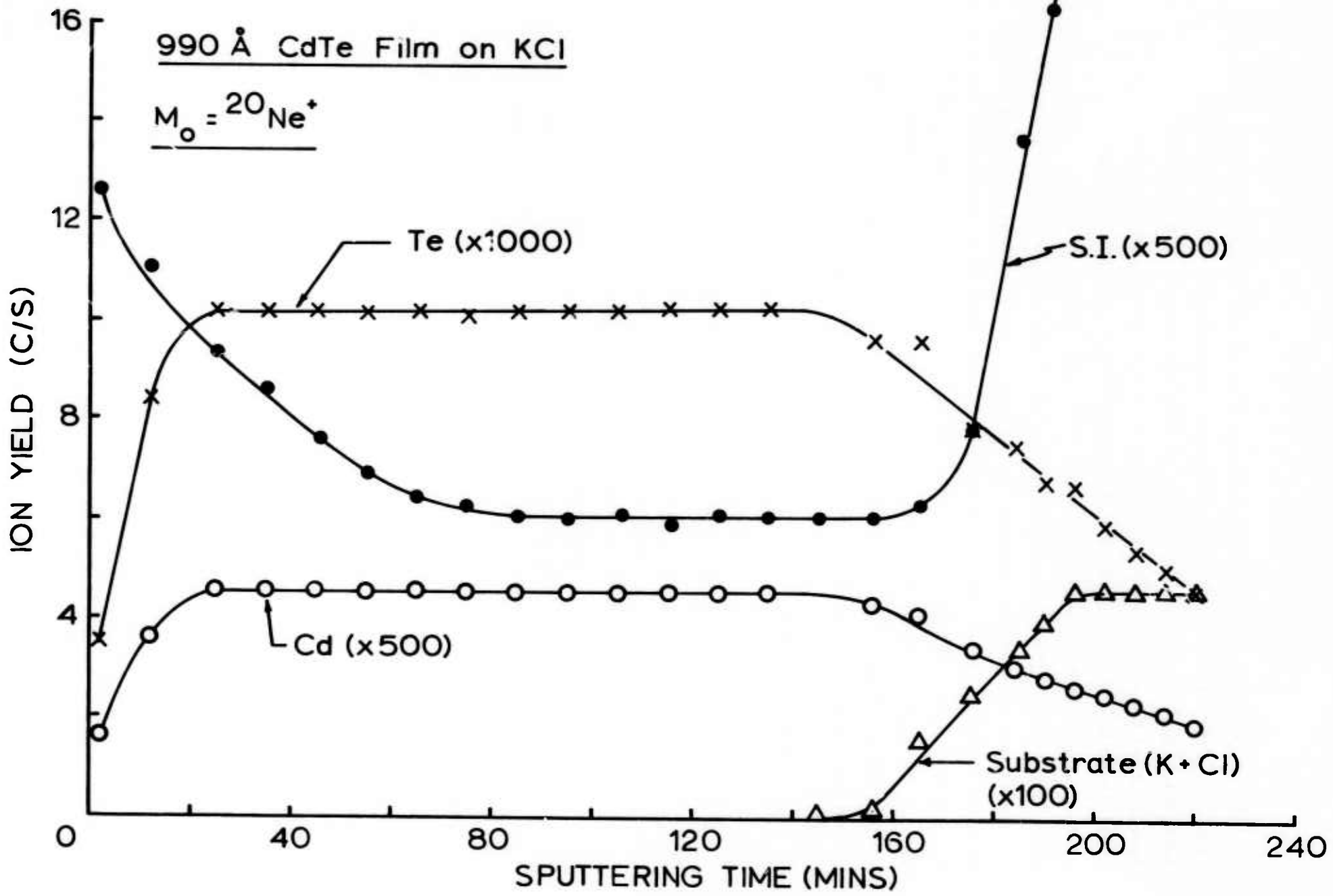

Figure 27. Compositional Profile of a Sputtered CdTe Film.

The diameter of the ion beam that was used in the ISS profile was nominally 1 mm. The beam was rastered over an area of approximately 0.16 cm^2, with the scattered signal electronically gated so that the signal from 25% of the rastered area entered the detection system. These added raster-gating capabilities of the ion scattering spectrometer are essential for more accurate compositional depth profiling, since the signals from the crater walls (generated by the Gaussian distribution of the ion beam) are minimized.

In Figure 27 the data taken at sputtering times of 2 and 12 minutes were obtained manually, while those obtained at longer times were taken with the spectrometer controlled by a PDP 11/20 computer. The computer print-out listing the chemical symbols of the elements, elapsed time per specified count, gain and count rate per channel, and time between scans are given in Appendix D. Eight (8) channels were programmed as follows:

Chemical Symbol	Description	Energy Ratio
SIL	Sputtered Ions Signal, Lower Limit	020
SIP	Sputtered Ions Signal, Maximum	025
SIH	Sputtered Ions Signal, Higher Limit	030
KL	Substrate (K) Signal, Lower Limit	320
KP	Substrate (K) Signal, Maximum	335
KH	Substrate (K) Signal, Higher Limit	360
CD	Cd peak	700
TE	Te peak	745

At sputtering times from 25 to 175 minutes, the time between starts of scans was 10 minutes, and each set of scans lasted for 2 minutes. For the sputtering times from 184 to 226 minutes, the time between starts of scans was changed to 6 minutes, with each set of scans lasting for 3 minutes. The printed data from T = 125 minutes to 226 minutes is also given.

The profile shown in Figure 27 shows that, as the interface between the film and KCl substrate is approached, the ion signals scattered from Cd and Te begin to decrease, while the sputtered ions peak rises very rapidly, since the latter peak consists of sputtered ions of Cd, Te, those from KCl and other impurities trapped at the interface. The slow decay in the Cd,Te signal was due to the slow sputtering rate used. From the measured film thickness and the ISS profile, a sputtering rate of about 6.7Å/min was calculated.

Modifications in the basic program are currently underway to enable the computer to:

(a) Detect the presence of peak, determine and store the count rate for each segment or channel;

(b) Plot the scattered ion yield for each channel as a function of sputtering time.

The modified program can readily follow shifts in peak position, which are indicative of the charged states of the surface.

9. PREPARATION OF COATINGS BY ION PLATING

9.1 Introduction

Ion plating is a vacuum coating technique in which a film is produced by depositing neutral atoms as well as ions on the substrate surface. There are two competing phenomena occurring at the surface of the substrate: the deposition of ionic and neutral species of the coating material; and the sputtering of the deposited film and substrate material by newly arriving ionic and neutral coating material species.

The substrate is placed at a high negative potential with respect to the evaporating material; thus any positive ions formed will be accelerated toward the substrate. The high velocity of these incoming ions will generally cause them to be buried deeper into the surface than the neutral atoms. This, coupled with the competing sputtering process, leads to greater adhesion of the deposited film than when only neutral atoms are deposited, even when a relatively small percentage of the coating species are ionized.

9.2 Apparatus and Procedure

A MRC electron beam zone refiner was modified for use in ion plating. A tungsten filament was used as an electron source to evaporate the coating material. The coating material was placed on a pedestal, at a high positive potential; the electrons emitted by the hot filament were thus accelerated toward the material. A relatively high ion production can be achieved when an electron beam is used rather than joule heating. Biasing the substrate produces an electric field between the coating material and the substrate which augments the production of ions, as well.

By changing the filament current and potential at which the coating material is maintained, the evaporation rate of the coating material can be controlled. By changing the substrate-to-coating material distance, one can control the ratio of ions/neutrals striking the substrate. Since the final velocity of the ions is a function of the potential difference between substrate and the coating material, increasing the substrate potential increases the velocity and hence the depth of penetration of the ions.

A thermistor located at the surface of the substrate was used to monitor the substrate temperature. A shutter was used to isolate the substrate while the coating material was being heated to a stable evaporation rate. Once a stable rate was achieved, the shutter was opened and plating allowed to take place until the desired thickness was obtained. The entire process was carried out in a vacuum chamber with a working pressure of between 10^{-4} and 10^{-5} torr.

9.3 Results

A number of germanium and cadmium telluride films were deposited on glass substrates. In addition, cadmium telluride was deposited on KCl substrates. The basic deposition parameters are shown in Table VI, where T_f is the final substrate temperature. Beam conditions refer to the electron beam used for heating and ionizing. The substrate-to-target distance is the measured distance between the surface of the coating materials to be evaporated and the substrate surface.

Germanium films were prepared in an attempt to study the film-character of coatings prepared by different processes, since we have thoroughly studied sputter-deposited germanium films. The cadmium telluride films were prepared for simultaneous characterization with sputter-deposited films of the same composition. Complete characterization of the ion-plated films was not done. However, the CdTe films appeared very uniform and adhered extremely well both to glass and to KCl.

10. PLASMA POLYMERIZATION OF THIN FILMS

Plasma polymerized organic films prepared as described in AFCRL-TR-75-0152 (1) were submitted to Mr. Joseph Comer of AFCRL for electron microscope characterization, specifically by transmission electron microscopy and diffraction. The samples were prepared and examined by Mr. Comer using a JEM-6A electron microscope with a

TABLE VI

ION PLATED FILMS*

No.	Material	Substrate	T_f (C)	Substrate Potential V_s (volts)	Ion Current (ma)	Filament Heating		Beam Conditions		Substrate-Target Distance D (cm)
						V_f (volts)	I_f (amps)	V_b (volts)	I_b (ma)	
1	Ge	Glass	-	-1000	>25	6	22	-	-	14
2	Ge	Glass	-	-1000	>25	6	20	1000-1500	>0	10
4	Ge	Glass	-	-1000	>25	7	25	2000	150	10
6	Ge	Glass	43	- 500	>25	6.5	22	1800	160	10
7	Ge	Glass	40	- 500--1500	>25	6-7	23-25	1800	150	10
11	CdTe	Glass KCl	60	-1000	4-7, >25	5.0	22-25	1400-2000	170-200	10
12	CdTe	Glass KCl	100	- 500	8-9	4.0	21	2000	220	7

*Vacuum system pressure 5×10^{-5} torr.

beam having an energy of 100 KV. He obtained electron micrographs for examining texture, selected area diffraction patterns, and high resolution electron diffraction patterns both to cover large areas in diffraction and also to examine the films using a grazing incidence electron beam.

Two of the films were completely amorphous. Two of the films were highly crystalline but also showed the presence of an amorphous phase. Crystallite size was about 100Å. Textural differences were thought to be caused only be regions of different thickness.

The selected area diffraction patterns taken on the crystalline films could be interpreted as a cubic structure which could be indexed as diamond. Table VII shows that the agreement with the diamond pattern is very good, although the measured values are close to certain reflections from graphite. A highly-oriented graphite film could produce a pattern with no 00ℓ reflection. To check for this the sample was tilted up to 20°, but no change in the diffraction pattern was recorded.

High resolution electron diffraction was used to confirm the selected area diffraction results. Table VIII shows the measured d-spacings for the same film as shown in Table VII (SAD). Tilting the sample as much as 45° produced no change in the diffraction pattern. A glancing angle electron diffraction pattern was obtained from the same film (mounted on a grid) in an attempt to find an (00ℓ) graphite reflection. The results compared with an ASTM pattern for graphite are shown in Table IX. By this technique the (002), (006) and (008) reflections show up, indicating the possibility of graphite being present. However, the glancing angle diffraction pattern was obtained from only a small portion of the sample because of the distortion of the grid from previous measurements. If these films are graphitic, then they must be highly oriented with the c-direction normal to the surface of the film. On the other hand, if they are diamond (or diamond-like) as indicated by SAD and high resolution diffraction patterns from two different films, then this technique presents a new method for producing diamond-like films for protecting optical components. Further studies to elucidate this are being conducted utilizing electron microscope facilities at Penn State.

TABLE VII

ANALYSIS OF SELECTED AREA DIFFRACTION PATTERNS
FROM FILM NO. 21, PLATES 4590C AND 4593C*

Measured d	Relative Intensity	Diamond d(Å)	(ASTM) hk	Graphite d(Å)	(ASTM) hk
				3.36	002
				2.13	100
2.06	vs	2.06	111	2.03	101
1.79	s	1.78*	200	1.800	102
				1.678	004
				1.544	103
1.26	m	1.261	220	1.232	10
				1.158	112
				1.138	105
				1.120	006
1.08	m	1.0754	311	1.054	201
1.03	w	1.03**	222	0.994	114,116
		.9816	400		
				.841	008
.82	vw	.8182	331	.829	116
				.801	211

*J. Comer, AFCRL

**Forbidden according to x-ray structure factor

TABLE VIII

HIGH RESOLUTION DIFFRACTION OF FILM NO. 21*

Measured d (Å) (Pattern 4599C)	Diamond d(Å)	(ASTM) hkℓ
2.06	2.06	111
1.795	1.78	200
1.265	1.261	220
1.082	1.0754	311
1.032		
	.892	400
	.82	331

*J. Comer, AFRCL

TABLE IX

GLANCING ANGLE ELECTRON DIFFRACTION FROM FILM NO. 21*

Pattern 4604C d(A)	Graphite (ASTM) d(A)	hk
3.36	3.36	002
2.12	2.13	100
	2.03	101
1.77	1.80	102
	1.678	004
1.30		
1.225	1.23	110
1.11	1.12	006
.84	.84	008
	.829	116
.79	.80	211

*J. Comer, AFCRL

11. REFERENCES

1. B. E. Knox and K. Vedam, "Coating Science and Technology," AFCRL-TR-75-0152, 31 January 1975.
2. B. E. Knox and K. Vedam, "Coating Science and Technology," AFCRL-TR-74-0085 (III), Special Reports, No. 1974, 14 February 1974.
3. B. E. Knox, J. Geneczko, L. Gilbert, R. Howard, G. Mariner and K. Vedam, "A Study of Sputtered Ge and CdTe Films on KCl," in Proceedings of the Fourth Annual Conference on Infrared Laser Window Materials, C. R. Andrews and C. L. Strecker (Eds.), Advanced Research Projects Agency, Arlington, Va., 1975, pp. 67-75.
4. K. V. Shalimova and V. A. Dmitriev, Sov. Phys.-Cryst. 17, 470 (1972).
5. H. M. Brown and F. D. E. Brodie, Can. J. Phys. 50, 2512 (1972).
6. K. V. Shalimova, O. S. Bulatov, E. N. Voronkov and V. A. Dmitriev, Sov. Phys.-Cryst. 11, 431 (1966).
7. R. Glang, J. G. Kren and W. J. Patrick, J. Electrochem. Soc. 110, 407 (1963).
8. V. Tolutis and V. Jasutis, Lietuvos Fiz. Rinkininys, Lietuvos TSR Mosklu Akad., Lietuvos TSR Aukstosios Mokyklos 5, 495 (1965).
9. K. V. Shalimova and E. N. Voronkov, Sov. Phys.-Solid State 9, -169 (1967).
10. Yu. P. Simanov, Zh. Fiz. Khim. 34, 1304 (1960).
11. V. Swaminathan, G. H. Narayanan and S. M. Copley, J. Appl. Phys. 46, 3716 (1975).
12. M. I. Abdalla and D. B. Holt, Phys. Stat. Sol. (a) 17, 267 (1973).
13. M. A. Short and E. B. Steward, Amer. Mineral. 44, 189 (1959).
14. J. W. Colby, "Quantitative Microprobe Analysis of Thin Insulating Films," Advances in X-ray Analysis, Vol. 11, Plenum Press, New York, 1968, pp. 287.
15. O. Brafman and I. T Steinberger, Phys. Rev. 143, 501 (1966).
16. N. K. Kiseleva and N. N. Pribytkova, Optics and Spect. 10, 133 (1961).
17. D. A. Vaugn, "Standard X-ray Diffraction Powder Patterns," N.B.S. Monograph #25, M. C. Morris, E. H. Evans and I Ulmer (Eds.), Washington, D. C., 1964, p. 21.
18. G. Jungk, Phys. Stat. Sol. (b) 44, 239 (1971).
19. G. A. N. Connel, R. J. Temkin and W. Paul, "Advances in Physics," 22, 643 (1973).

20. W. H. Knausenberger and K. Vedam, Phys. Lett. 29A, 428 (1969).

21. D. Haneman, Phys. Rev. 170, 705 (1968).

22. M. H. Brodsky, R. S. Title, K. Weiser and G. D. Pettit, Phys. Rev. B6, 2632 (1970).

23. S. C. Agarwal, Phys. Rev. B7, 685 (1973).

24. R. A. Street and N. F. Mott, Phys. Rev. Lett. 35, 1293 (1975).

25. P. W. Anderson, Phys. Rev. Lett. 34, 953 (1975).

26. D. E. Aspnes, Opt. Comms. 8, 222 (1973).

27. D. E. Aspnes, J. Opt. Soc. Am. 64, 812 (1974).

28. D. E. Aspnes and A. A. Studna, Appl. Opt. 14, 220 (1975).

29. M. Green, J. A. Kafalas and P. H. Robinson, in "Semiconductor Surface Physics," University of Pennsylvania Press, Philadelphia, Pa., 1957, p. 349.

30. C. R. Helms, W. E. Spicer and V. Pereskokov, Appl. Phys. Lett. 24, 318 (1974).

31. V. E. Henrich and J. C. Fan, J. Appl. Phys. 46, 1206 (1975).

32. J. C. C. Fan and V. E. Henrich, Appl. Phys. Lett. 25, 401 (1975).

33. G. A. N. Connell, R. J. Temkin and W. Paul, Appl. Phys. Lett. 24, 318 (1974).

34. R. Messier, Ph.D. Thesis, The Pennsylvania State University, University Park, Pa., 1973.

35. T. E. Gallon, I. G. Higginbotham, M. Prutton and H. Tokutaka, Surf. Sci. 21, 224 (1970).

36. P. W. Palmberg and T. N. Rhodin, J. Phys. Chem. Solids 29, 1917 (1968).

APPENDIX A

Program in BASIC Language for PDP 11/20
for Controlling the Automated Ellipsometer
and Collecting and Processing the Data.

```
KV91    11-FEB-76  BASIC V01-05

10 DIM I(30),R(30),S1(300),S2(300),P(300),W(300),N(300),V(300)
20 LET D1=3.14159/180
30 LET D2=12*D1
40 CALL "EINI"
50 FOR J=1 TO 30
60 LET R(J)=0
70 NEXT J
80 PRINT "HOW MANY SETS OF 100 TO BE AVERAGED?"
90 INPUT N
100 LET Y=0
110 IF Y=1 THEN 200
120 IF Y>0 THEN 210
130 PRINT "HOW MANY STEPS SHOULD MOTOR MOVE"
140 INPUT Q
150 PRINT "WHAT IS THE VALUE OF P0"
160 INPUT P0
170 PRINT "WHAT IS THE NUMBER OF 9.0E-3 DEGREE INCREMENTS PER STEP OF P0
180 INPUT K2
190 LET G=9.00000E-03*K2
200 FOR M=0 TO Q
210 FOR J=1 TO N
220 FOR K=1 TO 30
230 LET I(K)=0
240 NEXT K
250 FOR L=1 TO 100
260 FOR K=1 TO 30
270 CALL "FLIP"(X)
280 LET I(K)=I(K)+X
290 NEXT K
300 NEXT L
310 FOR K=1 TO 30
320 LET I(K)=I(K)/100
330 LET R(K)=0
340 LET R(K)=R(K)+I(K)
350 NEXT K
360 GO TO 410
370 PRINT "FOURIER TERMS"
380 PRINT I(1),I(2),I(3),I(4),I(5)
390 PRINT I(6),I(7),I(8),I(9),I(10)
400 PRINT I(11),I(12),I(13),I(14),I(15)
410 NEXT J
420 FOR K=1 TO 30
430 LET R(K)=R(K)/N
440 NEXT K
450 GO TO 530
460 PRINT "AVERAGE TERMS"
470 PRINT R(1),R(2),R(3),R(4),R(5)
480 PRINT R(6),R(7),R(8),R(9),R(10)
490 PRINT R(11),R(12),R(13),R(14),R(15)
500 PRINT R(16),R(17),R(18),R(19),R(20)
510 PRINT R(21),R(22),R(23),R(24),R(25)
520 PRINT R(26),R(27),R(28),R(29),R(30)
530 LET Z0=0
540 LET F1=0
550 LET F2=0
560 IF Y<2 THEN 600
570 LET S1=0
580 LET S2=0
590 GO TO 620
600 LET S1(M)=0
610 LET S2(M)=0
620 LET T1=0
630 LET T2=0
640 LET T3=0
650 LET F4=0
660 FOR L=1 TO 30
```

```
670 LET Z0=Z0+R(L)
680 LET A0=1*D1
690 LET A=A0-D2*(L-1)
700 LET F1=F1+R(L)*COS(A)
710 LET F2=F2+R(L)*SIN(A)
720 IF Y>1 THEN 760
730 LET S1(M)=S1(M)+R(L)*COS(2*(A))
740 LET S2(M)=S2(M)+R(L)*SIN(2*(A))
750 GO TO 780
760 LET S1=S1+R(L)*COS(2*(A))
770 LET S2=S2+R(L)*SIN(2*(A))
780 LET T1=T1+R(L)*COS(3*(A))
790 LET T2=T2+R(L)*SIN(3*(A))
800 LET F3=F3+R(L)*COS(4*(A))
810 LET F4=F4+R(L)*SIN(4*(A))
820 LET F5=F5+R(L)*COS(5*(A))
830 LET F6=F6+R(L)*SIN(5*(A))
840 LET S3=S3+R(L)*COS(6*(A))
850 LET S4=S4+R(L)*SIN(6*(A))
860 LET S5=S5+R(L)*COS(7*(A))
870 LET S6=S6+R(L)*SIN(7*(A))
880 LET E1=E1+R(L)*COS(8*(A))
890 LET E2=E2+R(L)*SIN(8*(A))
900 NEXT L
910 LET Z0=Z0/30
920 LET F1=F1/(15*Z0)
930 LET F2=F2/(15*Z0)
940 IF Y>1 THEN 980
950 LET S1(M)=S1(M)/(15*Z0)
960 LET S2(M)=S2(M)/(15*Z0)
970 GO TO 1000
980 LET S1=S1/(15*Z0)
990 LET S2=S2/(15*Z0)
1000 LET T1=T1/(15*Z0)
1010 LET T2=T2/(15*Z0)
1020 LET F3=F3/(15*Z0)
1030 LET F4=F4/(15*Z0)
1040 LET F5=F5/(15*Z0)
1050 LET F6=F6/(15*Z0)
1060 LET S3=S3/(15*Z0)
1070 LET S4=S4/(15*Z0)
1080 LET S5=S5/(15*Z0)
1090 LET S6=S6/(15*Z0)
1100 LET E1=E1/(15*Z0)
1110 LET E2=E2/(15*Z0)
1120 GO TO 1140
1130 PRINT "Z0 ="Z0
1140 GO TO 1160
1150 PRINT "F1 ="F1,"F2 ="F2
1160 IF Y>1 THEN 1200
1170 GO TO 1190
1180 PRINT "S1("M")="S1(M) "S2("M")="S2(M)
1190 GO TO 1210
1200 PRINT "S1 ="S1,"S2 ="S2
1210 GO TO 1240
1220 PRINT "T1 ="T1,"T2 ="T2
1230 PRINT "F3="F3,"F4="F4
1240 GO TO 1290
1250 PRINT "F5 ="F5,"F6 ="F6
1260 PRINT "S3 ="S3,"S4 ="S4
1270 PRINT "S5 ="S5,"S6 ="S6
1280 PRINT "E1 ="E1,"E2 ="E2
1290 IF Y>1 THEN 2040
1300 LET W(M)=1-S1(M)*S1(M)-S2(M)*S2(M)
1310 LET P(M)=(P0*D1)+(M*6*D1)
1320 LET N(M)=S2(M)/S1(M)
1330 LET V(M)=(ATN(N(M)))/2
1340 PRINT "P("M")="P(M)"W("M")="W(M)"V("M")="V(M)
```

```
1350 FOR K1=1 TO K2
1360 CALL 'ESTP'(1,1)
1370 NEXT K1
1380 NEXT M
1390 GOSUB 2430
1400 PRINT 'C0='C0,'C1='C1,'C2='C2
1410 IF Y>0 THEN 1480
1420 LET P1=-C1/(2*C2)
1430 PRINT 'P1 IN DEGREES='P1/D1
1440 LET U=1/SQR(1-C0+C1*C1/(4*C2))
1450 IF U>=0 THEN 1470
1460 LET U=-U
1470 IF Y=0 THEN 1510
1480 LET P2=-C1/(2*C2)-3.14159/2
1490 PRINT 'P2 IN DEGREES = 'P2/D1
1500 IF Y=1 THEN 1620
1510 LET G1=(12.3978/5461)
1520 LET G2=(12.3978/5461)
1530 LET G1=-G1
1540 LET G2=-G2
1550 PRINT 'WHAT ARE THE APPROXIMATE VALUES OF DELTA AND [illegible]"
1560 INPUT D3,P3
1570 LET M1=SIN(P3*D1)/COS(P3*D1)
1580 LET M2=P1-(G2*M1+G1*COS(D3*D1))/SIN(D3*D1)
1590 LET M3=M2/D1
1600 PRINT '(P SUB S) IN DEGREES ='M3
1610 IF Y=0 THEN 1670
1620 LET P7=COS(2*P3*D1)
1630 LET P8=(SIN(2*P3*D1)*SIN(D1*D3))
1640 LET P4=(P1+P2)/2+G2*P7/P8
1650 LET P5=P4/D1
1660 PRINT 'TRUE (P SUB S) IN DEGREES ='P5
1670 FOR M=0 TO Q
1680 LET W(M)=V(M)
1690 NEXT M
1700 GOSUB 2430
1710 PRINT 'V0='C0,'V1='C1,'V2='C2
1720 IF Y=1 THEN 1790
1730 LET A1=C0+(C1*P1)+(C2*P1*P1)
1740 PRINT 'A1 IN DEGREES='A1/D1
1750 LET M4=A1-(G1/M1+G2*COS(D3/D1))/SIN(D3*D1)
1760 LET M5=M4/D1
1770 PRINT '(A SUB S) IN DEGREES ='M5
1780 IF Y=0 THEN 1920
1790 LET A2=C0+C1*P2+C2*P2*P2
1800 PRINT 'A2 IN DEGREES='A2/D1
1810 LET A4=(A1+A2)/2-G1*P7/P8
1820 LET A3=A4/D1
1830 PRINT 'ACTUAL AZIMUTH A IN DEGREES='A3
1840 LET P9=SIN(2*P3*D1)
1850 LET D4=2*(COS(D3*D1)*(COS(D3*D1))-1/(P9*P9))
1860 LET G3=(((P1-P2)*COS(D1*D3)-(A1-A2)/P9)*SIN(D3*D1))*D4
1870 LET G4=(((A1-A2)*COS(D1*D3)-(P1-P2)/P9)*SIN(D3*D1))*D4
1880 PRINT 'CALCULATED VALUE OF G1='G3
1890 PRINT 'INPUT VALUE OF G1='G1
1900 PRINT 'CALCULATED VALUE OF G2='G4
1910 PRINT 'INPUT VALUE OF G2='G2
1920 LET Y=Y+1
1930 IF Y>1 THEN 1980
1940 PRINT 'WHAT IS THE VALUE OF P90 IN DEGREES?'
1950 INPUT P6
1960 LET P0=P6
1970 GO TO 110
1980 PRINT 'WHAT IS THE VALUE OF THE NEXT P IN DEGREES'
1990 INPUT P6
2000 LET P0=P6
2010 PRINT 'HOW MANY SETS OF 100 TO BE [illegible]"
2020 INPUT N
```

```
2030 GO TO 110
2040 LET N2=S2/S1
2050 IF S1>000 TO 2080
2060 LET Q1=(ATN(N2))/2+(3.14159/2)*(SGN(S2))
2070 GO TO 2090
2080 LET Q1=(ATN(N2))/2
2090 LET Z1=U*SQR((S1*S1)+(S2*S2))
2100 IF Z1>=0 THEN 2120
2110 LET Z1=-Z1
2120 LET A5=((-2*G4*Z1)+(1-G4*G4)*SQR(1-Z1*Z1))/((1+Z1)-(G4*G4)*(1-Z1))
2130 PRINT "LINE 2130  A5="A5
2140 IF A5>0 THEN 2170
2150 LET A5=((-2*G4*Z1)-(1-G4*G4)*SQR(1-Z1*Z1))/((1+Z1)-(G4*G4)*(1-Z1))
2160 PRINT " LINE 2160  A5="A5
2170 LET X1=(Q1-A4)
2180 LET Y1=P6*D1-P4
2190 LET X2=(COS(X1)*SIN(Y1))/(SIN(X1)*COS(Y1))
2200 LET X3=X2+A5*G3
2210 LET X4=1+(A5)*(G3)*(X2)
2220 LET X5=((G3)*COS(X1))/SIN(X1)
2230 LET X6=A5*SIN(Y1)/COS(Y1)
2240 LET X7=((G3)*SIN(Y1))/COS(Y1)
2250 LET X8=((A5)*COS(X1))/SIN(X1)
2260 LET Y2=(1+(X8)*(X8))*(1+(X7)*(X7))
2270 LET Y3=(((X3)*(X4))-(X5-X6)*(X7-X8))/Y2
2280 LET Y4=(((X3)*((X7)-(X8)))+(X4*((X5)-(X6))))/Y2
2290 LET Y5=(Y4)/(Y3)
2300 LET Y6=(ATN(Y5))/D1
2310 LET Y7=SQR((Y3)*(Y3)+(Y4)*(Y4))
2320 LET Y8=(ATN(Y7))/D1
2330 PRINT "DELTA="Y6,"PSI="Y8
2340 LET V1=(Y6)-(D3)
2350 LET V2=(Y8)-(P3)
2360 LET D3=Y6
2370 LET P3=Y8
2380 IF ABS(V1)<.0100 TO 2400
2390 GO TO 1570
2400 IF ABS(V2)<.0100 TO 2420
2410 GO TO 1570
2420 STOP
2430 LET B=0
2440 LET B1=0
2450 LET B2=0
2460 LET B3=0
2470 LET B4=0
2480 LET B5=0
2490 LET B6=0
2500 LET N1=Q+1
2510 FOR I=0 TO Q
2520 LET B=B+P(I)
2530 LET B1=B1+P(I)*P(I)
2540 LET B2=B2+P(I)*P(I+1)*P(I)
2550 LET B3=B3+P(I)*P(I)*P(I+1)*P(I)
2560 LET B4=B4+W(I)
2570 LET B5=B5+W(I)*P(I)
2580 LET B6=B6+W(I)*P(I)*P(I)
2590 NEXT I
2600 LET H1=B4*B2-B5*B1
2610 LET H2=B5*B3-B6*B2
2620 LET H3=B2*B3-B2*B2
2630 LET H4=B*B2-B1*B1
2640 LET H5=N1*B2-B*B1
2650 LET H6=B*B3-B1*B2
2660 LET H7=(H5*H3-H6*H4)
2670 LET C0=(H1*H3-H2*H4)/H7
2680 LET C1=(H2*H5-H1*H6)/H7
2690 LET C2=(B4-N1*C0-B*C1)/B1
2700 RETURN
2710 END
```

APPENDIX B

Program in BASIC Language for Controlling the Ion Scattering Spectrometer with the PDP 11/20 Data Processor.

```
JNISSC  12-JAN-76  BASIC V01-05

100 DIM B$(7),B(7,10),C(4),D(4)
120 PRINT "IF YOU WISH OUTPUT ON THE DECTAPE ENTER 1, OTHERWISE 0."
140 INPUT B7
160 PRINT "ENTER THE MAXIMUM NUMBER OF SECONDS THAT AN INDIVIDUAL"
180 PRINT "SCAN SHOULD LAST;  A NUMBER BETWEEN .1 AND 51.1"
200 INPUT Z3
220 LET J=1.5
240 LET Z3=Z3*10
260 IF Z3<.9 THEN 400
280 FOR B3=0 TO 9
300 IF Z3<J THEN 440
320 LET J=J*2
340 NEXT B3
360 PRINT Z3/10;"GREATER THAN MAXIMUM NUMBER OF SECONDS (51.2) RE-ENTER"
380 GO TO 200
400 PRINT Z3/10;"LESS THAN MINIMUM NUMBER OF SECONDS (.1-51.2) RE-ENTER"
420 GO TO 200
440 PRINT Z3/10;"APPROX =2 ** ";B3;" = ";J*6/30
460 PRINT "ENTER NUMBER OF MINUTES TO BE SPENT ON AN INDIVIDUAL SET OF"
480 PRINT "SCANS.  A NUMBER LESS THAN 1 CAUSES SINGLE PASSES"
500 INPUT B6
520 LET B6=B6-1
540 PRINT "ENTER THE TIME BETWEEN STARTS OF SCANS"
560 INPUT B5
580 REM
600 REM THESE NEXT FEW STATEMENTS BECOME UNNECESSARY IF B(?, 7) IS USED
620 REM
640 PRINT "ENTER THE NUMBER OF THOUSANDTHS YOU WISH AS A STEPSIZE FOR"
660 PRINT "CROSSING FROM ONE ENERGY RATIO BOUNDRY TO THE OTHER.  "
680 PRINT "ZERO CAUSES THE OPTION TO BE IGNORED, OTHERWIZE ENTER AN"
700 PRINT "INTEGER  BETWEEN 1 AND 999"
720 INPUT B4
740 IF B4>999 GO TO 640
760 IF B4=0 THEN 800
780 IF B4<1 GO TO 640
800 PRINT "ENTER THE TOTAL TIME IN MINUTES THAT THIS RUN MAY LAST"
820 INPUT B2
840 PRINT "ENTER THE NUMBER OF ENERGY RATIO RANGES TO BE USED FOR"
860 PRINT "THIS EXPERIMENT.  AT LEAST 1 MUST BE USED AND MAX IS 8"
880 INPUT B0
900 IF B0<1 THEN 840
920 IF B0>8 THEN 840
940 LET B0=B0-1
960 PRINT "ENTER THE NUMBER OF CONSECUTIVE  SCANS ACROSS AN INDIVIDUAL"
980 PRINT "ENERGY RATIO GAP THAT ARE TO BE USED:";
1000 PRINT " 1, 3, OR 5."
1020 INPUT B1
1040 IF B1<1 GO TO 1000
1060 IF B1>5 THEN 1000
1080 LET B1=B1-1
1090 LET D9=0
1100 PRINT "ENTER THE FOLLOWING DATA UNTIL YOU HAVE 2 LINES FOR EACH"
1120 PRINT "ELEMENT TO BE CONSIDERED.  THIS IS THE FORMAT:"
1140 PRINT "LINE 1 CHEM SYMBOL, LINES 2-5 NUMBERS SEPARATED BY COMMAS"
1160 PRINT "1. THE CHEMICAL SYMBOL"
1180 PRINT "2. LOWER ENERGY RATIO"
1200 PRINT "3. UPPER ENERGY RATIO"
1220 PRINT "4. GAIN SENSITIVITY 1, 2, 5, OR 10"
1240 PRINT "5. MAX COUNT - A NUMBER BETWEEN 16 AND 32768"
1260 REM PRINT "6. ZERO IF YOU WISH TO STEP ACROSS, STEPSIZE OTHERWISE"
1280 FOR K=0 TO B0
1300 INPUT B$(K)
1320 INPUT B(K,0),B(K,1),B(K,10),B(K,9)
```

```
1340 GO TO 1400
1360 PRINT "GAIN VALUE ENTERED IN ERROR PLEASE ENTER AGAIN"
1380 INPUT B(K,10)
1400 PRINT B$(K);B(K,0);B(K,1);B(K,10);B(K,7);B(K,9)
1420 LET I=0
1440 IF B(K,10)=1 THEN 1600
1460 IF B(K,10)=2 THEN 1580
1480 IF B(K,10)=5 THEN 1560
1500 IF B(K,10)=10 THEN 1540
1520 GO TO 1360
1540 LET I=1
1560 LET I=I+1
1580 LET I=I+1
1600 LET B(K,2)=I
1620 LET J=1.5
1640 LET Z=B(K,9)/16
1660 LET J=1.5
1680 FOR I=0 TO 11
1700 IF Z<J THEN 1840
1720 LET J=J*2
1740 NEXT I
1760 PRINT B(K,9);"GREATER THAN MAX COUNTS ENTER NUMBER LESS THAN"
1780 PRINT "32768 ENTER AGAIN:";
1800 INPUT B(K,9)
1820 GO TO 1640
1840 LET B(K,8)=I
1860 IF B(K,0)<=B(K,1) THEN 1950
1880 PRINT "LOWER LIMIT ";B(K,0);"  EXCEEDS UPPER LIMIT";B(K,1)
1900 PRINT "ENTER VALUES AGAIN"
1920 INPUT B(K,0),B(K,1)
1940 GO TO 1860
1950 IF D9=1 THEN 2842
1960 NEXT K
1970 IF B7<>1 THEN 2080
1980 OPEN "DT1:JMISSD.DAT" FOR OUTPUT AS FILE #7
2020 REM
2040 REM BEGIN CONTROL SECTION
2060 REM
2080 CALL "CTRL"(0,0,B5,0,3)
2100 CALL "REDC"(3,G0)
2120 REM START SLOW TIMER
2140 CALL "TIME"(1,0,B3)
2160 LET G=G0+B2
2180 LET T=G0
2200 LET G1=T+B6
2220 LET G2=T+B5
2240 PRINT
2260 PRINT "EL STR STOP  COUNT GAN CT*GN  COUNT RATES                ";
2280 PRINT "     TIME CTIM"
2300 FOR K=0 TO B0
2320 FOR J=0 TO B1
2340 LET D(J)=0
2360 LET C(J)=0
2380 LET Z=B(K,0)
2400 CALL "ENGY"(Z)
2420 CALL "CTRL"(B(K,2),1,B(K,8),0,1)
2440 IF B4=0 THEN 2500
2460 LET Z=Z+B4
2480 IF Z<=B(K,1) THEN 2520
2500 LET Z=B(K,1)
2520 CALL "ENGY"(Z)
2540 CALL "CTRL"(B(K,2),0,B(K,8),1,1)
2560 CALL "CTRL"(B(K,2),0,B(K,8),0,1)
2580 CALL "RED1"(R1,D8,R2,R3,R4,R5)
2600 CALL "CTRL"(B(K,2),0,B5,0,0)
2620 CALL "RED0"(S1,S2,S3)
```

```
2640 CALL "CTRL"(B(K,2),0,B5,0,3)
2660 CALL "REDC"(3,T)
2680 CALL "CTRL"(B(K,2),0,B5,0,2)
2700 CALL "REDC"(2,C)
2720 IF Z=S3 THEN 2860
2740 PRINT "THE SPECTROMETER IS PROBABLY ON 'INTERNAL' MODE. IF YOU"
2760 PRINT "WISH TO CONTINUE PRESS RETURN KEY. IF YOU WISH TO CHANGE"
2780 PRINT "THE ENERGY RATIO LIMITS TYPE C AND PRESS RETURN KEY"
2800 INPUT C$
2810 IF C$<>"C" THEN 2842
2820 IF C$<>"" THEN 3980
2840 GO TO 2420
2842 PRINT "GIVE THE CHEM SYMBOL(S) ONE AT A TIME FOR THE ONE(S) YOU"
2843 PRINT "WISH TO CHANGE. PRESS RET KEY IF YOU WISH NO MORE CHANGES"
2844 INPUT C$
2845 IF C$<>"" THEN 2420
2846 FOR I=0 TO B0
2847 IF B$(I)=C$ THEN 2851
2848 NEXT I
2849 LET B0=B0+1
2850 LET B$(B0)=C$
2851 PRINT "ENTER THE FOLLOWING NUMBERS SEPARATED BY COMMAS"
2852 PRINT "1. LOWER ENERGY RATIO",,,"2. UPPER ENERGY RATIO"
2853 PRINT "3. GAIN SENSITIVITY 1, 2, 5, OR 10"
2854 PRINT "4. MAX COUNT - A NUMBER BETWEEN 16 AND 32760"
2855 LET D9=1
2856 GO TO 1320
2860 LET B(J)=B(J)+B5
2880 LET C(J)=C(J)+C
2900 IF Z=B(K,1) THEN 2960
2920 LET Z=Z+1
2940 GO TO 2400
2960 NEXT J
2980 LET Y=0
3000 LET X=0
3020 FOR J=0 TO B1
3040 LET Y=Y+B(J)
3060 LET X=X+C(J)
3080 NEXT J
3100 LET B(K,3)=X/(J+1)
3120 LET B(K,4)=B(K,10)*B(K,3)
3140 LET B(K,5)=(Y/(J+1)/10)
3160 LET B(K,6)=B(K,4)/B(K,5)
3180 PRINT B$(K);B(K,0);B(K,1);B(K,3);B(K,10);B(K,4);
3200 IF K=0 THEN 3280
3220 FOR I=0 TO K-1
3240 PRINT "    ";
3260 NEXT I
3280 PRINT INT(B(K,6)+.5);
3300 IF K=7 THEN 3380
3320 FOR I=K TO 6
3340 PRINT "    ";
3360 NEXT I
3380 PRINT I;B(K,5)
3400 IF B7<>1 THEN 3460
3420 PRINT #7:B$(K);",";B(K,0);",";B(K,1);",";B(K,10);",";
3440 PRINT #7:B(K,3);",";B(K,4);",";B(K,6);",";T;",";B(K,5)
3460 IF T>G THEN 3920
3480 IF T>G1 THEN 3700
3500 CALL "ENGY"(999)
3520 CALL "TIME"(1,0,3)
3540 CALL "CTRL"(3,1,11,1,0)
3560 CALL "TIME"(1,0,B3)
3580 NEXT K
3600 REM WAIT 8 SECONDS
3620 CALL "TIME"(1,0,5)
```

```
3640 CALL 'CTRL'(3,0,11,1,0)
3660 CALL 'TIME'(1,0,B3)
3680 GO TO 2300
3700 IF T>G2 THEN 3840
3720 CALL 'ENGY'(999)
3740 CALL 'CTRL'(0,1,0,1,3)
3760 CALL 'CTRL'(0,0,0,0,3)
3780 CALL 'READC'(3,T)
3800 IF T>=G2 THEN 2200
3820 GO TO 3760
3840 PRINT 'ERROR ERROR TOO LITTLE TIME ALLOTTED BETWEEN STARTS ';
3860 PRINT 'OF SCANS.  THE OLD VALUE WAS ';B5;'ENTER NEW VALUE'
3880 INPUT B5
3900 GO TO 2200
3920 INPUT Z9
3940 IF Z9>5GO TO 840
3960 IF Z9=3 THEN 2080
3980 CALL 'TIME'(0,0,0)
4000 CLOSE #7
4020 END
```

APPENDIX C

Definitions of Variables in the Program Used for Controlling the Ion Scattering Spectrometer with the PDP 11/20 Data Processor.

```
JMISSV  18-DEC-75  BASIC V01-05

10 REM AUTOMATION OF ION SCATTERING SPECTROMETER
20 REM          JMM  JULY 16, 1975
30 REM
40 REM THE COMPUTER IGNORES THE HARDWARE WINDOWS AND TREATS THE
50 REM MACHINE AS IF IT WERE A SINGLE CHANNEL MACHINE
60 REM
70 REM INITIALIZATION OF THE PROGRAMME: DEFINITIONS OF VARIABLES
80 REM SCALER DEFINITIONS
85 REM
90 REM B0 NUMBER OF WINDOWS TO BE LOOKED THROUGH TO DETECT PRESENCE OF
100 REM VARIOUS ELEMENTS
110 REM
120 REM
130 REM B1 NUMBER OF SUCCESSIVE READINGS OF AN INDIVIDUAL WINDOW TO BE
140 REM     MADE BEFORE PROCEEDING TO THE NEXT WINDOW.
150 REM
160 REM B2 THE TOTAL TIME IN MINUTES WHICH THE EXPERIMENT MAY RUN.
170 REM    UP TO 4096 MINUTES (68.1 HOURS)
180 REM
190 REM B3 THE MAXIMUM NUMBER OF SECONDS THAT THE MACHINE MAY DEVOTE TO
200 REM     AN INDIVIDUAL PASS ACROSS THE WINDOW.
210 REM
220 REM B4 STEP SIZE IF USED TO STEP ACROSS A WINDOW TO DETERMINE THE
230 REM    PRESENCE OR ABSENCE OF THE ELEMENT BEING TESTED
240 REM
245 REM B5 MINUTES TO BE SPENT BETWEEN STARTS OF SCANNING PERIODS.
250 REM
255 REM B6 TIME TO BE SPENT SCANNING.0 MEANS ONE SCAN.
260 REM
265 REM B7 SWITCH TO DECIDE WHETHER OUTPUT IS TO GO TO DEC-TAPE
271 REM
280 REM
300 REM
310 REM K COUNTER FOR WHICH WINDOW IS CURRENTLY BEING LOOKED AT.
320 REM
330 REM I,J GENERAL USE COUNTERS
340 REM
350 REM D9 HARDWARE CHANNEL (WINDOW) BEING LOOKED AT CURRENTLY
360 REM
370 REM D8 DUMMY ARGUMENT BEING USED *BUSY*
380 REM
390 REM R1 GAIN VALUE RETURNED BY RED1 THIS SHOULD BE EQUAL TO B(K,2)
400 REM
410 REM R2 ARGUMENT TELLING IF MAXIMUM COUNT WAS ATTAINED
420 REM
430 REM R3 ARGUMENT TELLING IF MAXIMUM TIME WAS ATTAINED
440 REM
450 REM R4 ARGUMENT DUMMY? FROM RED1 TELLING IF COUNT EXCEEDED THE LIMIT
460 REM
470 REM R5 ARGUMENT CONTAINING THE FAST TIMER TIME FROM RED1
480 REM
490 REM T *REAL* TIME ELAPSED MINUTES FROM STARTING
500 REM
510 REM Z ARGUMENT FOR *ENGY* THAT CONTAINS THE MOST RECENT VALUE OF E/E
511 REM
515 REM C CURRENT E/E COUNT VALUE FOR CUMULATION
520 REM
525 REM C$ VALUE TO DETERMINE WHETHER TO CONTINUE IF ON INTERNAL MODE
526 REM     REQUIRES THAT IT BE SET TO EXTERNAL BEFORE GOING ON
530 REM G TIME THAT RUN IS TO END
531 REM
535 REM G0 INITIAL CLOCK TIME USUALLY 0
536 REM
```

```
540 REM G1 QUITTING TIME FOR SCANNING SET
541 REM
545 REM G2 BEGINNING TIME FOR NEXT SET OF SCANS
550 REM
560 REM Z3 SECONDS FOR MAXIMUM TIME
570 REM
580 REM
590 REM B$(7) AN 8 ELEMENT CHARACTER ARRAY CONTAINING THE CHEMICAL
600 REM SYMBOL (OR NAME) FOR THAT ELEMENT ASSOCIATED WITH THAT WINDOW
610 REM
620 REM
630 REM B(7,9 ) AN 8X10 ARRAY CONTAINING THE FOLLOWING:
640 REM I,0 LOWER ENERGY RATIO INPUT
650 REM I,1 UPPER ENERGY RATIO  INPUT
660 REM I,2 GAIN  SENSITIVITY FACTORS 0=> 1, 1=>2, 2=>5,3=>10
670 REM I,3 COUNT -AVERAGE OF THE SEVERAL PASSES(B(
680 REM I,4 PRODUCT OF THE PRECEDING TWO ACTUAL COUNTS
690 REM I,5 FAST TIMER TIME
700 REM I,6 COUNT RATE - DIVIDEND OF PRECEDING TWO.
710 REM I,7 SWITCH TO DECIDE BETWEEN TIME FOR COUNT:1, COUNT FOR TIME:0
720 REM I,8 MAX COUNT (POWER OF 2) FOR THIS ENERGY RATIO GAP
730 REM I,9 MAX COUNT (NUMBER) ENTERED
740 REM I,10 GAIN FACTOR VALUE =1,2,5, OR 10
770 REM
780 REM C(4) A 5 ELEMENT ARRAY TO HOLD INTERMEDIATE COUNT VALUES
790 REM      BEFORE AVERAGING THEM FOR B(I ,3)
800 REM
810 REM D(4) HOLDS THE CUMULATIVE INTERMEDIARY VALUES FOR FAST TIMER
830 REM
840 REM
850 REM
860 REM
870 REM
880 REM
890 END
```

APPENDIX D

CdTe Depth Profile Data Obtained with the Ion Scattering Spectrometer Controlled by the PDP 11/20 Data Processor.

```
LTISSE  18-DEC-75  BASIC V01-05

IF YOU WISH OUTPUT ON THE DECTAPE ENTER 1, OTHERWISE 0.
?0
ENTER THE MAXIMUM NUMBER OF SECONDS THAT AN INDIVIDUAL
SCAN SHOULD LAST;  A NUMBER BETWEEN .1 AND 51.1
?5
 5 APPROX =2 **  6  =  25.6
ENTER NUMBER OF MINUTES TO BE SPENT ON AN INDIVIDUAL SET OF SCANS
A NUMBER LESS THAN 1 CAUSES SINGLE PASSES
?2
ENTER THE TIME BETWEEN STARTS OF SCANS
?10
ENTER THE NUMBER OF THOUSANDTHS YOU WISH AS A STEPSIZE FOR
CROSSING FROM ONE ENERGY RATIO BOUNDRY TO THE OTHER.
ZERO CAUSES THE OPTION TO BE IGNORED. OTHERWISE ENTER AN
INTEGER BETWEEN 1 AND 999
?1
ENTER THE TOTAL TIME IN MINUTES THAT THIS RUN MAY LAST
?360
ENTER THE NUMBER OF ENERGY RATIO RANGES TO BE USED FOR
THIS EXPERIMENT.  AT LEAST 1 MUST BE USED AND MAX IS 8
?8
ENTER THE NUMBER OF CONSECUTIVE SCANS ACROSS AN INDIVIDUALENERGY RATIO G
AP THAT ARE TO BE USED1,3,OR 5.
?1
 ENTER THE FOLLOWING DATA UNTIL YOU HAVE 2 LINES FOR EACH
  ELEMENT TO BE CONSIDERED .  THIS IS THE FORMAT:
 LINE 1 CHEMICAL SYMBOL, LINE 2 NUMBERS SEPARATED BY COMMAS
1. THE CHEMICAL SYMBOL
2. LOWER ENERGY RATIO
3. UPPER ENERGY RATIO
4. GAIN SENSITIVITY 1, 2, 5, OR 10
5. MAX COUNT - A NUMBER BETWEEN 16 AND 32768
?

 SIL
?20,20,1,10000
SIL 20  20  1  0  10000
?SIP
?25,25,1,10000
SIP 25  25  1  0  10000
?SIH
?30,30,1,10000
SIH 30  30  1  0  10000
?KL
?320,320,1,1000
KL 320  320  1  0  1000
?KP
?335,335,1,1000
KP 335  335  1  0  1000
?KH
?360,360,1,1000
KH 360  360  1  0  1000
?CD
?700,700,1,5000
CD 700  700  1  0  5000
?TE
?745,745,1,15000
TE 745  745  1  0  15000
```

SPUTTERING TIME
125 MIN

EL	STR	STOP	COUNT	GAN	CT*GN	COUNT RATES	TIME	CTIM
SIL	20	20	3904	1	3904	610	1291	6.4
SIP	25	25	8192	1	8192	1575	1291	5.2
SIH	30	30	8192	1	8192	3034	1291	2.7
KL	320	320	1024	1	1024	379	1291	2.7
KP	335	335	1024	1	1024	394	1291	2.6
KH	360	360	1024	1	1024	445	1291	2.3
CD	700	700	4096	1	4096	2276	1291	1.8
TE	745	745	16384	1	16384		10240	1291
1.6								
SIL	20	20	3664	1	3664	573	1292	6.4
SIP	25	25	8192	1	8192	1517	1292	5.4
SIH	30	30	8192	1	8192	2926	1292	2.8
KL	320	320	1024	1	1024	394	1292	2.6
KP	335	335	1024	1	1024	394	1292	2.6
KH	360	360	1024	1	1024	410	1292	2.5
CD	700	700	4096	1	4096	2276	1292	1.8
TE	745	745	16384	1	16384		10240	1292
1.6								
SIL	20	20	3507	1	3507	548	1293	6.4

EL	STR	STOP	COUNT	GAN	CT*GN	COUNT RATES	TIME	CTIM
SIL	20	20	3885	1	3885	607	1301	6.4
SIP	25	25	8192	1	8192	1546	1301	5.3
SIH	30	30	8192	1	8192	3034	1301	2.7
KL	320	320	1024	1	1024	366	1301	2.8
KP	335	335	1024	1	1024	379	1301	2.7
KH	360	360	1024	1	1024	427	1301	2.4
CD	700	700	4096	1	4096	2276	1301	1.8
TE	745	745	16384	1	16384		10240	1301
1.6								
SIL	20	20	3587	1	3587	560	1302	6.4
SIP	25	25	8192	1	8192	1437	1302	5.7
SIH	30	30	8192	1	8192	2825	1302	2.9
KL	320	320	1024	1	1024	366	1302	2.8
KP	335	335	1024	1	1024	427	1302	2.4
KH	360	360	1024	1	1024	465	1302	2.2
CD	700	700	4096	1	4096	2276	1302	1.8
TE	745	745	16384	1	16384		10240	1302
1.6								
SIL	20	20	3422	1	3422	535	1303	6.4

EL	STR	STOP	COUNT	GAN	CT*GN	COUNT RATES	TIME	CTIM
SIL	20	20	3831	1	3831	599	1311	6.4
SIP	25	25	8192	1	8192	1463	1311	5.6
SIH	30	30	8192	1	8192	3034	1311	2.7
KL	320	320	1024	1	1024	379	1311	2.7
KP	335	335	1024	1	1024	379	1311	2.7

135 MIN

145 MIN

```
EL STR STOP  COUNT GAN CT*GN  COUNT RATES                TIME CTIM     156 MIN
SIL 20  20  3657  1  3657  571                          1322  6.4
SIP 25  25  8192  1  8192     1463                       1322  5.6
SIH 30  30  8192  1  8192        2825                    1322  2.9
KL 320  320  1024  1  1024           394                 1322  2.6
KP 335  335  1024  1  1024              394              1322  2.6
KH 360  360  1024  1  1024                 465           1322  2.2
CD 700  700  4096  1  4096                    2156       1322  1.9
TE 745  745  16384  1  16384                          9638  1322
 1.7
SIL 20  20  3346  1  3346  523                          1323  6.4

EL STR STOP  COUNT GAN CT*GN  COUNT RATES                TIME CTIM     165 MIN
SIL 20  20  4290  1  4290  670                          1331  6.4
SIP 25  25  8192  1  8192     1743                       1331  4.7
SIH 30  30  8192  1  8192        3151                    1331  2.6
KL 320  320  1024  1  1024           539                 1331  1.9
KP 335  335  1024  1  1024              512              1331  2
KH 360  360  1024  1  1024                 569           1331  1.8
CD 700  700  4096  1  4096                    2048       1331  2
TE 745  745  16384  1  16384                          9638  1331
 1.7
SIL 20  20  4138  1  4138  647                          1332  6.4
SIP 25  25  8192  1  8192     1638                       1332  5
SIH 30  30  8192  1  8192        3034                    1332  2.7
KL 320  320  1024  1  1024           569                 1332  1.8
KP 335  335  1024  1  1024              569              1332  1.8
KH 360  360  1024  1  1024                 539           1332  1.9
CD 700  700  4096  1  4096                    1950       1332  2.1
TE 745  745  16384  1  16384                          9102  1332
 1.8
SIL 20  20  4166  1  4166  651                          1333  6.4


EL STR STOP  COUNT GAN CT*GN  COUNT RATES                TIME CTIM     175 MIN
SIL 20  20  5562  1  5562  869                          1341  6.4
SIP 25  25  8192  1  8192     2482                       1341  3.3
SIH 30  30  8192  1  8192        3901                    1341  2.1
KL 320  320  1024  1  1024           640                 1341  1.6
KP 335  335  1024  1  1024              569              1341  1.8
KH 360  360  1024  1  1024                 683           1341  1.5
CD 700  700  4096  1  4096                    1638       1341  2.5
TE 745  745  16384  1  16384                          7802  1341
 2.1
SIL 20  20  5333  1  5333  833                          1342  6.4
SIP 25  25  8192  1  8192     2214                       1342  3.7
SIH 30  30  8192  1  8192        3901                    1342  2.1
KL 320  320  1024  1  1024           602                 1342  1.7
KP 335  335  1024  1  1024              640              1342  1.6
KH 360  360  1024  1  1024                 640           1342  1.6
CD 700  700  4096  1  4096                    1707       1342  2.4
TE 745  745  16384  1  16384                          7802  1342
 2.1
SIL 20  20  5400  1  5400  844                          1342  6.4
SIP 25  25  8192  1  8192     2214                       1343  3.7
```

```
EL STR STOP  COUNT GAN CT*GN  COUNT RATES                TIME CTIM      184 MIN
SIL 25  25  8192  1  8192  2926                        1350  2.8
SIP 30  30  8192  1  8192     5120                     1350  1.6
SIH 40  40  8192  1  8192        6827                  1351  1.2
KL 320  320  1024  1  1024           683                1351  1.5
KP 335  335  1024  1  1024              731             1351  1.4
KH 360  360  1024  1  1024                 683          1351  1.5
CD 700  700  4096  1  4096                    1517      1351  2.7
TE 745  745  16384  1  16384                      7447  1351
 2.2
SIL 25  25  8192  1  8192  2825                        1351  2.9
SIP 30  30  8192  1  8192     5120                     1351  1.6
SIH 40  40  8192  1  8192        6827                  1351  1.2
KL 320  320  1024  1  1024           731                1351  1.4
KP 335  335  1024  1  1024              731             1352  1.4
KH 360  360  1024  1  1024                 683          1352  1.5
CD 700  700  4096  1  4096                    1517      1352  2.7
TE 745  745  16384  1  16384                      7447  1352
 2.2
SIL 25  25  8192  1  8192  2825                        1352  2.9
SIP 30  30  8192  1  8192     5120                     1352  1.6
SIH 40  40  8192  1  8192        6827                  1352  1.2
KL 320  320  1024  1  1024           640                1352  1.6
KP 335  335  1024  1  1024              788             1352  1.3
KH 360  360  1024  1  1024                 683          1352  1.5
CD 700  700  4096  1  4096                    1517      1353  2.7

EL STR STOP  COUNT GAN CT*GN  COUNT RATES                TIME CTIM      190 MIN
SIL 25  25  8192  1  8192  3277                        1356  2.5
SIP 30  30  8192  1  8192     5851                     1356  1.4
SIH 40  40  8192  1  8192        7447                  1356  1.1
KL 320  320  1024  1  1024           731                1356  1.4
KP 335  335  1024  1  1024              788             1356  1.3
KH 360  360  1024  1  1024                 731          1356  1.4
CD 700  700  4096  1  4096                    1412      1356  2.9
TE 745  745  16384  1  16384                      6827  1356
 2.4
SIL 25  25  8192  1  8192  3034                        1356  2.7
SIP 30  30  8192  1  8192     5851                     1357  1.4
SIH 40  40  8192  1  8192        8192                  1357  1
KL 320  320  1024  1  1024           731                1357  1.4
KP 335  335  1024  1  1024              788             1357  1.3
KH 360  360  1024  1  1024                 731          1357  1.4
CD 700  700  4096  1  4096                    1365      1357  3
TE 745  745  16384  1  16384                      6554  1357
 2.5
SIL 25  25  8192  1  8192  2926                        1357  2.8
SIP 30  30  8192  1  8192     5851                     1357  1.4
SIH 40  40  8192  1  8192        8192                  1357  1
KL 320  320  1024  1  1024           788                1358  1.3
KP 335  335  1024  1  1024              788             1358  1.3
KH 360  360  1024  1  1024                 731          1358  1.4
CD 700  700  4096  1  4096                    1412      1358  2.9
TE 745  745  16384  1  16384                      6554  1358
 2.5
SIL 25  25  8192  1  8192  3151                        1358  2.6
SIP 30  30  8192  1  8192     5851                     1358  1.4
SIH 40  40  8192  1  8192        8192                  1358  1
KL 320  320  1024  1  1024           788                1358  1.3
KP 335  335  1024  1  1024              788             1358  1.3
KH 360  360  1024  1  1024                 683          1359  1.5
```

```
EL STR STOP  COUNT GAN CT*GN  COUNT RATES                    TIME CTIM        196 MIN
SIL 25  25  8192  1  8192  3413                             1362  2.4
SIP 30  30  8192  1  8192     6302                          1362  1.3
SIH 40  40  8192  1  8192        8192                       1362  1
KL 320  320  1024  1  1024           788                    1362  1.3
KP 335  335  1024  1  1024              788                 1362  1.3
KH 360  360  1024  1  1024                 788              1362  1.3
CD 700  700  4096  1  4096                    1321          1362  3.1
TE 745  745  16384  1  16384                          6302  1362
 2.6
SIL 25  25  8192  1  8192  3413                             1362  2.4
SIP 30  30  8192  1  8192     6827                          1363  1.2
SIH 40  40  8192  1  8192        9102                       1363  .9
KL 320  320  1024  1  1024           788                    1363  1.3
KP 335  335  1024  1  1024              788                 1363  1.3
KH 360  360  1024  1  1024                 788              1363  1.3
CD 700  700  4096  1  4096                    1321          1363  3.1
TE 745  745  16384  1  16384                          6068  1363
 2.7
SIL 25  25  8192  1  8192  3413                             1363  2.4
SIP 30  30  8192  1  8192     6827                          1363  1.2
SIH 40  40  8192  1  8192        9102                       1363  .9
KL 320  320  1024  1  1024           788                    1364  1.3
KP 335  335  1024  1  1024              853                 1364  1.2
KH 360  360  1024  1  1024                 731              1364  1.4
CD 700  700  4096  1  4096                    1280          1364  3.2
TE 745  745  16384  1  16384                          6068  1364
 2.7
SIL 25  25  8192  1  8192  3562                             1364  2.3
SIP 30  30  8192  1  8192     6827                          1364  1.2
SIH 40  40  8192  1  8192        9102                       1364  .9
KL 320  320  1024  1  1024           731                    1364  1.4
KP 335  335  1024  1  1024              853                 1364  1.2
KH 360  360  1024  1  1024                 731              1365  1.4

EL STR STOP  COUNT GAN CT*GN  COUNT RATES                    TIME CTIM        202 MIN
SIL 25  25  8192  1  8192  3901                             1368  2.1
SIP 30  30  8192  1  8192     7447                          1368  1.1
SIH 40  40  8192  1  8192        9102                       1368  .9
KL 320  320  1024  1  1024           853                    1368  1.2
KP 335  335  1024  1  1024              788                 1368  1.3
KH 360  360  1024  1  1024                 731              1368  1.4
CD 700  700  4096  1  4096                    1241          1368  3.3
TE 745  745  16384  1  16384                          5851  1368
 2.8
SIL 25  25  8192  1  8192  3901                             1368  2.1
SIP 30  30  8192  1  8192     7447                          1369  1.1
SIH 40  40  8192  1  8192        9102                       1369  .9
KL 320  320  1024  1  1024           853                    1369  1.2
KP 335  335  1024  1  1024              853                 1369  1.2
KH 360  360  1024  1  1024                 731              1369  1.4
CD 700  700  4096  1  4096                    1205          1369  3.4
TE 745  745  16384  1  16384                          5650  1369
 2.9
SIL 25  25  8192  1  8192  4096                             1369  2
SIP 30  30  8192  1  8192     7447                          1369  1.1
SIH 40  40  8192  1  8192        9102                       1369  .9
KL 320  320  1024  1  1024           853                    1370  1.2
KP 335  335  1024  1  1024              853                 1370  1.2
KH 360  360  1024  1  1024                 731              1370  1.4
CD 700  700  4096  1  4096                    1205          1370  3.4
TE 745  745  16384  1  16384                          5650  1370
 2.9
```

```
SIL 25  25  8192  1  8192  4096                          1370  2
SIP 30  30  8192  1  8192     8192                       1370  1
SIH 40  40  8192  1  8192        9102                    1370  .9
KL 320  320  1024  1  1024           788                 1370  1.3
KP 335  335  1024  1  1024              853              1370  1.2
KH 360  360  1024  1  1024                 788           1371  1.3

EL STR STOP  COUNT GAN CT*GN  COUNT RATES                TIME CTIM      208 MIN
SIL 25  25  8192  1  8192  4312                          1374  1.9
SIP 30  30  8192  1  8192     8192                       1374  1
SIH 40  40  8192  1  8192        10240                    1374  .8
KL 320  320  1024  1  1024           853                 1374  1.2
KP 335  335  1024  1  1024              853              1374  1.2
KH 360  360  1024  1  1024                 731           1374  1.4
CD 700  700  4096  1  4096                    1170        1374  3.5
TE 745  745  16384  1  16384                        5461  1374
 3
SIL 25  25  8192  1  8192  4551                          1374  1.8
SIP 30  30  8192  1  8192     8192                       1375  1
SIH 40  40  8192  1  8192        10240                    1375  .8
KL 320  320  1024  1  1024           853                 1375  1.2
KP 335  335  1024  1  1024              853              1375  1.2
KH 360  360  1024  1  1024                 788           1375  1.3
CD 700  700  4096  1  4096                    1138        1375  3.6
TE 745  745  16384  1  16384                        5461  1375
 3
SIL 25  25  8192  1  8192  4819                          1375  1.2
SIP 30  30  8192  1  8192     8192                       1375  1
SIH 40  40  8192  1  8192        10240                    1375  .8
KL 320  320  1024  1  1024           853                 1376  1.2
KP 335  335  1024  1  1024              853              1376  1.2
KH 360  360  1024  1  1024                 731           1376  1.4
CD 700  700  4096  1  4096                    1138        1376  3.6
TE 745  745  16384  1  16384                        5285  1376
 3.1
SIL 25  25  8192  1  8192  4819                          1376  1.7
SIP 30  30  8192  1  8192     8192                       1376  1
SIH 40  40  8192  1  8192        10240                    1376  .8
KL 320  320  1024  1  1024           853                 1376  1.2
KP 335  335  1024  1  1024              853              1377  1.2

EL STR STOP  COUNT GAN CT*GN  COUNT RATES                TIME CTIM      214 MIN
SIL 25  25  8192  1  8192  5120                          1380  1.6
SIP 30  30  8192  1  8192     9102                       1380  .9
SIH 40  40  8192  1  8192        10240                    1380  .8
KL 320  320  1024  1  1024           853                 1380  1.2
KP 335  335  1024  1  1024              931              1380  1.1
KH 360  360  1024  1  1024                 731           1380  1.4
CD 700  700  4096  1  4096                    1078        1380  3.8
TE 745  745  16384  1  16384                        5120  1380
 3.2
SIL 25  25  8192  1  8192  5461                          1380  1.5
SIP 30  30  8192  1  8192     9102                       1381  .9
SIH 40  40  8192  1  8192        10240                    1381  .8
KL 320  320  1024  1  1024           788                 1381  1.3
KP 335  335  1024  1  1024              931              1381  1.1
KH 360  360  1024  1  1024                 731           1381  1.4
CD 700  700  4096  1  4096                    1050        1381  3.9
TE 745  745  16384  1  16384                        4965  1381
 3.3
```

```
SIL 25  25  8192  1  8192  5461                          1381  1.5
SIP 30  30  8192  1  8192     9102                       1381  .9
SIH 40  40  8192  1  8192        10240                   1381  .8
NL 320  320  1024  1  1024           853                 1382  1.2
NP 335  335  1024  1  1024              853              1382  1.2
NH 360  360  1024  1  1024                 731           1382  1.4
CD 700  700  4096  1  4096                    1050       1382  3.9
TE 745  745  16384  1  16384                        5120  1382
 3.2
SIL 25  25  8192  1  8192  5851                          1382  1.4
SIP 30  30  8192  1  8192     9102                       1382  .9
SIH 40  40  8192  1  8192        10240                   1382  .8
NL 320  320  1024  1  1024           853                 1382  1.2
NP 335  335  1024  1  1024              853              1383  1.2

EL STR STOP  COUNT GAN CT*GN  COUNT RATES                TIME CTIM      229 MIN
SIL 25  25  8192  1  8192  5851                          1386  1.4
SIP 30  30  8192  1  8192     10240                      1386  .8
SIH 40  40  8192  1  8192        10240                   1386  .8
NL 320  320  1024  1  1024           853                 1386  1.2
NP 335  335  1024  1  1024              788              1386  1.3
NH 360  360  1024  1  1024                 731           1386  1.4
CD 700  700  4096  1  4096                    953        1386  4.3
TE 745  745  16384  1  16384                       4551  1386
 3.6
SIL 25  25  8192  1  8192  6302                          1386  1.3
SIP 30  30  8192  1  8192     10240                      1387  .8
SIH 40  40  8192  1  8192        10240                   1387  .8
NL 320  320  1024  1  1024           788                 1387  1.3
NP 335  335  1024  1  1024              853              1387  1.2
NH 360  360  1024  1  1024                 683           1387  1.5
CD 700  700  4096  1  4096                    931        1387  4.4
TE 745  745  16384  1  16384                       4551  1387
 3.6
SIL 25  25  8192  1  8192  6302                          1387  1.3
SIP 30  30  8192  1  8192     10240                      1387  .8
SIH 40  40  8192  1  8192        10240                   1388  .8
NL 320  320  1024  1  1024           788                 1388  1.3
NP 335  335  1024  1  1024              788              1388  1.3
NH 360  360  1024  1  1024                 731           1388  1.4
CD 700  700  4096  1  4096                    953        1388  4.3
TE 745  745  16384  1  16384                       4551  1388
 3.6
SIL 25  25  8192  1  8192  6827                          1388  1.2
SIP 30  30  8192  1  8192     10240                      1388  .8
SIH 40  40  8192  1  8192        10240                   1388  .8
NL 320  320  1024  1  1024           788                 1388  1.3
NP 335  335  1024  1  1024              853              1389  1.2


EL STR STOP  COUNT GAN CT*GN  COUNT RATES                TIME CTIM      226 MIN
SIL 25  25  8192  1  8192  6302                          1392  1.3
SIP 30  30  8192  1  8192     10240                      1392  .8
SIH 40  40  8192  1  8192        10240                   1392  .8
NL 320  320  1024  1  1024           853                 1392  1.2
NP 335  335  1024  1  1024              853              1392  1.2
NH 360  360  1024  1  1024                 683           1392  1.5
```